Fundamental Investigations on Multi-field Assisted Grinding of Difficult-to-machine Aeronautical Materials

（航空難加工材料のマルチフィールド援用研削の基礎研究）

by

Sisi Li
B.Eng., M.Eng.

A thesis submitted to Akita Prefecture University
in fulfillment of the requirements of the degree of
Doctor of Engineering

School of Graduate
Akita Prefecture University

2018

This page intentionally left blank.

Abstract

Poor machinability of hard-to-machine materials limits their applications in aircraft industries. From the viewpoint of cost reductions, it needs a more efficient and productive way to produce these materials. However, the grinding process is brittle material with small size grain, putting it at a disadvantage for large-variety production. In order to improve the grinding ability, one novel hybrid and two multi-filed assisted grinding technologies are proposed and experimental text with hard-to-machine materials in this study. The multi-field assisted machining are combined ultrasonic vibration, electrochemical and plasma electrolytic oxidation into grinding, meanwhile, named them as ultrasonic vibration assisted grinding, ultrasonic assisted electrochemical grinding and ultrasonic assisted plasma oxidation grinding, respectively.

First, the ultrasonic assisted grinding (UAG) apparatus was designed and constructed. An experimental apparatus was established by installing a commercially available ultrasonic spindle onto a commercially available NC grinder through a 3-components piezoelectric dynamometer. The dynamometer was located below the spindle and used for the measurement of grinding forces. In experiments, the workpiece specimen was fixed on a work-holder under which a Z-stage is located for determining the depth of cut. The working surface condition of abrasive tool is one of important issues in grinding process. This article discusses the effects of the ultrasonic vibration on the working surface condition involving chips adhesion and abrasive grains wear during UAG of Inconel 718 with an electroplated cBN grinding wheel as the abrasive tool. In this study, scanning electron microscopic (SEM) observations were performed on the wheel working surface before and after grinding at different vibration amplitudes and the SEM images were filtered, extracted and binarized by using Image-Pro Plus to evaluate the wheel working surface condition. The obtained

results demonstrated that (1) the wear of grinding wheel are dominantly attributed to chips adhesion, grains releasing and grains fracture, (2) both the percentage of chips adhesion area and the size of chips adhered tend to decrease as the vibration amplitude increases; in contrast, the effect of ultrasonic vibration on the number of chips adhesion are not noticeable, (3) the percentage of the number of grains released/fractured decreases as the vibration amplitude rises; e.g., the percentage in UAG at vibration amplitude of $A_{p\text{-}p}$=9.4 μm was decreased by 40 % compared to that in conventional grinding (CG), (4) higher distribution density of effective cutting edges can be achieved under larger vibration amplitude, and the mean area of effective cutting edges in UAG is smaller than that in CG, demonstrating that the ultrasonication enhances the grinding wheel sharpness.

In order to improve the grindability of Ti–6Al–4V, a hybrid material removal process was proposed in this study. This process was a combination of ultrasonic assisted grinding (UAG) and electrochemical grinding (ECG); hereafter named as ultrasonic assisted electrochemical grinding (UECG). In order to confirm the feasibility of the proposed technique, an experimental setup was constructed and the fundamental machining characteristics of UECG in the grinding of Ti–6Al–4V were experimentally investigated. The results obtained from the investigation summarized as follows: (1) The normal and tangential grinding forces in UECG were smaller than those in conventional grinding (CG) by 60 % and 65 %, respectively; (2) The work-surface roughness, Ra, both in ECG and UECG decreased with the increasing electrolytic voltage, U_I, and surface damage, such as plastic deformation and cracks, (which often occur in CG) were not observed in UECG; (3) The wheel radius wear in UECG was considerably smaller than that in ECG when U_I < 10 V. The wheel wear in CG was predominantly attributed to the grain drop out, whereas in ECG and UECG the working lives of the wheels were predominantly affected by the chip adhesion and the grain fracture; (4) A 78 nm thick titanium dioxide (TiO_2) layer was generated on the work-surface at U_I = 20 V, and thus the Vickers micro-hardness of work-surface in UECG was lower than that in CG/UAG by 15 %; (5) The weight percentages of oxygen elements on chips and work surfaces increased as the U_I increased in ECG and the ultrasonic treatment further enhanced the percentages of oxygen.

Then, the ultrasonic assisted plasma oxidation grinding (UPOG) was investigated. Before material removing, plasma oxidation are important issues in ultrasonic assisted

plasma oxidation grinding. In order to investigate grinding parameters to achieve high product quality and productivity, the relation between ultrasonic vibration and plasma oxidation is studied. Effects of grinding parameters (workpiece rotational speed, wheel feed rate, wheel rotational speed, ultrasonic vibration amplitude, and the oscillation frequency), on plasma oxidation are measured. The experiment results show once the plasma voltage was applied, the hardness became decreased. However, when the plasma voltage U_I was beyond 100 V, the plasma discharge intensity became higher locally, which resulted in the formation of melt-quenched, high-temperature oxides on the work surface.

To deeply investigate the material removal mechanism in UPOG of Ti-6Al-4V, the UPOG tests were performed on Ti-6Al-4V. The obtained results evidence that: The grinding forces decreased as the plasma voltage U_I and rotational speed n_g increased. The actual removal depth increased with the increase in input voltage. However, the benefit of the ultrasonication to the grinding efficiency would get smaller when the rotational speed has been set at a larger value. The roughness Ra both in POG and in UPOG decreased with the increasing of U_I and n_g; the roughness Ra in UPOG was smaller than that in POG regardless of the process parameters. The UPOG of Inconel 718 was also effective with high voltage.

The last part of this study is to extend the method on drilling with UPOG so as to open a door to potential industrial applications. The results show that material removal rate in UPOG is deeper than that CG, meaning that material removal is easily achieved in UPOG; high accuracy can be achieved by UPOG.

All in all, this study confirms that UPOG is a highly effective processing method for hard-to-machine material. The technology has the potential to being further extend to other materials.

This page intentionally left blank.

CONTENTS

Chapter 1 Introductions

With the fast growth of the aircraft industries, the needs for low cost with higher effectiveness force the machining process of difficult-to-machine material to another level. An example of this requirement can be seen in the evaluation of grinding process of aviation industry, where millions of dollars are used on replacing grinding wheel and the price continues to increase greatly. From the manufacturing point of view, the waste of grinding wheel can be reduced with improve grinding effectiveness. However the traditional manufacturing processes can no longer satisfy the needs for high accuracy and free of damage on grinding wheel. The development of high grinding effectually grinding process has thus become more important than ever before.

1.1 Difficult-to-machine material

Hard-to-machine materials are very often used in the mechanical engineering industry, for example in production of machining tools, work hold or molds. Especially, Ni and Ti alloy are usually applied to jet engine machining industry as shown in Fig.1.1.

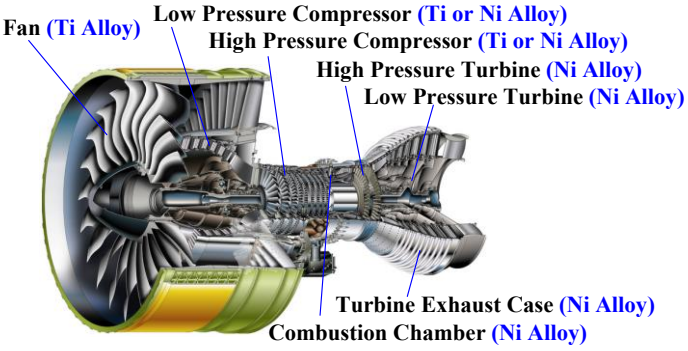

Fig. 1.1 Cross section of a jet engine[1] .

Ti-6Al-4V and Inconel 718 are two famous hard-to-machine. Due to Ti-6Al-4V and Inconel 718 have high strength, melting temperature and corrosion, a wide range of industries shown a great interesting in the application of them [2]. Due to the advantages of nickel-based alloys over Ti alloys, a number of material for aerospace industries have made by nickel-based alloys. Nickel based alloys have very broad operational temperatures. However, they are classified as extremely difficult to machine material, owing to several inherent properties of materials, e.g., low thermal conductivity, high specific strength and exceptional resistance to corrosion [3]. Currently, most of Ti-6Al-4V and Inconel 718 production is precision cast, subsequent grinding is carried out in order to remove excess material [4]. Because good surface finish and high from/dimension accuracy can be reached by use grinding. In conventional machining process also need grinding process to semi-precision. However, ether Ti-6Al-4V or Inconel 718 are very difficult to grinding because of its inherent properties such as the ability to retain high strength at elevated temperatures and low thermal conductivity [5]. These issues in turn result in faster grinding tool wear [6].Due to high strength at elevated temperatures and low thermal conductivity, the grinding process of Ti-6Al-4V and Inconel 718 need to face a serious heat problem and high fiction between grain and work surface. This is the reason why several studies focus on improve the grindability of Ti-6Al-4V and Inconel 718 [7-10].

1.2 Hybrid Assisted Machining

Hybrid assisted machining is a combination of two or more processes to remove material. Recently researches are aimed to enhance grinding efficiency and improve work-surface quality in a hybrid assisted technique [11]. In manufacturing environment, many technological developments can be defined as hybrid machining. Schuh G[12] writes this kind technology is the “1+1=3” effect, meaning the benefit is more than double of the advantages of the single process.

1.2.1 Cutting process

The cutting process such as drilling, turning, milling has lots of hybrid assisted

process. The ultrasonic vibration cutting is an important hybrid assisted process. In turning, the vibration assisted turning will lead to chip breakage and resulting in discontinuous chips [13]. Besides, the number of built-up edges on grains and burrs on the workpiece side were decreased by the vibration assisted cutting. According to the study of Pujana et al. [14], vibration assisted drilling of Ti6Al4V is also effectually. They found feed force was decreased 20 % with high amplitudes compared to conventional drilling. In the study of Baghlani et al. [15], the lower grinding forces, better surface and better chip breakage also can be found in the vibration assisted drilling of Inconel 728LC. However, most of ultrasonic vibration cutting is forced on the single ultrasonic vibration assistance and ignored its potential of multi-filed assistance. This is the reason why most of ultrasonic assisted cutting are carried out with low cutting speed to enlarge the affection of ultrasonic.

The application of laser assisted machining (LAM) is also used in the turning of difficult-to-machining materials. The laser beam make machining becomes easier by soften material. In recent decade, research also used laser assisted milling [16] and shearing of sheet material [17]. According to the investigation of Attia et al. [18], an improvement of the surface integrity is showed in the LAM of Inconel 718 by the observation of machined surface is carried out by SEM analyses and microstructure. Brecher et al. [19] reports 40–60 % of force is reduced and tool life is improved during LAM of Inconel alloys. By use LAM, Lei et al. made precise ceramic parts [20]. The surface heating of laser assisted process prepared uniformly material for machining. After the observation of LAM samples no sub-surface cracks can be found. On the other hand, the pre-heating process of laser also leads to thermal stress layer on the work surface. In order to remove this thermal stress layer, the work need to semi precision.

Another important hybrid machining process is combine by use the supply of high pressure lubrication coolants, which is also can be called „„Media-assisted Processes“. Flow rate and pressure have a significant influence on chip formation (chip shape, chip breakage), tool life and tool wear behavior and on the metallurgical structure of workpiece and chip due to considerable temperature and lubrication changes (reduction of contact length between chip and rake face [21]). Therefore, it is also called „„high-pressure lubricoolant supply“ [22]. Lopez de Lacalle found that super alloys can be machined with improved surface integrity and/or with higher cutting

speeds during the turning and milling of Ti6Al4V and Inconel 718 by media-assisted [23]. Ezugwu et al. also found the wear of cutting reduced up to 350 % was identified by during finish machining of Inconel 718 [24] as well as other more classical steels [25]. Sharman et al. found residual stresses decreased in the sub-surface layer during ultra-high pressure turning of Inconel 718 [26]. However, due to media-assisted processes waste a huge number of coolants, media-assisted processes still costly.

1.2.2 Grinding process

Electrochemical grinding, combines electrolytic activity with the physical removal of material by means of charged grinding wheels. In ECG, the metallic bond material over the abrasive coated tool generates the electrochemical reaction and electrochemical reaction only appeared in the space between abrasive particles. The abrasive cutting action removes the oxide material from work surface through mechanical abrasion [27]. Fig. 1.2 shows the schematic view of material removal mechanism for ECG process [28]. In order to achieve the better surface quality and higher material removal rates, experimental observations have revealed that there should be low gap and maximum contact area between abrasive tool and work surface. This offers thin gas film with maximum cutting edges. In order to make the appropriate contact between the abrasive particles and work surface, tool feed rate is mentioned as a critical parameter. Thus it can produce burr free and stress free parts without heat or other metallurgical damage caused by mechanical grinding, eliminating the need for secondary machining operations [29]. By the use of these advantages, the electrolytic grinding has been also employed for the grinding of Ti-6Al-4V [30]. However, in precision elecyrolytic grinding with a fine grinding wheel, the clearance between the wheel metal bond and the workpiece is very small, leading to the frequent occurrence of sparks within the clearance and consequently damaging the work-surface. In addition, the formed debris during electrolytic grinding should be promptly removed from the clearance so that the electrolytic action can be continued. Nowadays, a high accuracy can be reached by electrochemical grinding, but the efficiency still no good enough.

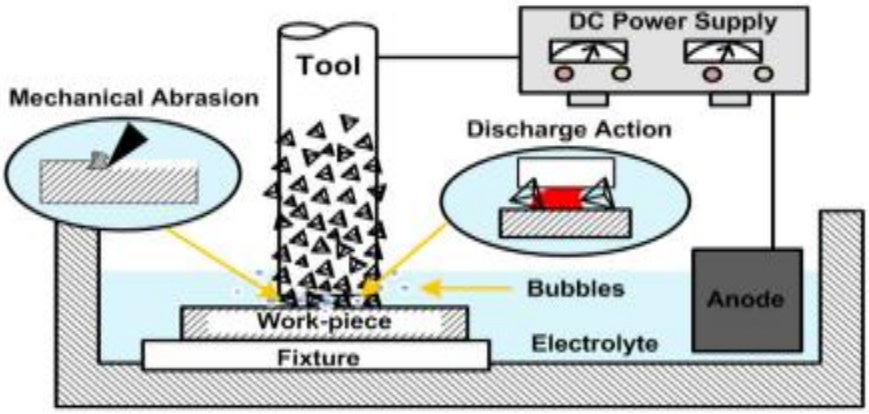

Fig. 1.2 Schematic of electrochemical discharge grinding mechanism.

Ultrasonic assisted grinding (UAG), a hybrid machining process combining grinding and ultrasonic vibration, can enhance grinding efficiency and improve work-surface quality owing to its decreased grinding forces and reduced wheel wear compared with CG [31-33]. Thus, UAG is considered to be a promising technique for ceramics grinding. Different types of UAG techniques, e.g., one-dimensional UAG (1D-UAG), two-dimensional UAG (2D-UAG), and elliptical-UAG (EUAG), have been proposed. In 1D-UAG, the ULTRASONIC VIBRATION is usually applied to the grinding wheel in either the vertical direction or parallel to the work surface. The former is called VUAG (vertical UAG), and the latter is called AUAG (axial UAG) [34]. VUAG is characterized by a much lower grinding force and higher material removal rate (MRR) while maintaining slightly increased wheel wear and surface roughness [35]; the AUAG benefits the grinding process, significantly, by decreasing the thermal load and improving the surface quality [36]. To combine the merits of both VUAG and AUAG, Liang and Wu proposed the EUAG technique [34, 37] and their experimental investigations involving monocrystal sapphire with a resin bond diamond wheel showed that the grinding forces and the work-surface roughness can be decreased by 30 % and 20 %, respectively, compared to CG. To further improve the work-surface quality, Yan and Zhao developed the 2D-UAG technique [38, 39]. In this method, the ULTRASONIC VIBRATION is simultaneously applied to the workpiece from two directions; one is in the same direction as that of the wheel peripheral speed and the other is along the wheel axis. The experimental results involving nano-ZrO_2 ceramics indicated that the quality of the work surface attained

is even better than that obtained from AUAG [38]. However, in either EUAG or 2D-UAG, the ULTRASONIC VIBRATION must be simultaneously generated in two directions, resulting in complicated machining equipment structures. This further increases the equipment expense and multiplies the difficulty in equipment maintenance. Consequently, in practical UAG, the predominant approach is types of 1D-UAG, i.e., AUAG or VUAG rather than 2D-UAG and EUAG.

Utilizing the advantages of the 1D-UAG methods, research attempts have been devoted to the application of both AUAG and VUAG to hard and brittle materials. The results showed that the work surface quality can be greatly improved with a slight decrease in grinding force in the AUAG of the Al_2O_3 ceramic workpiece [40] compared to CG; the grinding force can also be significantly reduced. Particularly, Mult et al. found that utilizing VUAG resulted in a slight increase in wheel wear due to the grinding wheel striking the machined workpiece [35]. To elucidate the material removal mechanism in the 1D-UAG methods, some studies focused on the change pattern and grinding force reduction in AUAG [41-43] by using a combination of numerical simulation and experimentation. Lee and Chan found that the increased vibration amplitude resulted in an increased MRR in AUAG due to the increased energy imparted to the material [43]. Zhang et al. thought the average cutting velocity in AUAG was higher than that in CG, which is a main factor contributing to the reduction of force [40]. Additionally, Farhadi et al. believed that the elimination of the sliding and plowing region along the cutting path during VUAG was the reason for force reduction, as determined by the numerical simulation investigation [42].

On the other hand, 1D-UAG methods has been introduced into internal grinding. Kumabe [44, 45] performed ultrasonic assisted internal grinding (UAIG) of metal materials such as aluminum, copper and steel. The obtained results showed that the grinding efficiency was improved and grinding forces were reduced for the sake of the presence of ultrasonic vibration. Wu et al. [46] found that the normal and tangential forces in UAIG of stainless steel were smaller by 65 % and 70 %, respectively, and the surface roughness was smaller by 20 % than those in CIG. In M. Fujimoto et al.'s work [47], the machining characteristics of the UAIG of tungsten were experimentally compared with those of the CIG, showing that the normal and tangential grinding forces and the surface roughness in UAIG were smaller by 11 %, 41 %, and 53 %, respectively, than those in CIG. This study confirms that UAIG is a highly effective

processing method. Obviously, ultrasound-assisted grinding technology, especially for axial ultrasonic-assisted grinding, has the potential to simultaneously improve material removal and surface quality, reducing abrasive and even abrasive wear.

1.2.3 Multi-filed machining

The hybrid machining process imposed by the short product development cycles and the growing cost pressures. However, tool wear and chip adhesion has under mined the full potential of the hybrid machining process and drastically reduced the efficiency and accuracy. Therefore, this study adds two assistance processes in one conventional machining process and defined it as multi-filed machining. The aim is to discuss the possible trends for future multi-filed machining research.

1.3 Plasma electrolytic oxidation

In order to further improve the accuracy and efficiency of grinding, the work material need do a soften treatment. Plasma electrolytic oxidation (PEO) is an anodizing process with high-voltage. It produces a stable oxidation layer on the surface of a number of light weight metals (aluminum, titanium, magnesium, zirconium, etc.) or metallic alloys. It is widely used to soften work surfaces by oxidizing the work materials [48]. This process involves anodizing above the dielectric breakdown voltage and leads to the formation of plasma micro-discharges [49].

In particular, Dang Van Thanh et al. found in their work on the preparation of graphene sheets using electrochemical discharge (plasma electrolytic oxidation) [50] that the ultrasonic vibration of cathode strengthen the plasma electrolysis phenomenon. This is achieved by the breaking of van der Waals bonds, which increases the synthesis efficiency of plasma oxidation. This implies that the PEO phenomenon would be promoted by the ultrasonic vibration. However, no studies have been reported so far on grinding processed with the assistance of both ultrasonic vibration and PEO. Consequently, a hybrid process is proposed in this study to further improve the grindability of the titanium alloy Ti-6Al-4V.

In order to develop a high accuracy and efficiency grinding method, PEO process is

added to the UAG process in this study, hereafter referred to as ultrasonic-assisted plasma oxidation grinding (UPOG). After the processing principle of UPOG and the experimental details have been introduced, the experimental results are described. Then, the discussion of the results is presented, and the feasibility of using UPOG for the improvement in grindability of Ti-6Al-4V is confirmed.

1.4 Objective of the study

As described above, the ultrasonic, electrochemical and plasma is added into grinding process and named this two new multi-field assisted grinding technology as ultrasonic assisted electrochemical grinding (UECG) and ultrasonic assisted plasma oxidation grinding (UPOG), respectively. In order to compare multi-filed grinding with hybrid assisted grinding, ultrasonic assisted grinding (UAG) is also be studied. This research attempts to improve grinding ability of different to machine materials. Due to its wide applications, Ti-6Al-4V and Inconel 718 are used as the specimen in this study. Specifically, this project aims to achieve the following objectives:

- To develop multi-field assisted grinding system incorporating an ultrasonic, electrochemical and plasma components to perform the hybrid grinding process.
- To understand the effects of process parameters on the grinding forces and material removal rate, including the interactions of above three kinds of multi-field assisted grinding technology.
- To investigate the effect of process parameters on the wheel wear with multi-field assisted grinding technology.

1.5 Thesis organization

This thesis is divided into 6 chapters. The outline of thesis organization is shown in Fig. 1.3.

In chapter 1, hard-to-machine materials were briefly introduced. Prevailing technologies, i.e., ultrasonic assisted grinding, electrochemical grinding and plasma electrolytic oxidation is outlined.

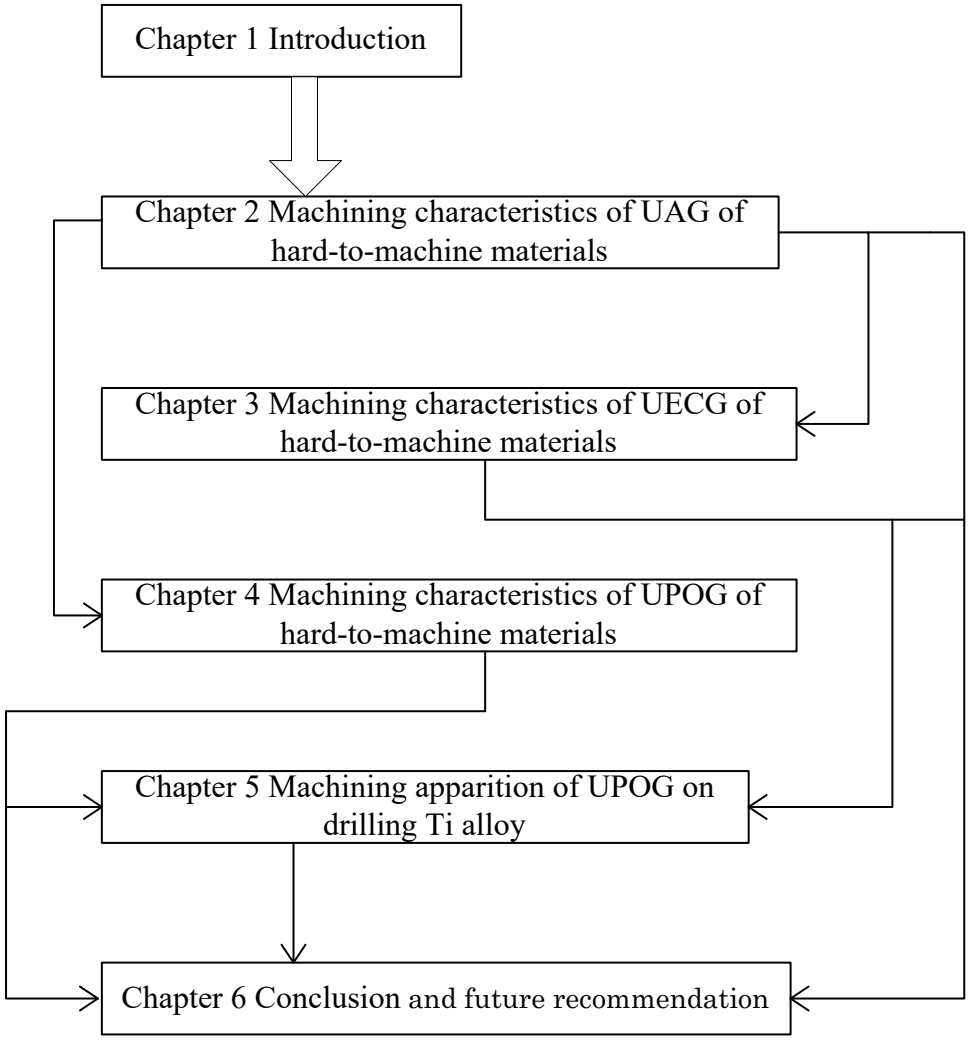

Fig. 1.3 Outline of thesis organization

In chapter 2, the investigations on the machining characteristics of UAG of Inconel 718 workpiece are performed on the constructed rig. CG tests involving the same workpiece are also carried out on the same experimental rig for comparison. The effects of the ultrasonic vibration on the grinding forces, the surface roughness, the form accuracy, and grinding wheel wear are revealed. Meanwhile, the topographic features of work-surfaces and the subsurface damages are observed as well to clarify the material removal behavior.

In chapter 3, aiming at the development of a novel grinding technology for the high efficient machining of difficult to machine materials such as titanium alloy Ti-6Al-4V, an ultrasonic assisted electrolytic grinding (UECG) method was proposed. Firstly, an experimental apparatus was constructed by installing an electrolytic mechanism on an

existing 3D CNC machine tool attached with an ultrasonic spindle. Then, after the performance test has been carried out for the constructed apparatus, UECG experiments of Ti-6Al-4V specimen were conducted on the apparatus to investigate the effects of the ultrasonic vibration of grinding wheel and the electrolytic phenomenon on the grinding force and the work surface quality. The experimental results indicate that the ultrasonic assisted electrolytic grinding is greatly beneficial to the decrease in grinding force and the improvement in the work surface quality compared to conventional grinding.

In chapter 4, a novel grinding technique is proposed with the goal of improving the grindability of Ti–6Al–4V and Inconel 718. This technique is a combination of ultrasonic-assisted grinding and plasma-electrolytic oxidation. To determine its performance in the grinding of Ti-6Al-4V, experiments were conducted to investigate the effect of ultrasonic vibration on grinding forces and work-surface roughness under the presence of plasma oxidation. The results showed that the technique drastically reduced the normal and tangential grinding forces by 60 % and 70 %, respectively, and decreased the work-surface roughness by 46 % compared to conventional grinding, which uses neither ultrasonic assisted grinding nor plasma-electrolytic oxidation.

In chapter 5, a novel grinding technique is proposed for drilling these materials. The proposed technique is a combination of ultrasonic assisted grinding and plasma electrolytic oxidation; hence named as ultrasonic assisted plasma oxidation grinding (UPOG). A thin oxidized layer is formed on the largest surface of the workpiece in the grinding zone by plasma. The oxidized layer would be much softer than the original material. To reveal its fundamental performance in the drilling of Ti-6Al-4V, experiments were conducted to investigate the effect of ultrasonic vibration on grinding forces and tool wear under the presence of plasma oxidation. The results showed that the technique drastically stabilize the grinding force and avoid the tool wear/damage.

In chapter 6, conclusions, and contributions of this research is presented. It also provided recommendations for further work in this direction.

Reference

[1] Ulutan D, Ozel T. Machining induced surface integrity in titanium and nickel alloys: A review. International Journal of Machine Tools and Manufacture. 2011;51:250-80.

[2] Hong SY, Markus I, Jeong W-c. New cooling approach and tool life improvement in cryogenic machining of titanium alloy Ti-6Al-4V. International Journal of Machine Tools & Manufacture. 2001;41:16.

[3] Ezugwu EO, Wang ZM. Titanium alloys and their machinability - a review. Journal of Materials Processing Technology. 1997;68:12.

[4] Thakur A, Gangopadhyay S. State-of-the-art in surface integrity in machining of nickel-based super alloys. International Journal of Machine Tools and Manufacture. 2016;100:25-54.

[5] Ezugwu EO. Key improvements in the machining of difficult-to-cut aerospace superalloys. International Journal of Machine Tools and Manufacture. 2005;45:1353-67.

[6] Setti D, Sinha MK, Ghosh S, Venkateswara Rao P. Performance evaluation of Ti–6Al–4V grinding using chip formation and coefficient of friction under the influence of nanofluids. International Journal of Machine Tools and Manufacture. 2015;88:237-48.

[7] Sun S, Brandt M, Dargusch MS. Machining Ti–6Al–4V alloy with cryogenic compressed air cooling. International Journal of Machine Tools and Manufacture. 2010;50:933-42.

[8] Bermingham MJ, Palanisamy S, Kent D, Dargusch MS. A comparison of cryogenic and high pressure emulsion cooling technologies on tool life and chip morphology in Ti–6Al–4V cutting. Journal of Materials Processing Technology. 2012;212:752-65.

[9] Palanisamy S, McDonald SD, Dargusch MS. Effects of coolant pressure on chip formation while turning Ti6Al4V alloy. International Journal of Machine Tools and Manufacture. 2009;49:739-43.

[10] Dandekar CR, Shin YC, Barnes J. Machinability improvement of titanium alloy (Ti–6Al–4V) via LAM and hybrid machining. International Journal of Machine Tools and Manufacture. 2010;50:174-82.

[11] Bert Lauwers, Fritz Klocke, Andreas Klink, A. Erman Tekkaya, Reimund Neugebauer, Don Mcintosh, Hybrid processes in manufacturing, CIRP Annals, 2014;63:561-583

[12] Schuh G, Kreysa J, Orilski S, Roadmap „„Hybride Produktion"". Zeitschrift fu¨r Wirtschftlichen Fabrikbetrieb, 2009, 104(5):385–391.

[13] Bulla B, Klocke F, Dambon O, Hu¨ nten M, Ultrasonic Assisted Diamond Turning of Hardened Steel for Mould Manufacturing. Key Engineering Materials, 2012, 516:437–442.

[14] Pujana J, Rivero A, Celeya A, Lo´pezde Lacalle LN, Analysis of Ultrasonic-Assisted Drilling of Ti6Al4V. International Journal of Machine Tools &Manufacturing, 2009, 49:500–508.

[14] Baghlani V, Mehbudi P, Akbari J, Sohrabi M, Ultrasonic Assisted Deep Drilling of Inconel 738LC Superalloy. 17th CIRP Conference on Electro Physical and Chemical Machining, 2013, 6: 571–576.

[15] Ruszaj A, Skoczypiec S, Czekaj J, Miller T, Dziedzic J, Surface Micro and Nanofinishing Using Pulse Electrochemical Machining Process Assisted by Electrode Ultrasonic Vibrations. 15th International Symposium on Electromachining (ISEM XV), 2007, 309–314.

[16] Romero P, et al, Laser Assisted Conical Spin Forming of Dual Phase Automotive Steel. Physics Procedia, 2003, 5:215–225.

[17] Emonts M, Laserunterstu¨tztes Scherschneiden von hochfesten Blechwerkstoffen, (Dissertation) RWTH Aachen, Apprimus-Verlag, 2010, ISBN 3940565601.

[18] Attia H, Tavakoli S, Vargas R, Thomson V, Laser-Assisted High-Speed Finish Turning of Superalloy Inconel 718 Under Dry Conditions. CIRP Annals – Manufacturing Technology, 2010, 59(1):83–88.

[19] Brecher C, Emonts M, Rosen CJ, Hermani JP, Laserunterstu¨ tzte Fra¨sbearbeitung. WT Werkstattstechnik Online, 2012, 102(6):353–356.

[20] Lei S, Shin Y, Experimental Investigation of Thermo-Mechanical Characteristics in Laser-Assisted Machining of Silicon Nitride Ceramics. Journal of Manufacturing Science and Engineering, 2001, 123:639–646.

[21] Kaminiski J, Alvelid B, Temperature Reduction in the Cutting Zone in Water-Jet Assisted Turning. Journal of Materials Processing Technology, 2000, 106(1):68–73.

[22] Klocke F, Sangermann H, Kra¨mer A, Lung D (2010) Influence of a High-Pressure Lubricoolant Supply on Thermo-Mechanical Tool Load and Tool Wear Behaviour in the Turning of Aerospace Materials. Proceedings of the IMechE 225(B):52–61.

[23] Lo´ pez de Lacalla LN, Pe´ rez-Bilbatua J, Sa´nchez JA, Llorente JI, Gutie´ rrez A, Albo´ niga J, Using High Pressure Coolant in the Drilling and Turning of Low Machinability Alloys. International Journal of Advanced Manufacturing Technology, 2000, 16(2):85–91.

[24] Ezugwu EO, Bonney J, Effect of High-Pressure Coolant Supply When Machining Nickel-Base, Inconel 718, Alloy With Coated Carbide Tools. Journal of Materials Processing Technology, 2004, 153:1045–1050.

[25] Paul S, Dhar NR, Chattopadhyay AB, Benificial Effects of Cryogenic Cooling Over Dry and Wet Machining on Tool Wear and Surface Finish in Turning AISI 1060 Steel. Journal of Materials Processing Technology, 2001, 116:44–48.

[26] Sharman ARC, Hughes JI, Ridgway K, Surface Integrity and Tool Life When Turning Inconel Using Ultra-High Pressure and Flood Coolant Systems. Proceedings of the Imech E, 2008, 222:653–663.

[27] K.C. Sanjay, P.V. Rao, The drilling of Al2O3 using a pulsed DC supply with a rotary abrasive electrode by the electrochemical discharge process, Int. J. Adv. Manuf. Technol. 39;2008:633–641.

[28] V.K. Jain, S.K. Choudhury, K.M. Ramesh, On the machining of alumina and glass, Int. J. Mach. Tools Manuf. 42;2002:1269–1276.

[29] Maksoud TMA, Brooks AJ. Electrochemical grinding of ceramic form tooling. Journal of Materials Processing Technology. 1995;55:70-5.

[30] Itoh N, Ohmori H. Grinding characteristic of hard and bittle materials by fine grain lapping wheels with ElID. Journal of Materials Processing Technology. 1996;62:315-20.

[31] Peng Y, Liang Z, Wu Y, Guo Y, Wang C. Characteristics of chip generation by vertical elliptic ultrasonic vibration-assisted grinding of brittle materials. Int J Adv Manuf Technol. 2012;62:563-8.

[32] Peng Y, Wu YB, Liang ZQ, Guo YB, Lin X. An experimental study of ultrasonic vibration-assisted grinding of polysilicon using two-dimensional vertical workpiece vibration. Int J Adv Manuf Technol. 2011;54:941-7.

[33] Qu W, Wang K, Miler MH, Huang Y, Chandra A. Using vibration-assisted grinding to reduce subsurface damage. Precis Eng. 2000;24:329-37.

[34] Liang Z, Wu Y, Wang X, Zhao W. A new two-dimensional ultrasonic assisted grinding (2D-UAG) method and its fundamental performance in monocrystal silicon machining. Int J Mach Tools Manuf. 2010;50:728-36.

[35] Mult H, Spur G, Holl S. Ultrasonic assisted grinding of ceramics. J Mater Process Technol. 1996;62:6.

[36] Denkena B, Friemuth T, Reichstein M, Tönshoff H. Potentials of different process kinematics in micro grinding. CIRP Annals-Manufacturing Technology. 2003;52:463-6.

[37] Liang Z, Wang X, Wu Y, Xie L, Liu Z, Zhao W. An investigation on wear mechanism of resin-bonded diamond wheel in Elliptical Ultrasonic Assisted Grinding (EUAG) of monocrystal sapphire. J Mater Process Technol. 2012;212:868-76.

[38] Yanyan Y, Bo Z, Junli L. Ultraprecision surface finishing of nano-ZrO2 ceramics using two-dimensional ultrasonic assisted grinding. Int J Adv Manuf Technol. 2009;43:462-7.

[39] Gao GF, Zhao B, Xiang DH, Kong QH. Research on the surface characteristics in ultrasonic grinding nano-zirconia ceramics. J Mater Process Technol. 2009;209:32-7.

[40] Zheng Jx, XU Jw. Experimental Research on the Ground Surface Quality of Creep Feed Ultrasonic Grinding Ceramics (Al_2O_3). Chin J Aeronaut. 2006;19:359-65.

[41] Klecka M, Subhash G. Grain size dependence of scratch-induced damage in alumina ceramics. Wear. 2008;265:612-9.

[42] Farhadi A, Abdullah A, Zarkoob J, Pak A. Analytical and Numerical Simulation of Ultrasonic Assisted Grinding. ASME 2010 10th Biennial Conference on Engineering Systems Design and Analysis. 2010;4:763-8.

[43] Lee T, Chan C. Mechanism of the ultrasonic machining of ceramic composites. J Mater Process Technol. 1997;71:195-201.

[44] Kumabe J. Study on Ultrasonic Internal Grinding by Using the Longitudinally Vibrated Grinding Wheel : 1st Report, Traverse Ultrasonic Cutting. Transactions of the Japan Society of Mechanical Engineers. 1961;27:1404-11.

[45] Kumabe J, Ito Y. Study on Ultrasonic Internal Grinding by Using the Longitudinally Vibrated Grinding Wheel : 2nd Report, The Outline of the Effects. Transactions of the Japan Society of Mechanical Engineers. 1961;27:1412-8.

[46] Wu Y, Nomura M, Kato M, Tachibana T. Fundamental Investigation of Internal Ultrasonic Vibration Assisted Grinding of Small Holes. Proceedings of International Conference on Leading Edge Manufacturing in 21st century : LEM21. 2003;2003:145-50.

[47] Fujimoto M, Wu Y, Cao J. High Precision Ultrasonically Assisted Internal Grinding (UAIG) of Difficult-to-machining Materials using Metal Bonded Diamond Wheels. The 6th International Conference on Leading Edge Manufacturing in 21st Century2011.

[48] A.L. Yerokhin, X. Nie, A. Leyland, A. Matthews, Characterisation of oxide films produced by plasma electrolytic oxidation of a Ti-6Al-4V alloy, Surface and Coatings Technology, 2000, 130:195-206.

[49] Stevan Stojadinović, Rastko Vasilić, Jelena Radić-Perić, Miljenko PerićCharacterization of plasma electrolytic oxidation of magnesium alloy AZ31 in alkaline solution containing fluoride, Surface & Coatings Technology, 2015, 273: 1-11.

[50] Dang Van Thanh, Phung Phi Oanh, Do Tra Huong, Phuoc Huu Le, Ultrasonic-assisted cathodic electrochemical discharge for graphene synthesis, Ultrasonics Sonochemistry, 2017, 34:978-983.

This page intentionally left blank.

Chapter 2 Machining characteristics of the UAG of difficult-to-machine materials

This chapter mainly focuses on the UAG apparatus. First, the principle of UAG is described. Then, in order to realize the processing principle of UAG in practice, an experimental rig is constructed. Before UAG tests, the ultrasonic vibration amplitude of the grinding wheel should be measured. Thereby, the measurement method of ultrasonic vibration amplitude and results are presented. At last, the detailed experiment conditions are also listed out along with machining characteristics evaluation method.

2.1 Machining Principal of UAG

Fig. 2.1 shows the processing principle of UAG schematically. A grinding wheel is ultrasonically vibrating along its own axis (y-direction) at a frequency of f and peak-to-peak amplitude of $A_{p\text{-}p}$, and rotating clockwise around its own axis at a rotational speed of n_g. When a depth of cut is given between the ultrasonically vibrating grinding wheel and the workpiece that is fed rightward in x-direction at a feed rate of v_w, an ultrasonic assisted surface grinding operation is performed. Once the spindle has been released from the ultrasonic vibration, a conventional surface grinding is carried out.

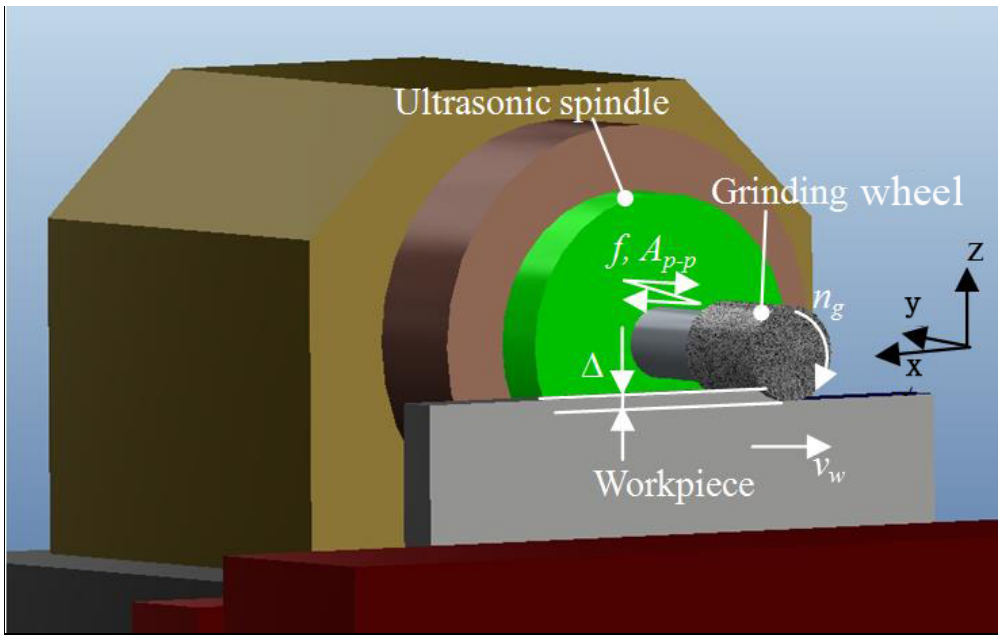

Fig. 2.1 Schematic illustration of the principle for UAG

In order to actually realize the above-described processing principle, an experimental apparatus was established by installing a commercially available ultrasonic spindle (URT40 by Takesho Co., Ltd.) onto a commercially available NC grinder (GRIND-X IGM15EX by Okamoto Machine Tool Works Co., Ltd.) through a 3-components piezoelectric dynamometer (9256A by Kistler Co., Ltd.) as shown in Fig.2. The dynamometer was located below the ultrasonic spindle and used for the measurement of grinding forces. In this work, an electroplated cBN grinding wheel of ϕ8mm×L8mm in dimensions with the mesh number of #140 was employed as the abrasive tool which is attached on the left end of the ultrasonic spindle, and a plate-shaped Inconel 718 specimen with dimensions of L48 mm×W 36 mm×T3 mm was used as the workpiece. In experiments, the Inconel 718 specimen was fixed on a work-holder under which a Z-stage is located for determining the depth of cut Δ. As the purpose of this work is to investigate the effect of the ultrasonic vibration of grinding wheel on the wheel working surface condition, grinding parameters, i.e., the depth of cut, the work feed rate and the wheel rotational speed, in experiments were kept constant at Δ=80 μm, v_w=15 mm/min and n_g=4000 rpm, respectively, while the vibration amplitude was varied in a range of A_{p-p}=0 to 9.4 μm as exhibited in Table 1. In addition, dry grinding operations were performed without coolant supplying.

2.2 Experimental apparatus, procedure and conditions

The ultrasonic spindle for UAG (URT40 by Takesho Co., Ltd.) was showed in Fig. 2.2. The frequency of the rotary spindle is 40 kHz and vibration in the axis direction. The rotational speed of the spindle is change from 0 to 8000 rpm. Ultrasonic spindle controller is used to control the rotational speed and vibration power as shown in Fig. 2.3. This spindle incorporated a rotary spindle with resonance frequency of 40 kHz. The maximum rotational speed of the spindle is 8000 rpm.

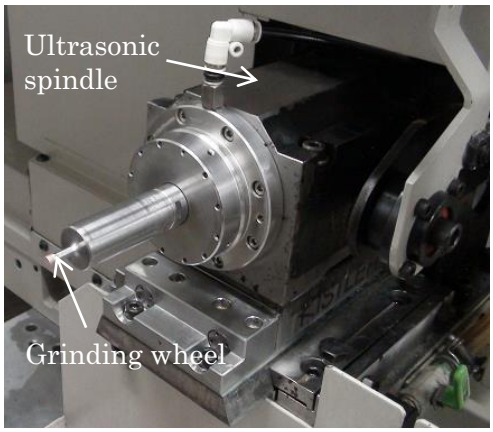

Fig. 2.2 Ultrasonic spindle

Fig. 2.3 Ultrasonic spindle controller

2.2.1. Apparatus (Ultrasonic spindle, Workpiece and Experiment setup)

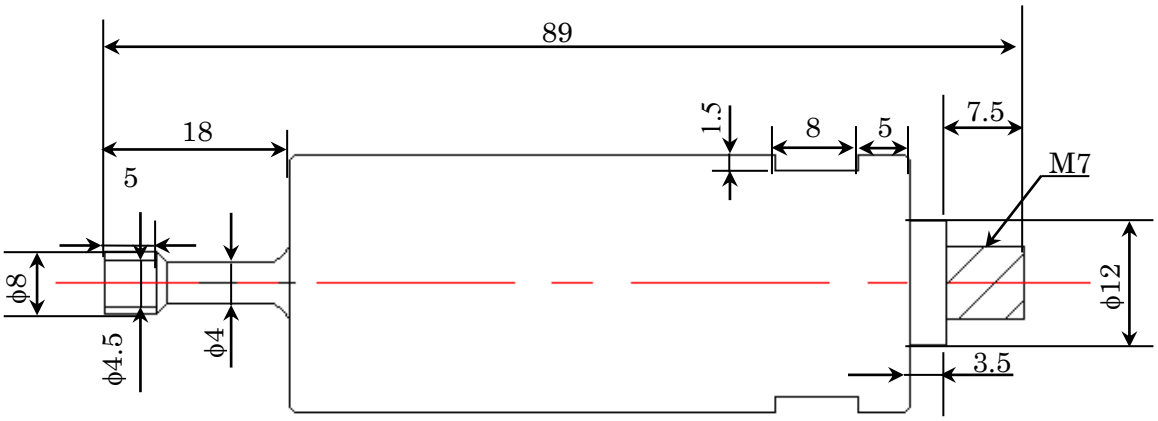

(a) Structure of grinding wheel

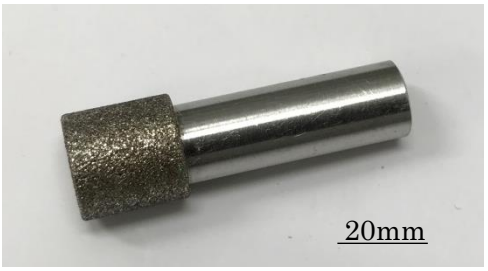

(b) Grinding wheel

Fig. 2.4 Grinding wheel for UAG

Fig. 2.4 shows the grinding wheel used for UAG tests. The diameter of the grinding wheel is ϕ 8 mm, length is 5 mm. Grinding wheel is metal bond cBN wheel with mesh size #140 and concentration 100.

Due the research of UAG of Inconel 718 have been widely proved to be effective. Therefore, the Ti-6Al-4V was selected to be study in this research. Fig. 2.5 show workpieces used for UAG tests. Plate-shaped Inconel 718 and Ti-6Al-4V specimen with dimensions of L48 mm×W36 mm×T3 mm were used as the workpieces and the material properties are shown in table 1.1.

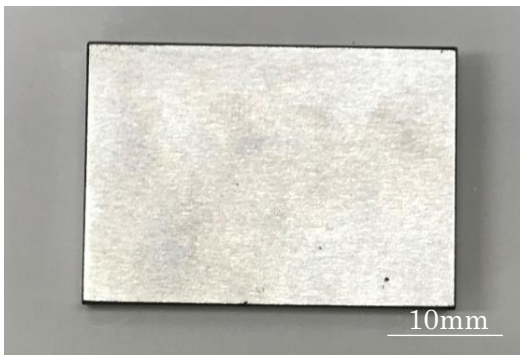

Fig. 2.5 Workpieces used for UAG tests

In order to actually realize the above-described processing principle, an experimental apparatus was established by installing a commercially available ultrasonic spindle (URT40 by Takesho Co., Ltd.) onto a commercially available NC grinder (GRIND-X IGM15EX by Okamoto Machine Tool Works Co., Ltd.) through a 3-components piezoelectric dynamometer (9256A by Kistler Co., Ltd.) as shown in Fig.2.6. The dynamometer was located below the ultrasonic spindle and used for the measurement of grinding forces.

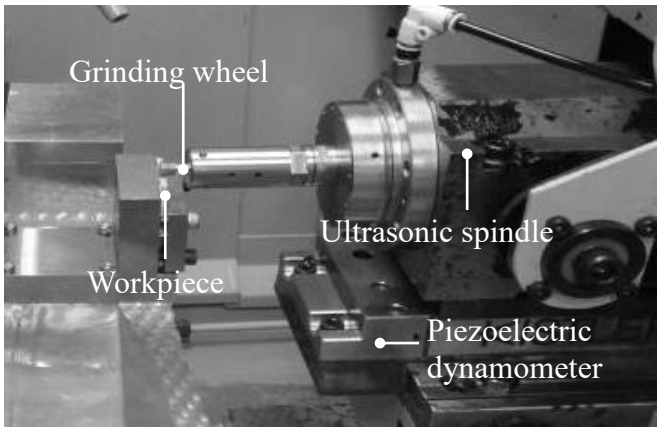

Fig. 2.6 Schematic illustration of the ultrasonic assisted truing and dressing

2.2.2 Procedure (Measurement of UV amplitude)

Before UAG tests, it is necessary to confirm the performance of the ultrasonic spindle. Fig. 2.7 shows the UV amplitude measurement method. Laser Doppler vibrometers (LV-1610 by Ono Sokki Co., Ltd.) was used for measuring the UV amplitude of the grinding wheel. Grinding wheel was screw into the end surface of the UV spindle. Laser light strikes on the center of the end surface of the grinding wheel. Thus, the UV amplitude in the grinding wheel axial direction can be measured.

Fig. 2.7 UV amplitude measurement method.

2.2.3 Experiment conditions

The abrasive grains on the working surface of the wheel employed were observed by a 3D SEM (ERA-8900 by ELIONIX.Co., Ltd), showing that most of the grains were cone-shaped and their vertical angles and average diameter were around 120° and 105 μm, respectively. In experiments, the Inconel 718 specimen was fixed on a work-holder under which a Z-stage is located for determining the depth of cut Δ. Typically, cBN abrasives require a speed of over 50 m/min for grinding Inconel 718 [1]. In this work, the grinding wheel diameter was 8 mm, indicating that the wheel rotational speed n_g should be over 2000 rpm; therefore the value of n_g was set at 5500rpm. Meanwhile, for precision grinding, usually the workpiece feed rate should be a relatively low value, consequently the v_w was set at 15 mm/min in this work. In this case, the depth of cut should be a relatively large value in order to ensure the material removal rate; hence the value of Δ was set to 80 μm. As the purpose of this work is to investigate the effect of the ultrasonic vibration of grinding wheel on the wheel working surface condition, grinding parameters, i.e., the depth of cut, the work feed rate and the grinding speed, in experiments were kept constant at Δ=80 μm, V_w=15 mm/min and V_c=100.5-138.2 mm/min, respectively, while the vibration amplitude $A_{p\text{-}p}$ was measured by the Laser Doppler vibrometers (LV-1610 by On Sokki Co., Ltd.), and it was varied in a range of $A_{p\text{-}p}$=0 to 9.4 μm as exhibited in Table 2.1. In addition, dry grinding operations were performed without coolant supplying.

Table 2.1 Experimental conditions.

Workpiece	Inconel 718, L48 mm×W36 mm×T3 mm
Grinding wheel	Electroplated cBN#140, ϕ8×L8 mm
Ultrasonic Vibration	Frequency f=40kHz Amplitude $A_{P\text{-}P}$=9.4μm, 7.7μm, 5.8μm, 4.1μm, 2.2μm, 0μm
Process parameters	Workpiece feed rate V_w=0.2 mm/min Grinding speed V_c=100.5 mm/min, 113.0 mm/min, 125.6 mm/min, 138.2 mm/min Depth of cut Δ=10, 20, 30, 40, 50, 60, 70, 80 μm
Coolant	Without (Dry grinding)

2.3 Results and discussions

2.3.1 Grinding forces

With the assistance of ultrasonication, the shear angle φ is increased. For confirming this issue, it is perfect to directly measure the shear angle; however, this is an extremely difficult task in fact. Therefore, given the grinding force is the function of the shear angle [2], the effect of the ultrasonic vibration on the grinding force is considered as belows in order to indirectly measure the shear angle in the absence and presence of ultrasonication.

As shown in Fig.2.8, the direction of the tangential grinding force f_{gt} acting on the grain cutting edge along the real grain cutting speed V is determined with the engagement angle γ and thus oscillates between $-\gamma_{max}$ and $+\gamma_{max}$ during one cycle of vibration during grinding. Thus, the instantaneous tangential grinding force f_t(t) at time t along the wheel-workpiece contact arc l can be expressed as:

$$f_t(t) = f_{gt}\cos\gamma \tag{1}$$

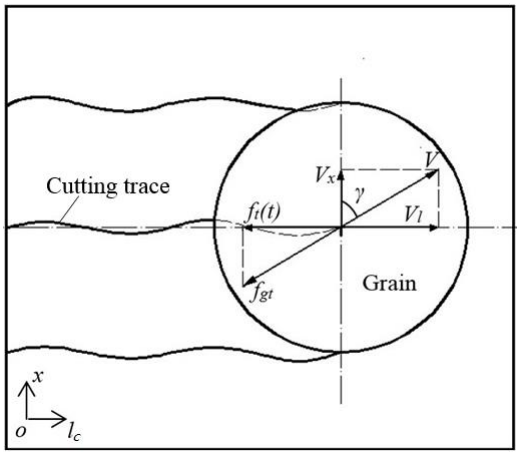

Fig. 2.8 Cutting trace in grinding zone and grinding forces on the grain in UAG.

Following the oscillation of γ, the $f_t(t)$ varies periodically, and its time-averaged value over one cycle with the period of T, f_t, is obtained by:

$$f_t = \frac{1}{T}\int_0^T f_t(t)dt = \frac{1}{T}\int_0^T f_{gt}\cos\gamma dt \tag{2}$$

The total time-averaged tangential grinding force F_t can be calculated by Eq.(3)

$$F_t = \frac{N_g}{T}\int_0^T f_{gt}\frac{V_c + V_w}{\sqrt{4\pi^2 f^2 A_{p-p}\cos^2(2\pi f) + (V_c + V_w)^2}}dt \quad (3)$$

Eq.(3) indicates that the grinding force in UAG (i.e., $A_{p\text{-}p}>0$) would be smaller than that in CG (i.e., $A_{p\text{-}p}=0$), and in particular the force F_t would be decreased as the ultrasonic vibration amplitude $A_{p\text{-}p}$ increases but linearly increases with the increase in the wheel peripheral speed of V_c.

To confirm this issue, grinding forces were measured under various values of $A_{p\text{-}p}$ and V_c. In practice, the F_t approximately equals the component of grinding force in y-direction (see Fig.1) F_y and hence the F_y was experimentally obtained. Also, the component F_z in z-direction was measured for comparison. Figs.2.9 (a) and (b) show the obtained effects of the $A_{p\text{-}p}$ and the V_c on the two components of grinding force. Evidently, either the F_y or the F_z monotonously decreased as the $A_{p\text{-}p}$ increased (Fig.15(a)), and almost linearly decreased with the increasing V_c (Fig.2.9 (b)). It should be noticed, for example, that at V_c=138.2m/min, once the ultrasonic vibration at $A_{p\text{-}p}$=9.4 μm has been applied, the values of F_y and F_z were dropped by 51.9% and 38.6 %, respectively, compared with that without ultrasonication ($A_{p\text{-}p}$=0 μm). These results agreed well with those predicted by Eq.(3). Also the grinding force ratio of F_z/F_y was obtained as exhibited in the same Fig.2.9, showing that the ratio increased with the increasing ultrasonic vibration amplitude $A_{p\text{-}p}$ (Fig.2.9(a)), whereas little effect of the wheel peripheral speed V_c can be observed on the ratio (Fig.2.9(b)) either in CG or in UAG. As revealed by Dong Kun Zhang [3], the larger grinding force ratio indicates that the grinding process mainly involves the friction ploughing and the deformation of chip is small. The obtained results shown in Fig.2.9(a) accordingly demonstrated that the ultrasonic vibration indeed contributed to the occurrence of the friction ploughing and the reduction in chip deformation. This would in turn result in the reduction in grinding energy consumption; in other word, in the case of the same specific grinding energy consumption, a greater material removal rate, i.e., a higher grinding efficiency, would be achieved at a larger vibration amplitude.

Furthermore, the specific grinding energy in UAG was compared with that in CG. As the specific grinding energy is defined as the energy per unit volume of material removed [4], in CG without ultrasonication, the specific grinding energy u can be expressed by following equation:

$$u = F_y V_c / 1000\, b\Delta V_w \quad (4)$$

where F_y [N] is the tangential grinding force, V_c [m/min] is the wheel grinding speed, b [mm] is the grinding width, Δ [mm] is the wheel depth of cut, and V_W [m/min] is the workpiece feed rate. On the other hand, the specific grinding energy in UAG would be:

$$u = (F_y V_c + F_x V_x)/1000\, b \Delta V_w \tag{5}$$

where F_x [N] is the grinding force in x-direction due to the wheel ultrasonic vibration and V_x [m/min] is the wheel ultrasonic vibration speed; both of them are varied periodically at the frequency of f during grinding.

In the current work, the values of V_c, b, Δ and V_w have been already known as exhibited in Table 1 and that of F_y is also the already known one as shown in Fig.15. Then the F_x was actually measured with the same dynamometer used for F_y and F_z, and the value of V_x was calculated by substituting the f and $A_{p\text{-}p}$ given in Table 2.1. Table 2.2 exhibits the results typically obtained at V_c=138.2 m/min for various values of $A_{p\text{-}p}$. It can be seen that in a vibration cycle of wheel, the F_xV_x varied from 0 to the respective peek values for different $A_{p\text{-}p}$ while the F_yV_c decreased as the $A_{p\text{-}p}$ increased.

Table 2.2 V_x, F_x, F_xV_x and F_yV_c typically obtained at V_c=138.2 m/min for various values of $A_{p\text{-}p}$

$A_{p\text{-}p}$ [mm]	0	2.2×10^{-3}	4.1×10^{-3}	5.8×10^{-3}	7.7×10^{-3}	9.4×10^{-3}
V_x [m/min]	0	-16.6~16.6	-31~31	-44~44	-58~58	-71~71
F_x [N]	0	-0.1~0.1	-0.1~0.1	-0.1~0.1	-0.1~0.1	-0.1~0.1
F_xV_x	0	0~1.7	0~3.1	0~4.4	0~5.8	0~7.1
F_yV_c	718.6	552.8	483.7	428.4	387.0	345.5

Subsequently, substituting the data shown in Table 2.2 and the values of b, Δ and V_w shown in Table 2.1 into Eq.(5) yielded the relationship between the u and the $A_{p\text{-}p}$ as shown in Fig.2.10. It can be seen from this figure that although the specific grinding energy u varied between u_L and u_H at the given $A_{p\text{-}p}$ for the sake of the ultrasonic vibration, the u intended to decrease as the $A_{p\text{-}p}$ increases, confirming that the ultrasonication benefits the reduction in the specific grinding energy significantly.

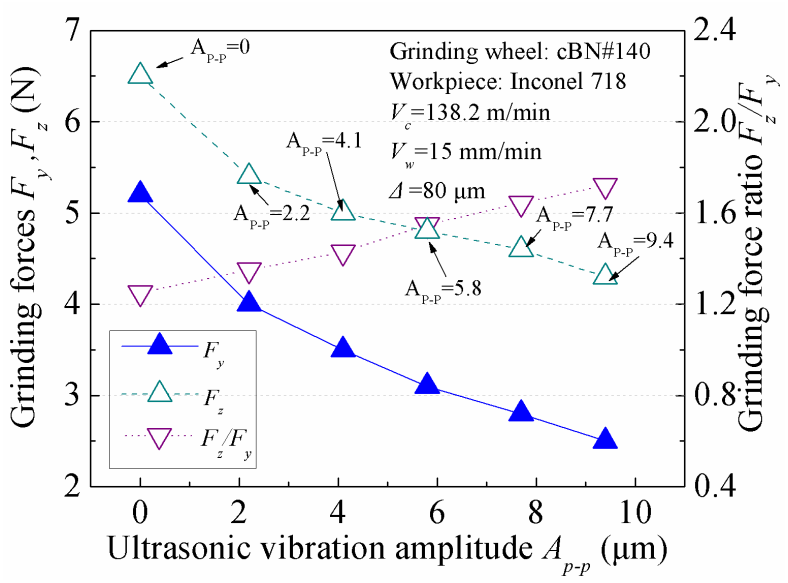

(a)

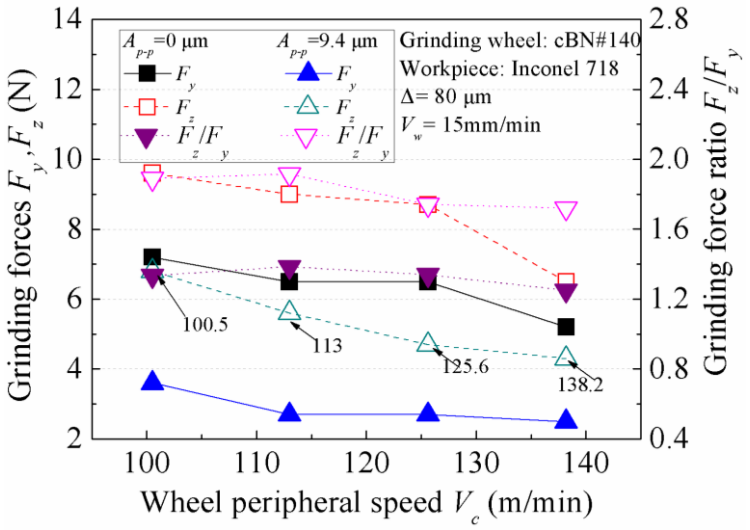

(b)

Fig. 2.9 Effects of (a) vibration amplitude and (b) wheel peripheral speed on grinding forces and grinding force ratio

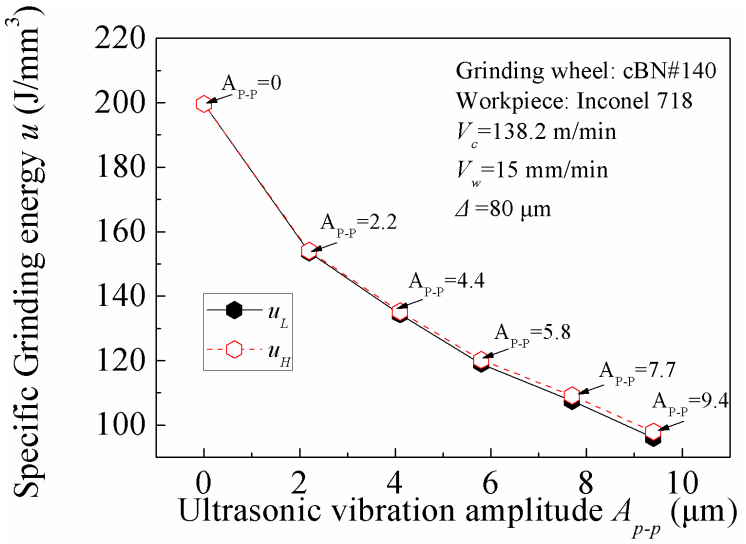

Fig. 2.10 Effects of vibration amplitude on specific grinding energy.

2.3.2 Form accuracy and surface roughness

To investigate the grinding efficiency of the UAG process, actual removal depth/rate are studied with the parameters $A_{p\text{-}p}$, V_c, Δ. Fig.2.11 shows the effect of actual removal depth/rate by process parameters. It shows a high level of vibration amplitude and rotational speed can be verified that a evidently contributes to a high actual removal depth Δ_r=9.8 μm , both in UAG and CG. In addition, actual removal rate were defined as:

$$\eta = \frac{\Delta_r}{\Delta} \times 100\% \quad (1)$$

The values of η were obtained for different depth of cut as shown in Fig. 4c. When depth of cut increases, the actual removal rate in UAG is significantly larger than those in CG. Moreover, according to the graph gradient of η, it can be verified that deep depth of cut led to a lower actual removal depth η=81 % in CG, but UAG can remained keep η at 98 %. In other words, the effect of UV on the actual removal depth can be enhanced with the increasing of $A_{p\text{-}p}$ and V_c, but V_c can hardly contributes to η with deep cut of depth, as high level UV ($A_{p\text{-}p}$= 9.4 μm) does.

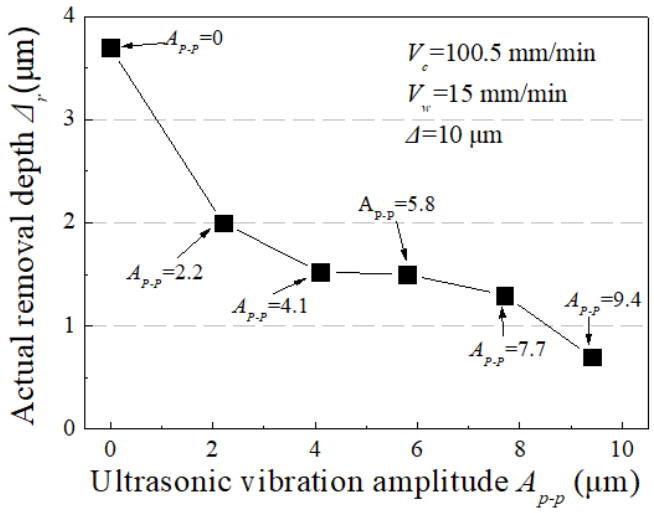

(a) Influence of vibration amplitude $A_{p\text{-}p}$

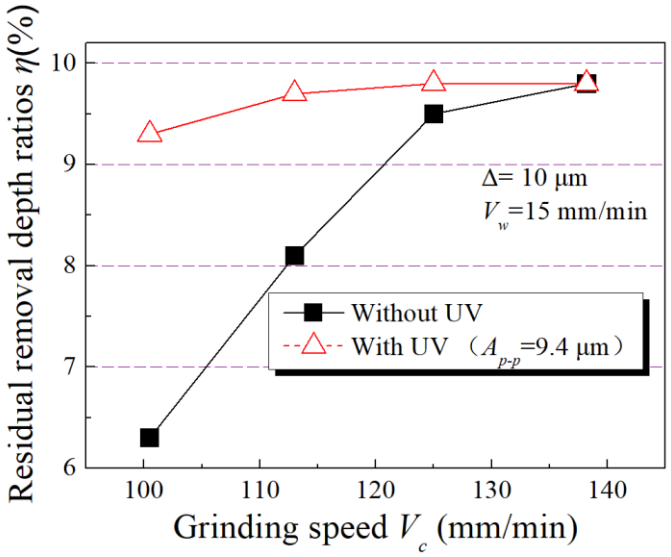

(b) Influence of grinding speed V_c

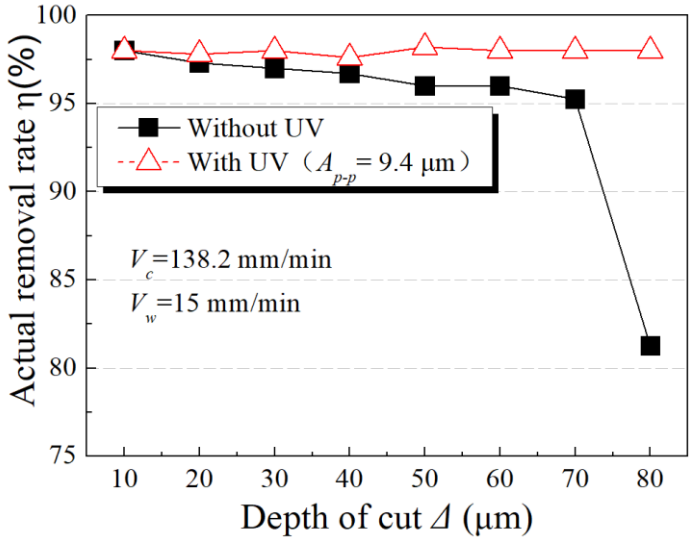

(c) Influence of depth of cut Δ

Fig.2.11 Actual removal depth/rate versus process parameters

Furthermore, the effect of process parameters on the surface roughness in CG and UAG are shown in Fig. 2.12. It is found that both roughness in CG and in UAG decrease with increasing of vibration amplitude and rotational speed, but increase with increasing of cut of depth. Additionally, it is noticed that the roughness Ra in UAG are smaller than those in CG, meaning the presence of the UV improves the surface roughness significantly. The improvement of surface quality in UAG can be considered to be the contribution of the grinding forces reduction.

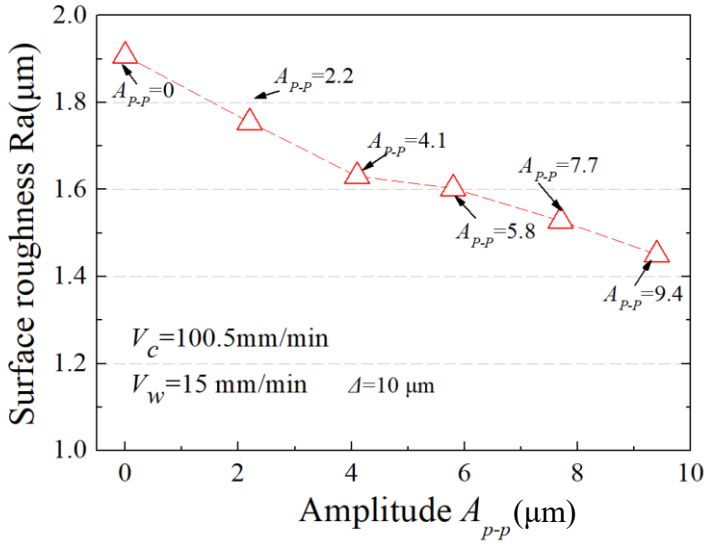

(a) Influence of vibration amplitude A_{p-p}

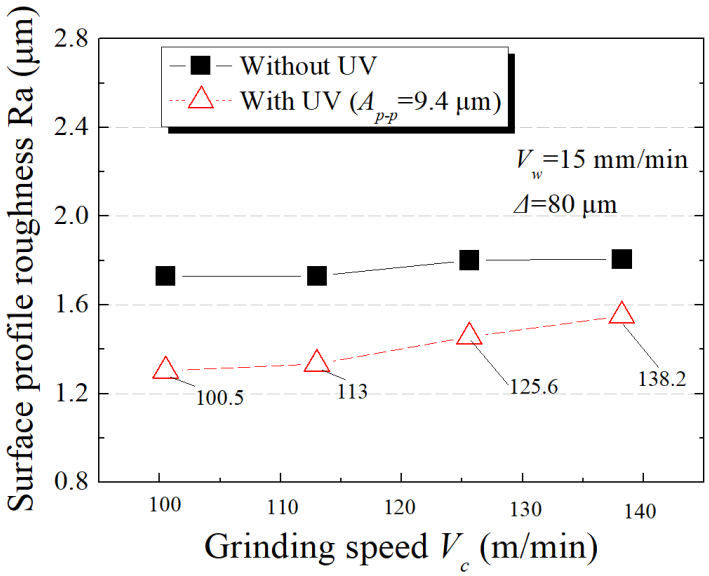

(b) Influence of grinding speed V_c

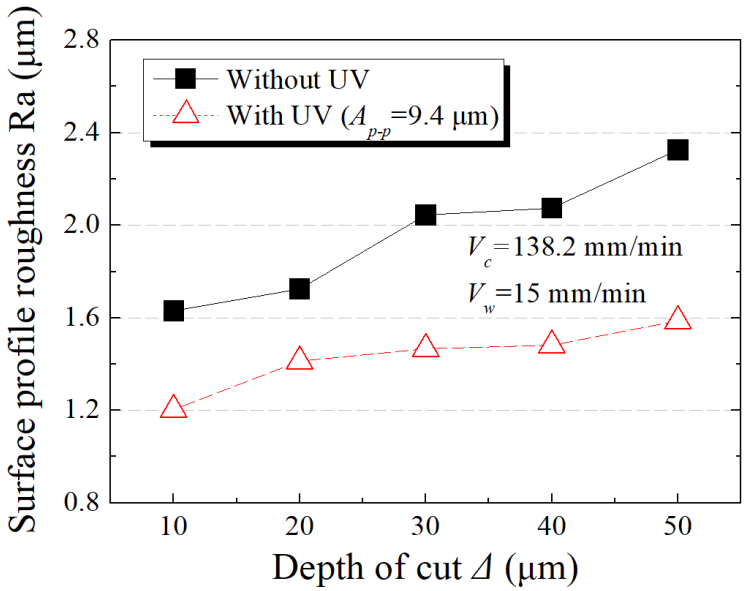

(c) Influence of depth of cut Δ

Fig.2.12 Surface roughness versus process parameters

Furthermore, Taghi Tawakoli [5] proved ultrasonic vibrations caused significant improvements on surface roughness for dry grinding 42CrMo4, which was caused by friction. This issue could increase material removal rate Q with better surface roughness. To investigate the effect of vibration amplitude on work-surface form accuracy, the roughness of workpiece surface and material removal rate Q were measured and shown in Fig.2.11 and 2.12. It could be seen from this Fig. 2.11 that the surface roughness of workpiece improved with the increase of ultrasonic vibration. This suggested that, for Inconel 718, the ultrasonic vibration also contributed to workpiece form accuracy.

2.3.3 Work surface integrity

2.3.4 Grinding wheel wear

At first, a comparison between the grinding wheel working surface conditions with and without ultrasonic vibration was carried out by SEM observation. Fig.2.13 shows the SEM images of typical fragments on the wheel working surface before and after grinding with and without ultrasonication. As can be seen that either in CG without ultrasonication (A_{P-P}=0 μm) or in UAG with ultrasonication (A_{P-P}=9.4 μm), both chips adhesion and grains releasing/fracture occurred after grinding, indicating

the wear of electroplated cBN grinding wheel in grinding of Inconel 718 are dominantly attributed to chips adhesion, grains releasing and grains fracture; however, comparing the right sides of Figs.2.13(a) and (b) revealed distinctly that the ultrasonic vibration of grinding wheel reduced both the chips adhesion and grains releasing/fracture significantly.

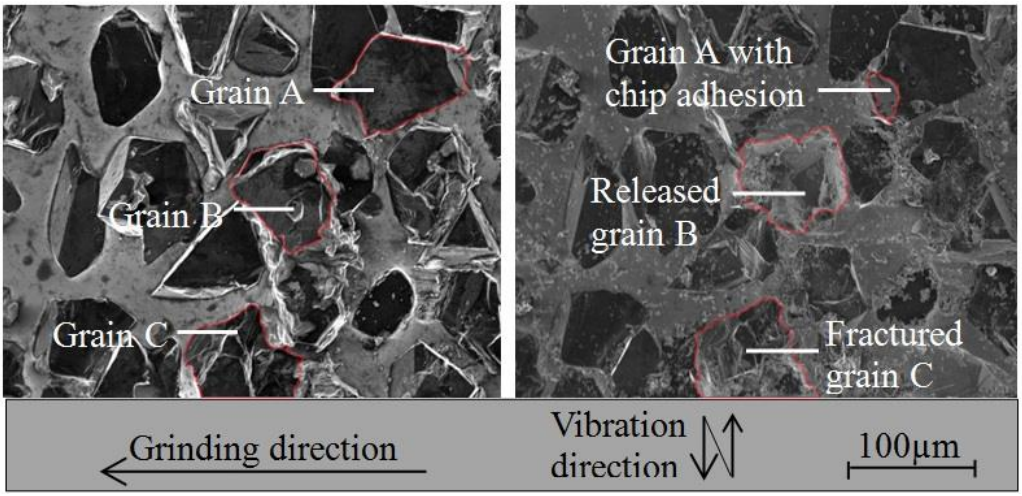

(a) without ultrasonication, i.e. CG, $A_{p\text{-}p}$=0 μm, V_c=138.2 mm/min

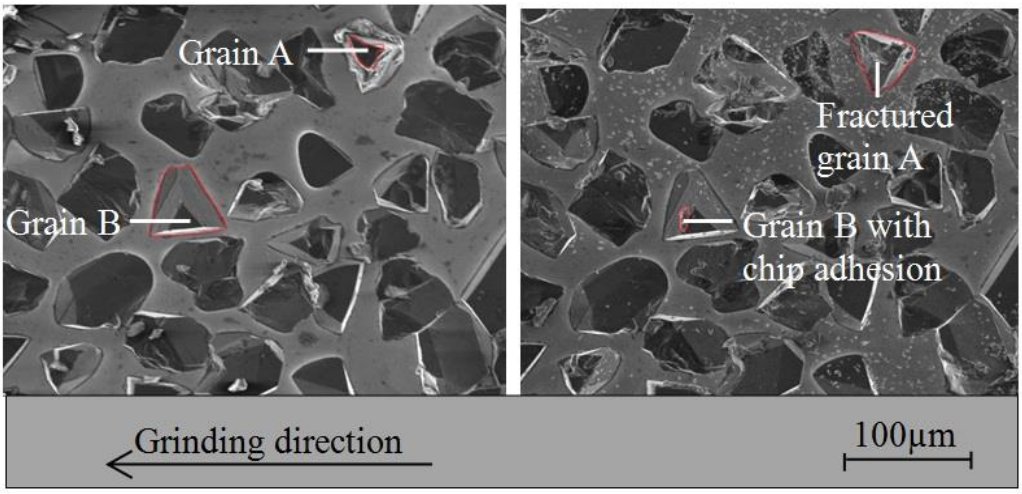

(b) with ultrasonication, i.e., UAG, $A_{p\text{-}p}$=9.4 μm, n_g=138.2 mm/min

Fig.2.13 SEM images of the grinding wheel working surfaces before (left sides) /after (right sides) grinding of Inconel 718 (a) without and (b) with ultrasonication

To begin with, the chips adhesion phenomenon was quantitatively estimated. For this purpose, the extraction and binarisation processing of the chips adhered in a

certain zone of working surface (1.13 mm×6 mm in the current work) were performed on the SEM images of grinding wheel working surface using Image-Pro Plus software followed by calculating their areas with the same software. In the extraction, as the colors of the chips adhered differ from those of the cBN grains and the bond materials (see right sides of Fig.4), the chips adhere were extracted according to their colors by using threshold and segmentation tools of the Image-Pro Plus software which can distinguish colors of SEM images. After the extracted chips have been binarized, their numbers and areas were calculated using the Count/Size command of the same software. As the typical results obtained, Fig.2.14 shows the binarized SEM images, on which only the adhered chips appeared, for different ultrasonic vibration amplitudes. It can be seen from the figures that the smaller the ultrasonic vibration amplitude was, the heavier chips adhesion became. This result demonstrated that the assistance of ultrasonic vibration improves the grinding wheel working surface condition from the view point of chip adhesion, as the chips adhesion leads to not only a loss of abrasive grain sharpness but also an increase in the contact area and frictional interaction between abrasive grains and the workpiece.

By using the data of binarized SEM images, the effect of the ultrasonic vibration amplitude on the chips adhesion was discussed quantitatively in terms of the percentage of chips adhesion area in the total wheel working surface area estimated, the number and mean area of chips adhered on the same wheel working surface area examined as shown in Fig.2.15. Obviously, the percentage of chips adhesion area decreased with the increase in the vibration amplitude (Fig.2.15(a)); a decrease by 72.4 % at $A_{P\text{-}P}$=9.4 μm compared with that in CG at $A_{P\text{-}P}$=0 μm. In contrast, no noticeable tendency can be observed on the effect of the amplitude on the number of chips adhered (Fig.2.15(b)), implying that the mean area, i.e., size of chips adhered tend to decrease as the vibration amplitude increases (Fig.2.15(c)). This phenomenon is considered to be due to that the larger vibration amplitude leads to the formation of smaller chips [6]. Small-sized chips adhered in chip pocket do not pose a friction-triggered intensive heating in grinding zone [7]. Larger vibration amplitude makes the grinding process of Inconel 718 more effective owing to the huge motion acceleration of chips which is induced by the ultrasonic vibration of grinding wheel.

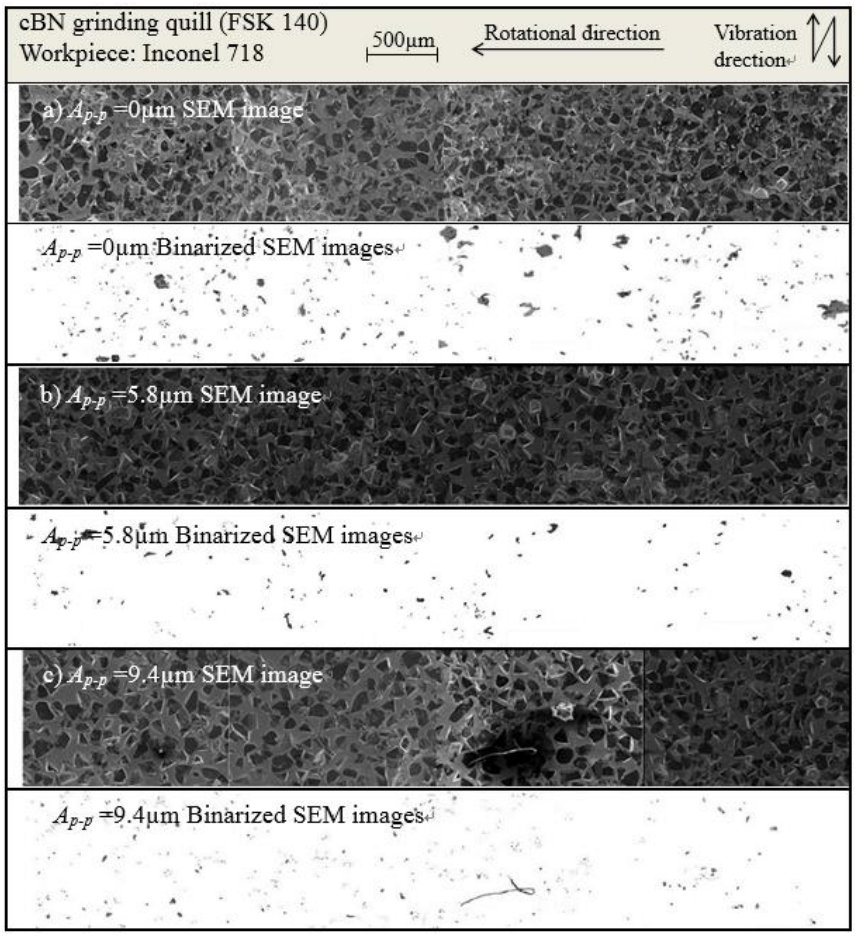

Fig.2.14 SEM images of chips adhered on the grinding wheel working surface with and without ultrasonication

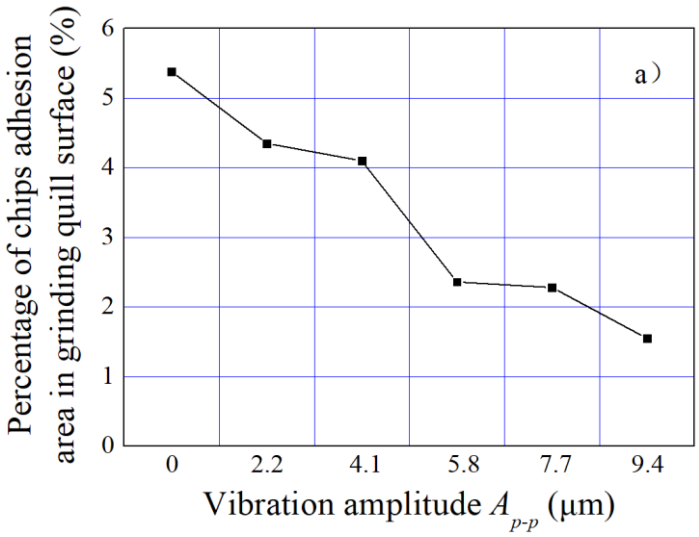

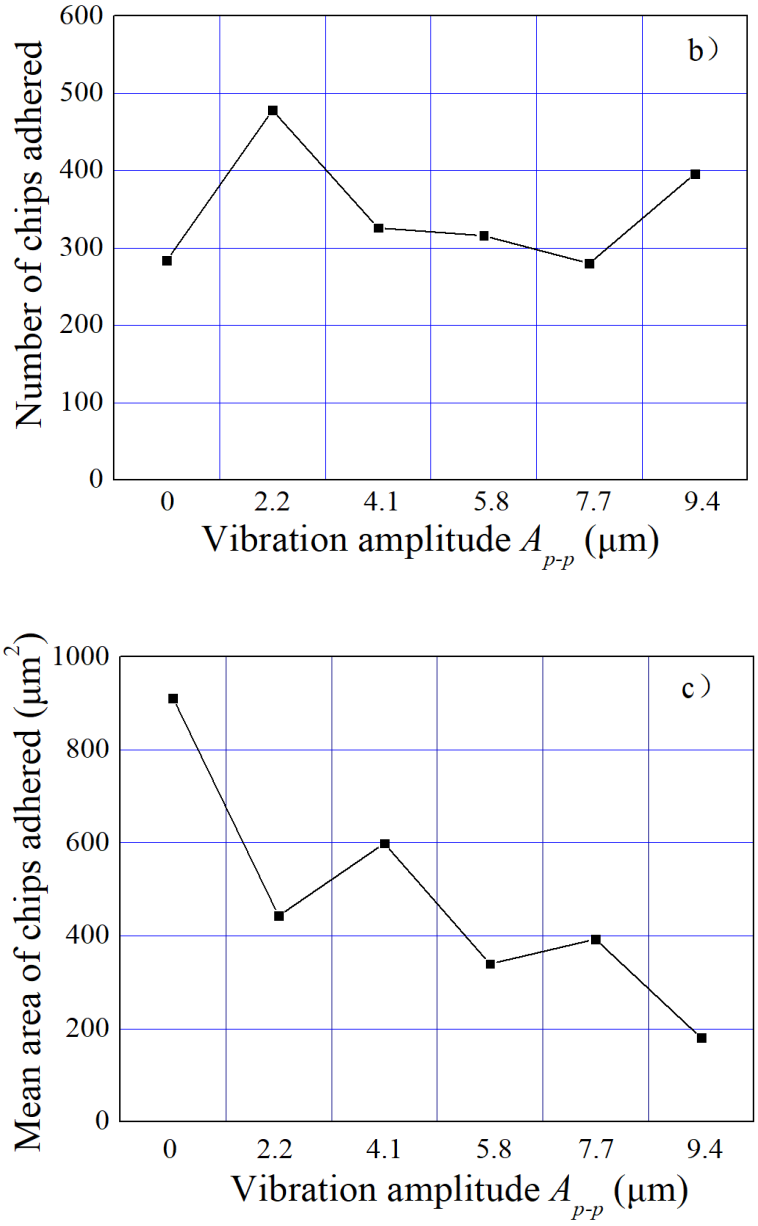

Fig.2.15 Effects of vibration amplitude on chips adhesion: (a) percentage of chips adhesion area; (b) number of chips adhered; (c) mean area of chips

Next, the releasing and fracture of abrasive grains were also quantitatively investigated in terms of the percentages of the number of abrasive grains released/fractured in the total number of abrasive grains in the estimated wheel working surface area both in CG and UAG of Inconel 718. Fig.2.16 shows the obtained results. Evidently, in CG (A_{P-P}=0 μm) the percentage reached 44 %, indicating that almost the half of the abrasive grains were released/fractured during grinding without ultrasonication, whilst once the ultrasonic vibration has been imposed on the grinding wheel even at a relatively small amplitude of A_{P-P}=2.2 μm,

the percentage was significantly decreased to less than 20 %, demonstrating that the presence of ultrasonic vibration restraints the grain releasing/fracture phenomenon considerably. It is also noticed that the percentages of the number of grains released/fractured decreased as the vibration amplitude rose, implying that the larger the amplitude was, the smaller the damage to grains became.

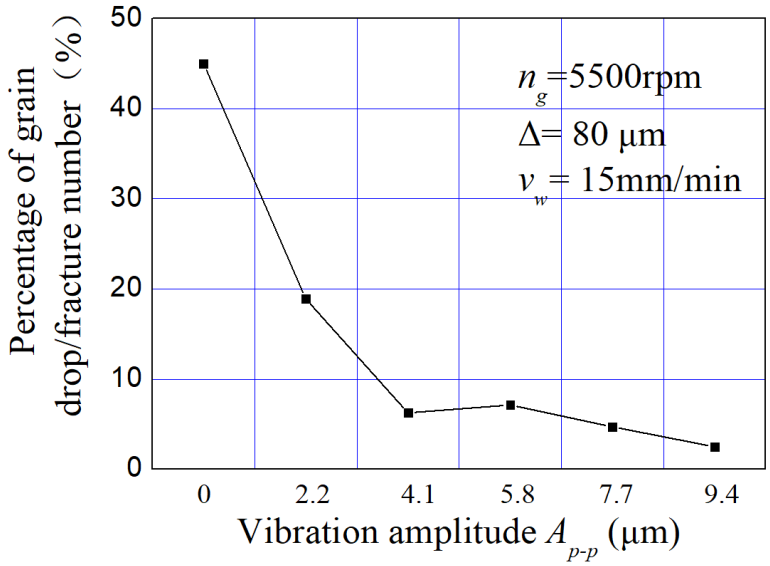

Fig.2.16 Effect of ultrasonic vibration amplitude on the percentage of the grain releasing/fracture number in CG and UAG of Inconel 718

As clarified above, the abrasive grains are released from the wheel working surface due to the bond fracture, and the grains fracture also occurs because of the grinding forces during grinding. These facts would in turn cause the decrease in the distribution density of effective grain cutting edges seriously, subsequently leading to the deterioration of the wheel performance. In order, therefore, to maximize the effort of ultrasonic vibration on keeping the grinding wheel performance, the distribution density of effective grain cutting edges on the wheel working surface were investigated for various ultrasonic vibration amplitudes by the island analysis.

In the island analysis, 3D (three dimensional) topographies of wheel working surface were firstly obtained by means of the 3D-observation function of the used SEM. As an example, Figs.2.17(a) and (b) show the 3D-topographies of a grinding wheel working surface in a typical area of 1.5 mm×1.13 mm before and after UAG at A_{p-p}=9.4 μm , respectively. As can be seen from the figures that the grains with sharp cutting edges were distributed uniformly on the working surface before UAG;

however after grinding the grains releasing occurred and the grains fracture took place which resulted in the reduction of cutting edge protrusion.

Figs.2.18(a) and (b) exhibit the islands obtained by the island analysis, for example, using the data in Figs.2.17(a) and (b), respectively, at z=30 μm. These islands stands for the effective cutting edges in the case of the maximum grain depth of cut g_m=z=30 μm .Comparing Figs.2.18(a) and (b) with each other revealed that after UAG either the distribution density or the size of the islands, i.e., the effective cutting edges, at z=30 μm were changed. By similarly doing, the distribution densities of the effective cutting edges at different values of z were quantitatively investigated under various values of $A_{P\text{-}P}$. Fig.2.19 shows the obtained results, indicating that the distribution density increased as the value of z rose. When the value of z was smaller than 10μm, no considerable difference between the distribution densities with and without ultrasonication was observed; however, once the z was beyond 20 μm the larger the vibration amplitude was, the higher the distribution density became. On other words, as mentioned in the last sub-section, the presence of ultrasonic vibration restraints the grains releasing/fracture, and in turn maintains the effective cutting edge density at a high level. In addition, micro self-sharpening or self dressability effect contributes to such an increase in the effective cutting edges density as well [8].

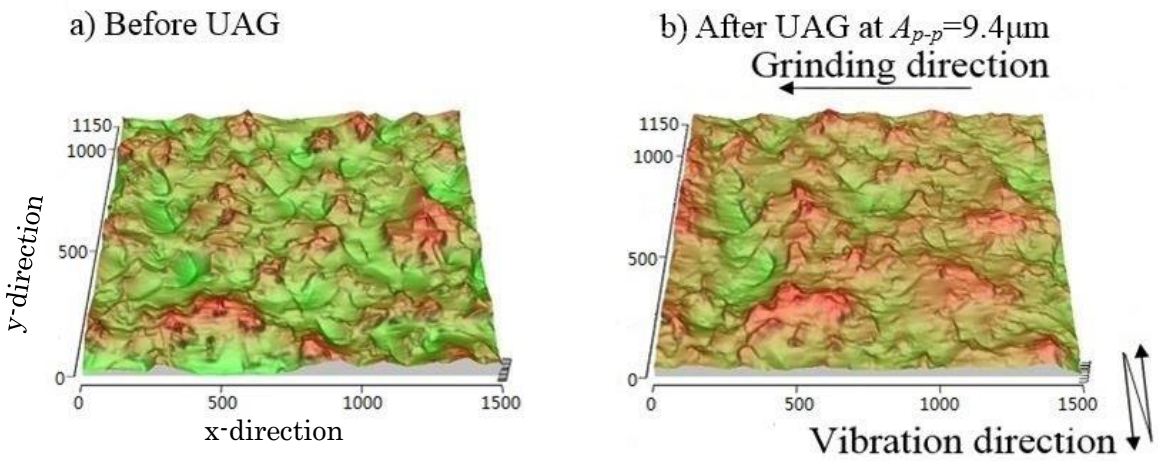

Fig.2.17 3D topographies of wheel working surface (a) before and (b) after UAG

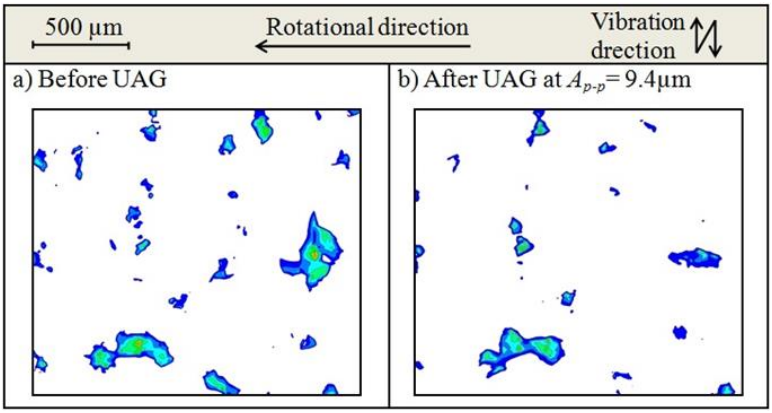

Fig.2.18 Islands, i.e., effective grain cutting edges, distributions at z=30 μm

Given that the mean area of the islands (i.e., the effective cutting edges) denote the sharpness of the grinding wheel, it is of importance to investigate the effects of the vibration amplitude on the mean area of effective cutting edges for various values of *z*. Fig.2.20 shows the results obtained by averaging the areas of effective cutting edges. Evidently similar with that in Fig.2.19, the mean cutting edge area increased as the *z* rose. It is, however, worthy to note that overall the mean area of effective cutting edges in UAG is smaller than those in CG, demonstrating that the presence of ultrasonication enhanced the grinding wheel sharpness, namely, reduced the dulling degree of abrasive grains and hence improved the wheel performance. At larger amplitude, this fact appeared more outstandingly.

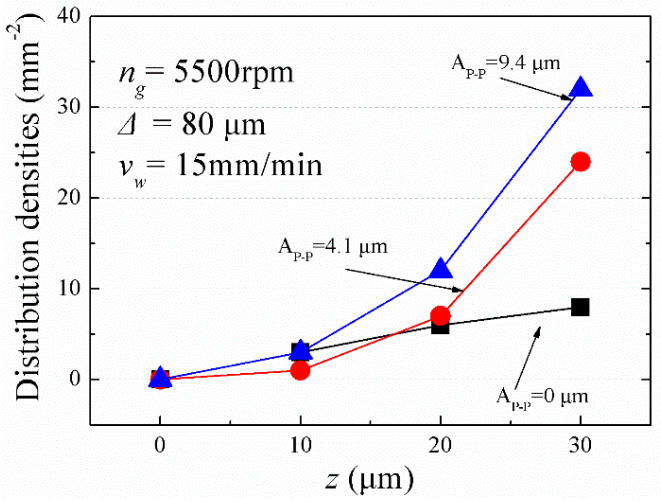

Fig.2.19 Variations of the distribution densities along the radial depth at different amplitudes

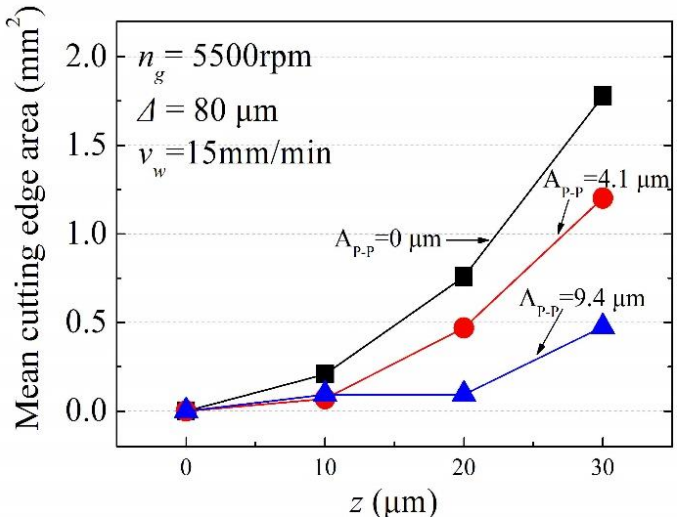

Fig.2.20 Variations of the mean cutting edge area along the radial depth

The aforementioned comparison between the wheel surface conditions after grinding with and without ultrasonication revealed that the ultrasonic vibration plays an essential role in inhibiting the grinding wheel wear and promoting the chip removal during grinding of Inconel 718. Jianguo Cao, et al. [9] pointed out that in UAG sinusoidal grain cutting traces are formed on the workpiece in the contact zone between the wheel and the workpiece with an arc length of l_c and a width of b owing to the synthesis of two motions, i.e., the wheel rotation around its own axis and the wheel ultrasonic vibration along its own axis as shown in Fig.2.21(a). For convenience, the 3D spatial cutting trace is re-drawn on a 2D *yol* plane, which is fixed on the workpiece as in Fig.2.21(b). Thus the *l*- and *y*-coordinates of an ultrasonically vibrating grain at time t in the *yol* plane can be expressed by Eqs.(6) and (7), respectively, when assuming both the initial *l*- and *y*-coordinates of the grain are 0 at time t=0 and the work feed rate is small enough to be ignored compared with the wheel peripheral speed.

$$x(t) = \pi d_g n_g t \tag{6}$$

$$y(t) = 0.5 A_{p-p} \sin(2\pi f t) \tag{7}$$

Differentiating Eqs. (6) and (7) with respect to time t twice yielded the acceleration of the grain in *l*-axis being zero regardless of the time t but that in *y*-axis at time t being given with Eq. (8).

$$a_y(t) = -2\pi^2 f^2 A_{p-p} \sin(2\pi f t) \tag{8}$$

Essentially, the occurrence of chips adhesion and grains releasing/fracture during

grinding is due to the physical interaction between the grain and the workpiece. Assuming a chip with a mass of m has been adhered on the front face, i.e., the rake face, of the grain cutting edge (Fig.2.21(b)) and motions along with the grain, an inertia force in y-direction would be caused by the acceleration of the chip according to Newton's second law and acts on itself as expressed with Eq.(9).

$$F_v(t) = -2m\pi^2 f^2 A_{p-p} \sin(2\pi ft) \tag{9}$$

It can be figured out from Fig.2.21(b) that when the grain motions to any of the sinusoidal peaks, the inertia force reaches maximum, for example, with a value of $2\times3.14^2\times40^2\times9.4$ m=296577 m in the case of f=40 kHz and $A_{p\text{-}p}$=9.4 μm , meaning the inertia force would reach a huge value of 30263 times as great as chip weight, which is only 9.8 m. This inertia force has non-significant effect on the material removal [2], but will bring a sake of the chip leave out from the grain surface because the inertia force acts in a direction opposite to the grain motion direction. According to Eq.(9), higher amplitude leads to larger inertia force, and hence results in a better chip removal, which can not only encourage the decrease in the chips adhesion but also reduce the damage to grains and bonds [3].

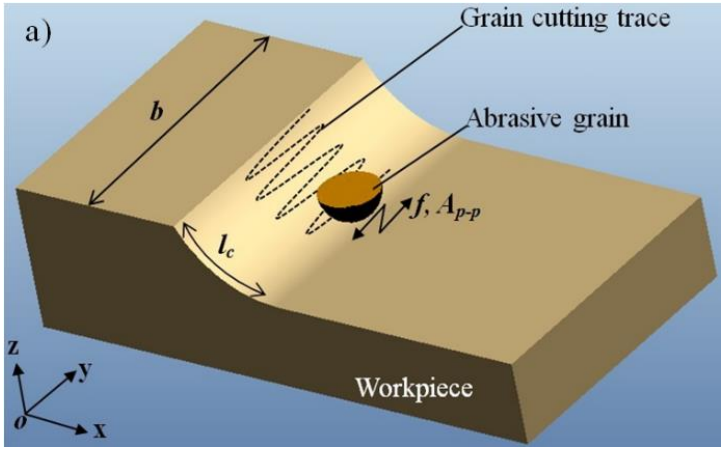

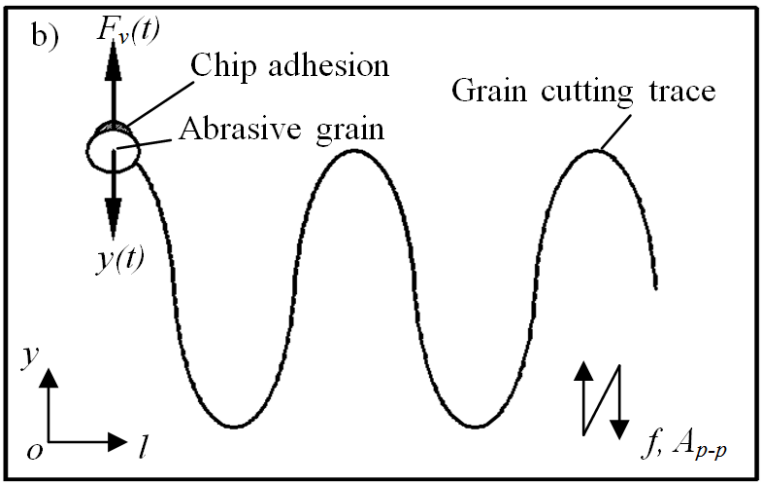

Fig.2.21 Grain cutting trace on workpiece: (a) 3D image of UAG; (b) grinding area of UAG

In addition, one of the present authors concluded in his previous work [10] that for the sake of the sinusoidal trace the cross section area of the un-deformed chip becomes smaller once the ultrasonic vibration has been imposed on the vitrified-bond cBN grinding wheel in the UAG of stainless steel (SUS440C). This subsequently not only results in the minimization of chips and makes it easier to remove the chips from the grinding zone but also decreases the grinding force.

2.3.5 Chip deformation

Figs.2.22 (a) and (b) show the 3D SEM images of chips formed in UAG ($A_{P\text{-}P}$=9.4 μm) and CG at V_c=138.2 m/min, respectively. The majority of chips in UAG seems smaller than those in CG. Subsequently, 50 chips formed in each test were properly collected and their 3D SEM images were obtained to achieve their sizes (lengths and cross section areas). As a result, the chip length and its cross section area at different vibration amplitudes for various wheel peripheral speeds were obtained as shown in Figs.2.22 (c) and (d), respectively, where the error bars indicate the size variations of 50 chips in the corresponding test with the same grinding conditions. It is evident in Fig.2.22 (c) that both the mean length and the mean cross section area of 50 chips were decreased monotonously with the increasing vibration amplitude. It is further worthy to note that the cross-section area of chips became smaller by 64.3 %, and the mean length decreased by 36.3 %, respectively, once the ultrasonic vibration with an

amplitude of $A_{p\text{-}p}$=9.4 μm has been imposed to the grinding wheel. Shifting the attention to the effect of the wheel peripheral speed (Fig.2.22 (d)) revealed that the cross-section area either in UAG or in CG decreased slightly with the increasing peripheral speed; however, the effect of the speed on the chip length either in UAG or in CG were not obvious. In a word, the chip size is distinctly affected by the ultrasonication but little effect of wheel peripheral speed was observed. Given that in grinding the normal force acting on the grain cutting edge rake face is increased with the increasing contact area between the chip and the cutting edge [11] and the grain cutting force is proportional to the chip cross section area [12], these experimental observations on chip size imply that the grinding force would be reduced as the ultrasonic vibration amplitude increases.

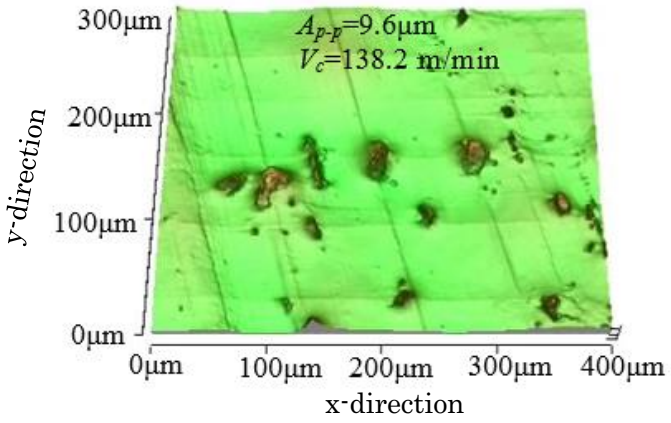

(a)

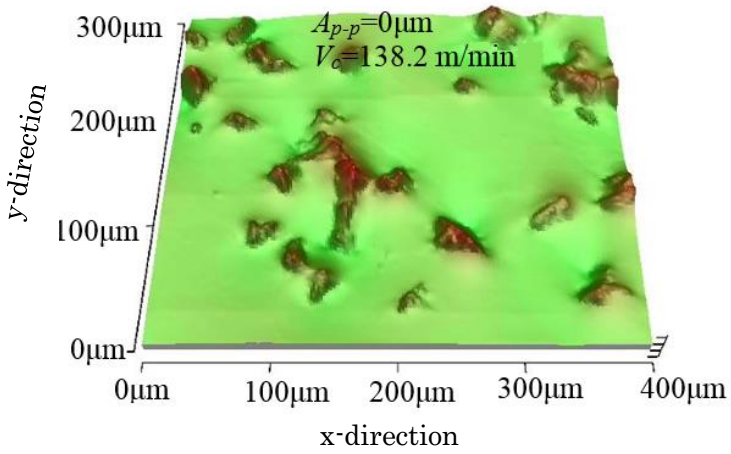

(b)

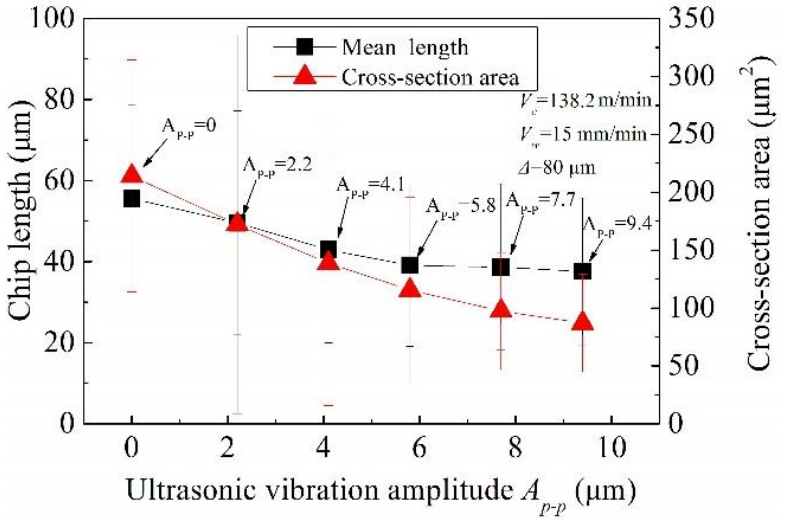

(c)

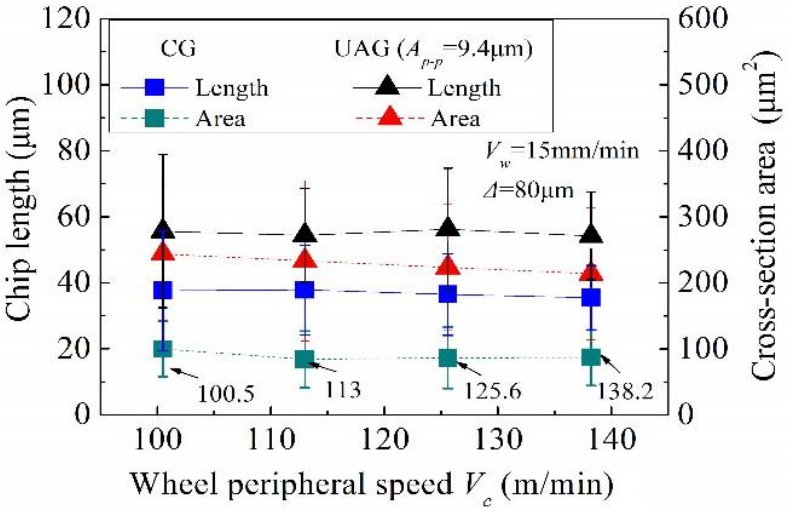

(d)

Fig. 2.22 Effects of ultrasonic vibration amplitude and wheel peripheral speed on chip size: (a) 3D SEM images of chips in UAG at A_{p-p}=9.4 μm, (b) 3D SEM images of chips in CG, (c) Chip lengths and cross section area vs. vibration amplitude, (d) Chip lengths and cross section area vs. wheel peripheral speed.

As revealed by Pei-Lum Tso [13], in conventional grinding of Inconel 718, the formed chips can be in general classified to six types, i.e., flow, shear, rip, knife, slice and melt. In the present work involving the same workpiece, although all the six types of chips were also observed, the great majority of them were the shear, knife and flow types either in UAG or in CG as typically shown in Fig.2.23. Shifting the attention to the number percentages of each type under different grinding conditions, it can be found from Fig.2.24 that the majority of chips in CG were shear type, whereas most of them in UAG were flow type especially at larger vibration amplitude ($A_{p-p} \geq$ 4.1

μm). This indicates that the UAG of Inconel 718 is potentially avoiding the formation of shear chips and prefers the flow chips especially at larger amplitude.

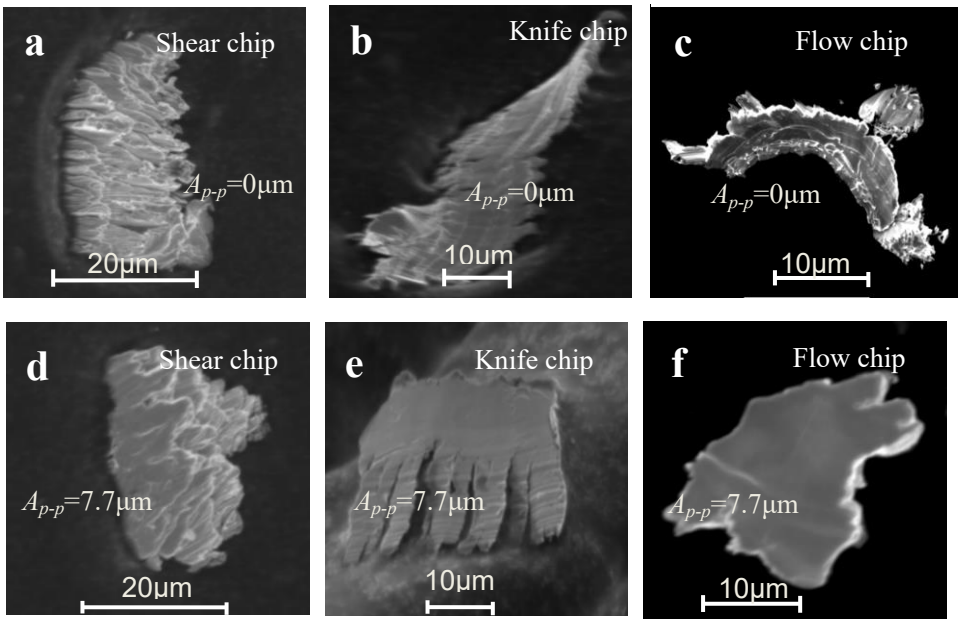

Fig. 2.23 Type of chips at Δ=80 μm and V_c=138.2 m/min: (a) shear chip in CG ; (b) knife chip in CG; (c) Flow chip in CG; (d) shear chip in UAG; (e) knife chip in UAG; (f) Flow chip in UAG.

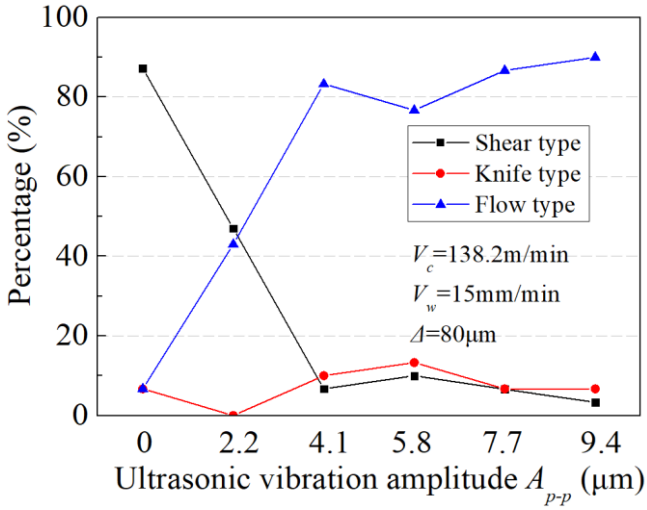

Fig. 2.24 Effect of vibration amplitude on chip type.

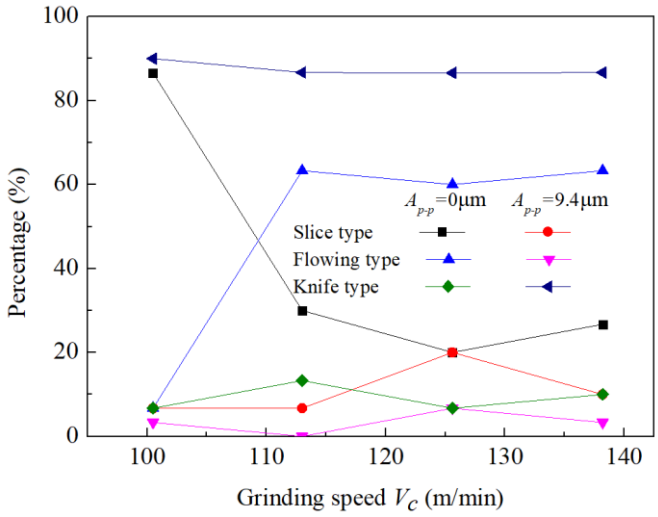

Fig. 2.25 Effect of wheel peripheral speed on chip type.

As for the effect of the wheel peripheral speed V_c, it can be found from Fig.2.25 that in CG at the beginning as the V_c increased from 100.5 m/min to 113 m/min, the percentage of the flow chip rapidly rose from 4 % to 63 % and little change can be found on the percentage of knife chip, whilst that of the shear chips dropped considerably from 86% to 30%, and then as the V_c continued to increase, significant variations cannot be observed on the percentages of all the three types of chips. However, in UAG, little changes can be found on the percentages of all the three types of chips as the V_c increased from 100.5 m/min to 138.2 m/min. These facts revealed that in CG of Inconel 718, the wheel peripheral speed would affect the chip formation significantly, whereas in UAG the chip formation is hardly affected by the wheel peripheral speed. The reason for these differences will be discussed in next section.

As afore-revealed, the great majority of chips formed in UAG were smaller than those in CG. In order to find the reason why the ultrasonication resulted in the formation of smaller chips, the cutting traces of a single grain with and without ultrasonication in the grinding zone and the formation behavior of a chip by the grain are considered as illustrated in Figs.2.26(a) and (b), respectively.

In CG without ultrasonication (Fig.2.26 (a)), the grain's cutting trace is a 2D curved line in the *yz*-plane and the undeformed chip length is supposed to be equal to the length of the cutting trace, whereas in UAG the cutting trace is a 3D curved line that looks like a spatial sinusoidal curve and its length would be longer than that in CG, indicating that the undeformed chip length in UAG would be longer than that in

CG. One of the present authors presented in his earlier work [14] on the UAG of SUS440C steel that the materials removed by a single abrasive grain with ultrasonication equals that without ultrasonication and thus the longer cutting trace results in the smaller cross section area of chip. This would be one of the reasons why the cross section area of chips in UAG is smaller than that in CG. Meanwhile, the ultrasonic vibration benefits the reduction of the friction coefficient between the grain and the chip and the ground work-surface for the sake of the so-called ultrasonic lubrication [15]; the larger the vibration amplitude is, the smaller the friction coefficient becomes, leading to the increase in shear angle and eventually decrease the chip thickness. This might be one of the reasons why the chip cross section area decreased with the increasing ultrasonic vibration amplitude.

Fig.2.26(b) illustrates the instantaneous chip formation behavior at a moment in UAG. Although the ultrasonic vibration is purposely imposed on the grinding wheel along the wheel axis (*x*-direction), usually it also occurs in the wheel radial direction owing to the LR transferring effect [16]. In the current work, for confirming this issue, the radial and axial ultrasonic vibration of the wheel were measured using a laser Doppler vibrometer (LV-1610 by Onosokki) and the obtained results indicated that the actual vibration amplitude in the radial direction (A_r) was about 0.4 μm whereas about 9.4 μm in the axial direction. Therefore, even the amplitude in the radial direction was much smaller than that in the axial direction, the impact effect of the ultrasonically vibrating grain takes place in the radial direction and the chip breakage is promoted, resulting in the formation of shorter chips compared with that in CG without the impact effect. This might be one of the reasons why the chips length in UAG was smaller than that in CG.

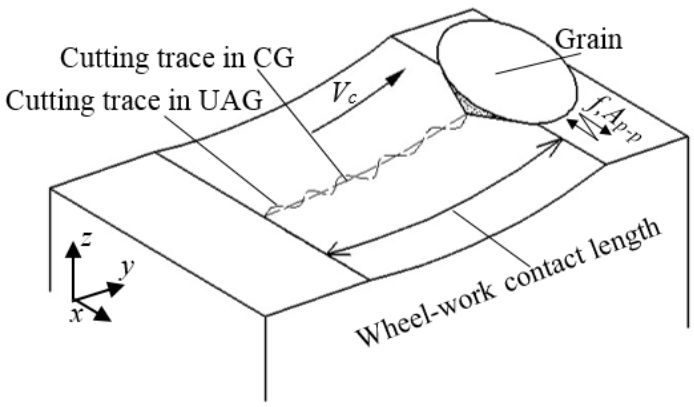

(a)

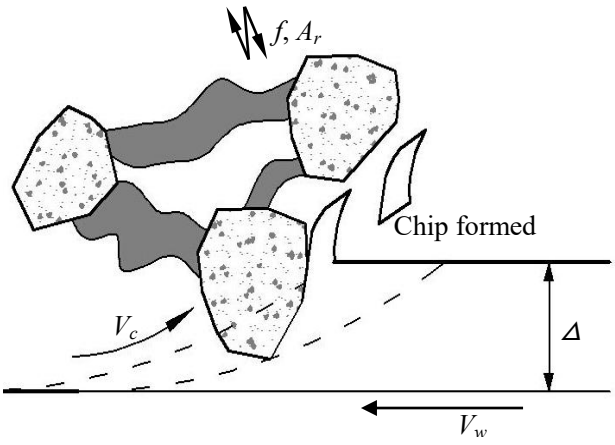

(b)

Fig.2.26 (a) Grain cutting traces (b) impact effect of grain on chip in UAG

The generally accepted mechanism of chip formation in grinding is that of extrusion-like action [12] as shown in Fig.2.27 (a). Between points A and C, grain and workpiece are just in contact without cutting action. At the very first stage of the interaction between grain and workpiece, plastic deformation occurs, the temperature rises and normal stress exceeds the yield stress. The work material is abruptly sheared as it crosses the primary shear zone along the shear plane A-D that is determined by the shear angles φ. When the shear angle φ is small, the material in the front of grain is predominantly deformed and piled up due to shearing action, which is more relevant to high compressive stress, leading to the formation of a shear chip (Fig.2.27(b)). The material piled up in the front of grain partially flows under the cutting edge, resulting in the generation of many cutting marks on the chip surface, which was frequently observed in the CG of Inconel 718 [17]. This kind of chips will bring a large specific grinding force, increase the grinding temperature and cause serious grain wear.

The formation mechanism of flow chip is similar with that of shear chip, but the shear angle φ is larger compared with that in shear chip formation (Fig.2.27(c)). When the shear angle is large, the flow chip formed with a narrow primary shear zone. In this case, there is low residual stress, and practically all of the energy consumed ends up in the chips instead of workpiece. In addition, the material is removed with a low strain and the contact condition turns into sliding. This phenomenon can be observed by scanning the chip grinding surface (Figs.2.23(c) and (f)), which is smoother than shear chip (Figs.2.23(a) and (d)).

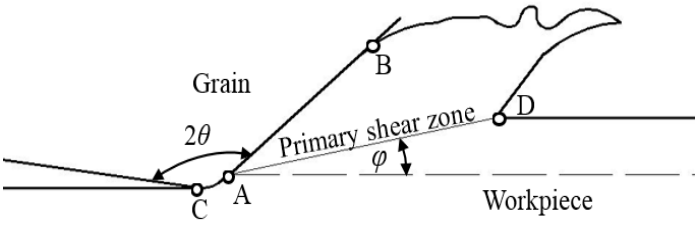

(a) Extrusion-like behavior in chip formation in grinding

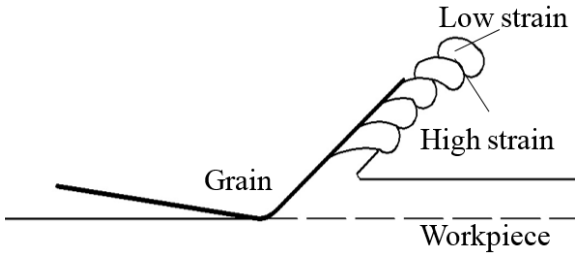

(b) Shear chip formation

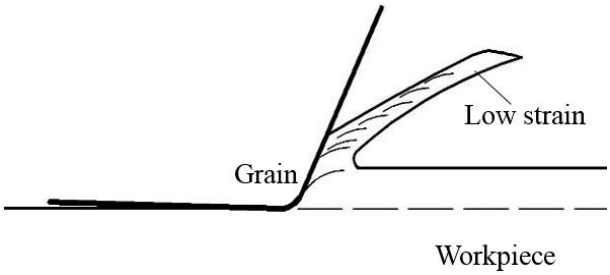

(c) Flow chip formation

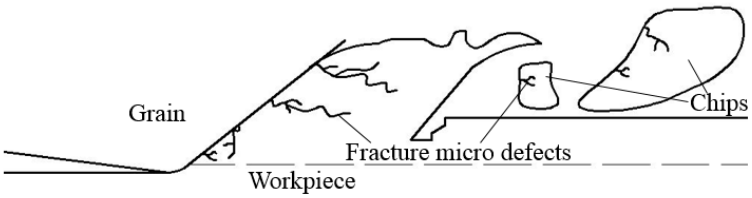

(d) Fracture mechanism in knife chip formation

Fig. 2.27 Shear and fracture of chip in single grain

The knife chip is formed frequently with fracture micro defects in work material (Fig.2.27 (d)). This kind of chips was actually found to occur when a relatively large depth of cut was applied [18]. This phenomenon brings a serious compressive force and ends up the occurrence of high compressive stress in the primary deformation zone, eventually inducing compressive residual stresses in the machined surfaces [19]. Due to the high compressive residual stress, the subsequently passing grain leads to fracture micro defects below the surface. This is the reason why the knife chip was formed with crack, as shown in Figs.2.23 (b) and (e).

Armarego and Brown [21] concluded that the shear angle φ is independent of both the grain width of cut and the chip thickness and can be determined by Eq. (10).

$$\tan(\varphi+\beta)=\cot\alpha \tag{10}$$

where β is the friction angle and determined by the friction coefficient μ_g between the

rake face of cutting edge and the chip through the relationship of $\tan\beta=\mu_g$ and α is the rake angle of cutting edge. In CG, the angle α is usually the same with the half vertical angle θ of the grain; hence, it can be figured out from Eq.(10) that as long as the grinding is performed with a given grinding wheel at a given wheel depth of cut, the α will be a given constant, consequently the φ would increases as the β decreases. Elena Teidelt [15] pointed out that the ultrasonic vibration benefits the reduction of the friction coefficient μ_g; the larger the vibration amplitude is, the smaller the friction coefficient becomes, implying that a larger vibration amplitude leads to a larger shear angle φ according to Eq.(10). This is considered to be one of reasons why the formation of flow chips was promoted by the ultrasonication of wheel, in particular, at a larger amplitude.

For convenience, the 3D spatial cutting trace is re-drawn on a 2D l_cox plane, which is fixed on the workpiece as in Fig. 2.28. A sinusoidal cutting trace is generated on the work-surface due to the grain vibration velocity V_x in the wheel axis (x-direction) and the grinding speed V_l along the contact arc where the V_l and the V_x can be expressed as:

$$V_l(t) = V_c + V_w \tag{11}$$

$$V_x(t) = \pi f A_{p-p} \cos(2\pi f t) \tag{12}$$

It can be figured out from Eqs. (11) and (12) that the direction of the real grain cutting speed V varies in a sinusoidal pattern and quantitatively is indicated by the engagement angle γ determined by Eq. (13):

$$\gamma = \tan^{-1}(V_x / V_l) \tag{13}$$

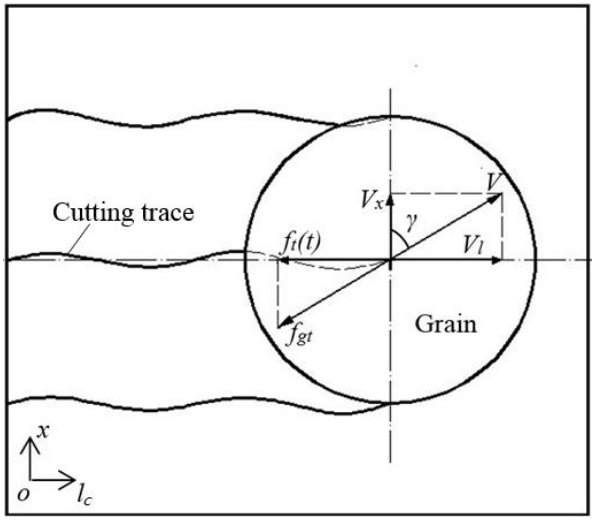

Fig. 2.28 Cutting trace in grinding zone and grinding forces on the grain in UAG.

Under the experimental conditions in the current work, the max value of V_x was similar with the value of V_l, resulting in the γ will oscillated in the range of -27°(-γ_{max}) to 27°(+γ_{max}). It is also inferred from Eqs. (6)-(8) that the engagement angle increases as the vibration amplitude increases. Thus, the chip hardly forms in same plastic deformation during a vibration cycle. Hence, the ultrasonic vibration eliminates the accumulation of chip compressive stress and makes the flow chip form easily. Meanwhile, flow chip formation leads to a low compressive residual stresses of chip, which make the formed chip break easily under the impact from the vibrating grain in plane *zl*.

2.4 Summary

The working surface condition of electroplated cBN grinding wheel and chip deformation in ultrasonic assisted grinding (UAG) of Inconel 718 was investigated for different ultrasonic vibration amplitudes. The obtained results can be summarized as followings:

(1) In UAG at the ultrasonic vibration amplitude of $A_{p\text{-}p}$=9.4μm the normal and tangential grinding forces were smaller by 42.5 % and 40 %, respectively, compared to those in CG, when the wheel peripheral speed was 138.2 m/min.

(2) The specific grinding energy u in UAG is smaller than that in CG and intended to decrease as the $A_{p\text{-}p}$ increases, demonstrating that the ultrasonication benefits the reduction in the specific grinding energy.

(3) The wear of electroplated cBN grinding wheel in grinding of Inconel 718 are dominantly attributed to chips adhesion, grains releasing and grains fracture. Both the percentage of chips adhesion area and the size of chips adhered tend to decrease as the vibration amplitude increases; in contrast, the effect of ultrasonic vibration on the number of chips adhesion are not noticeable;

(4) The percentage of the number of grains released/fractured decreases as the vibration amplitude rises; e.g., the percentage in UAG at $A_{p\text{-}p}$=9.4 μm was decreased by 40 % compared to that in CG;

(5) The chip size, i.e., cross-section area and length, are distinctly affected by the ultrasonication but little effect of wheel peripheral speed is observed. The UAG is potentially avoiding the formation of shear chips and prefers the flow chips especially at larger amplitude;

(6) In conventional grinding (CG) without ultrasonication the wheel peripheral speed would affect the chip formation significantly, whereas in UAG the chip formation is hardly affected by the speed.

Reference

[1] Z.J. Pei, P.M. Ferreira, S.G. Kapoor, M. Haselkorn, Rotary ultrasonic machining for face milling of ceramics, International Journal of Machine Tools and Manufacturel, 1995; 35(7):1033-1046.

[2] Ioan D. Marinescu, Mike P. Hitchiner, Eckart Uhlmann, W. Brian Rowe, Ichiro Inasak, Handbook of Machining with Grinding Wheels, CRC Press, Technology & Engineering, 2006; 632:124.

[3] Wojciech Kapłonek, Krzysztof Nadolny, Assessment of the grinding wheel active surface condition using SEM and image analysis techniques, Journal of the Brazilian Society of Mechanical Sciences and Engineering, 2013;35 (3):207-215.

[4] D.F. Liu, W.L. Cong, Z.J. Pei, YongJun Tang, A cutting force model for rotary ultrasonic machining of brittle materials, International Journal of Machine Tools & Manufacture, 2012;52:77–84.

[5] K.W. Sharp, M.H. Miller, R.O. Scattergoodc, Analysis of the grain depth-of-cut in plunge grinding, Precision Engineering, 2000;24:20–230.

[6] D. Bhaduri, S.L. Soo, D. Novovic, D.K. Aspinwall, P. Harden, C. Waterhouse, S. Bohr, A.C. Mathieson, M. Lucas, Ultrasonic assisted creep feed grinding of Inconel 718, Procedia CIRP, 2013;6:616-621.

[7] K. Nadolny, W. Sienicki, M. Wojtewicz, The effect upon the grinding wheel active surface condition when impregnation with non-metallic elements during internal cylindrical grinding of titanium, Archives of Civil and Mechanical Engineering, 2014;15: 529-533.

[8] Pei-Lum Tso, 1995, Study on the grinding of Inconel 718, International Journal of the Materials Processing Technology, 55, pp. 421-426.

[9] Jianguo Cao, Yongbo Wu, Dong Lu, Masakazu Fujimoto, Mitsuyoshi Nomura, 2014, Material removal behavior in ultrasonic-assisted scratching of SiC ceramics with a single diamond tool, International Journal of Machine Tools

& Manufacture, 79, pp. 49–61.

[10] Wojciech Kapłonek, Czesław Łukianowicz, Krzysztof Nadolny, 2012, Methodology of the assessment of the abrasive tool's active surface using laser scatterometry, Transactions of the Canadian Society for Mechanical Engineering, 36, 1, pp. 49-66.

[11] Taghi Tawakoli Bahman Azarhoushang Mohammad Rabiey (2009) Ultrasonic assisted dry grinding of 42CrMo4, The International Journal of Advanced Manufacturing Technology 42: 883-891.

[12] Milton C. Shaw (1996) Principles of abrasive processing, Mech. Chem. Engng., Inst. Engrs, Australia MC8, 73

[13] Pei-Lum Tso (1995) An investigation of chip types in grinding, Journal of Materials Processing Technology 53:521-532.

[14] Y.B. Wu, M. Nomura, Z.J. Feng, M. Kato (2004) Modeling of Grinding Force in Constant-depth-of-cut Ultrasonically Assisted Grinding, Materials Science Forum 471-472:101-106.

[15] Elena Teidelt, Jasminka Starcevic, Valentin L. Popov, Influence of Ultrasonic Oscillation on Static and Sliding Friction, Tribol Lerr, 2012;48:51-62.

[16] Chul H. Park, Daniel J. Inman, Enhanced piezoelectric shunt design, Shock and Vibration,2003;10(2):127-133.

[17] D.Aslan, E.Budak, Surface roughness and thermo-mechanical force modeling for grinding operations with regular and circumferentially grooved wheel, International Journal of Machine Tools and Manufacture, 2015.

[18] Zhiqiang Liang, Yongbo Wu, Xibin Wang, Wenxiang Zhao, A new two-dimensional ultrasonic assisted grinding (2D-UAG) method and its fundamental performance in monocrystal silicon machining, International Journal of Machine Tools and Manufacture, 2010;5 (8):728–736.

[19] Brian Griffith, Manufacturing, Surface Technology-Surface Integrity and Functional Performance, Penton Press, London, 2001.

This page intentionally left blank.

Chapter 3 Machining characteristics of the UECG of the difficult-to-machine materials

3.1 Machining Principal of UECG

Figure 3.1 illustrates the processing principle of the proposed UECG method. A metal bonded cBN grinding wheel ultrasonically vibrating in its own axis, i.e., Y-axis, at a frequency of f and a peak-to-peak amplitude of $A_{p\text{-}p,}$ is rotated clockwise at a peripheral speed of V_g. When a cut depth, Δ, is given between the wheel and an electrically conductive workpiece, and the wheel is simultaneously fed to the left at a feed rate of V_w, an ultrasonic assisted surface grinding operation is performed. Let the grinding wheel be the cathode and the workpiece be the anode. Thus, the grinding wheel and the workpiece are negatively and positively charged, respectively, when a pulsed electric voltage is applied between them. In the meantime, if an electrolyte fluid is supplied to the grinding zone between the wheel and the workpiece, the work-material is oxidized and a thin oxidized layer is formed on the work-surface in the grinding zone (this layer is conducive to an electrochemical reaction). Then, the weakened thin layer is easily removed by the cBN abrasive grains which are moving along with the peripheral surface of the rotating grinding wheel. The electrolyte is a key part of the ECG process because the electrochemical reaction forms the oxygen layer. KNO_3 solution is selected as the electrolyte. The values of Δ, V_g, and $V_{w.}$ are determined such that the maximum grain depth of cut, i.e., the maximum undeformed chip thickness, t_m, is less than the extrusion height of the grain on the wheel working surface, h. This is to prevent the metal bond from contacting the work-material, otherwise electric short may occur, which will deteriorate the stability of the electrochemical reaction. In order to discuss t_m, several assumptions and

simplifications are made and are shown below:

- The cBN grains are rigid cones of the same size.
- The active cBN grains located on the wheel working surface have the same extrusion height, and all of them take part in cutting during grinding.
- The volume of material removed by a single grain is approximately equal to the intersection volume between the grain and the workpiece.

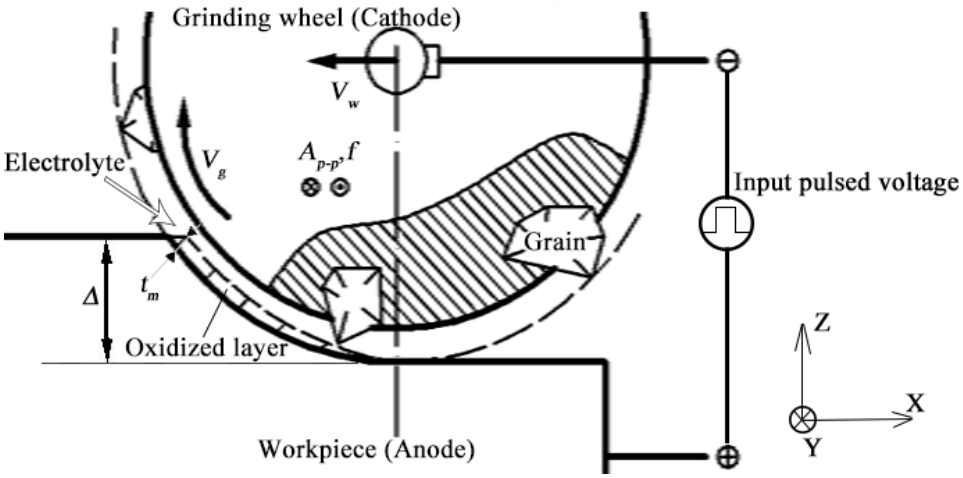

Fig. 3.1 Illustration of the principle of UECG

3.2 Experiment apparatus and conditions

3.2.1 Apparatus(Electrochemical unit, Workpiece and Experiment setup)

Fig.3.2 shows the schematic drawing of experimental setup constructed. A commercially available ultrasonic spindle (R2 by industria Co., Ltd., Japan) capable of vibrating at f=40 kHz and $A_{p\text{-}p}$≦8 μm was installed on the vertical axis of an existing desk-top sized 3-axes CNC machine tool (Multi Pro III by Takashima Sangyo Co., Ltd., Japan). On the lower end of the spindle, a metal bonded cBN grinding wheel of d_s=1.8mm in diameter was screwed. A coolant nozzle was employed to supply the electrolyte fluid into the grinding zone. As the workpiece, a Ti-6Al-4V specimen (L14×W10×T6mm) was held on the work-table of the machine tool through a 3D-dynamometer (9254 by Kistler Co., Ltd.) and a work-holder. An electrochemical

power supplier composed of a high frequency switch and a DC power was employed to induce the electrochemical reaction between the electrodes; the anode output of the power supplier was connected to the work-holder directly, whereas the cathode output was to the spindle though a spring/carbon brush mechanism.

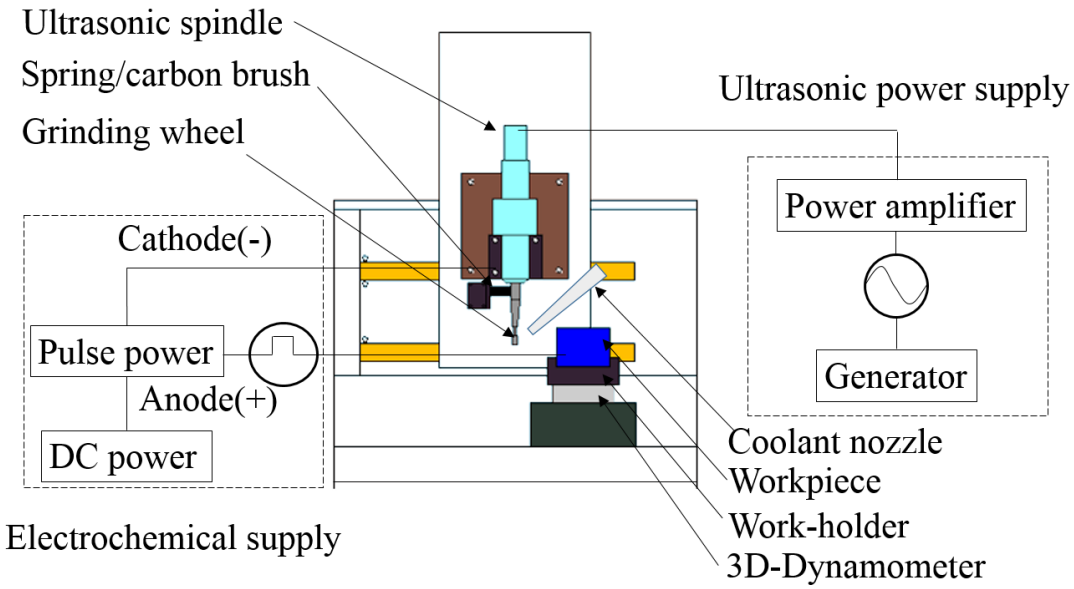

Fig.3.2. The schematic drawing of experimental setup

3.2.2 Experiment conditions

In grinding, the maximum undeformed thickness t_m of the chip which is formed by the cutting action of the cone-like abrasive grain can be expressed as [1]:

$$t_m \approx 2a\frac{V_w}{V_g}\sqrt{\frac{\Delta}{d_s}} \tag{1}$$

Where a is the successive cutting point spacing. Accordingly, in order to determine the processing parameters of Δ, V_g and V_w under the precondition of $t_m<h$, first the values of a and h were obtained by measuring the 3D size of grains and observing the grains geometry using an electron scanning microscope (SEM) with 3D measurement/observation functions (ERA-8900 by ELIONIX Co., Ltd.). Figs.3.3 (a) and (b) show the 2D SEM image of a typical area on the wheel working surface and the 3D SEM image of a representative grain, respectively. For obtaining the mean value of a, the distances a_i (i=1, 2,…, N) between two neighbored grains along the grinding direction were measured (Fig.3.3 (a)); in this work one hundred

measurements, i.e., N=100, were attained as shown in Fig.3.3 (c). It can be seen that although the value of a_i varied in the range of 0 – 35 μm, more than 90 % of them were in the range of 5 – 20 μm and hence the mean value can be determined as a=11.88 μm. As for the extrusion height of grains h, the 3D SEM observation results revealed that most of the grains exhibited cone-shaped (Fig.3.3 (b)), and one hundred grains were randomly selected for measuring their extrusion heights. Fig.3.3 (d) shows the obtained height distribution percentage of the 100 grains. It can be seen that although the values of h varied in the range of 1 – 14 μm, over 74 % of them were 1 – 6 μm, resulting in the mean values of h=2.7 μm.

Table 3.1 Experimental conditions

Ultrasonic vibration	Frequency	f	40 kHz
	Amplitude	A_{p-p}	8.0 μm
Grinding wheel	cBN1000N100M		
	Diameter	d_s	1.8 mm
	Grinding speed	V_g	84.78 m/min
	Depth of cut	Δ	3 μm
	Grinding width	b	2.5 mm
	Wheel feed rate	V_w	2.0 mm/s
Workpiece	Ti-6Al-4V(L14× W10 × T6 mm)		
Pulse electrolytic power supplying	Pattern		Triangle
	Input voltage	U_I	0~20 V
	Pulse frequency	f_d	0~0.2 MHz
	Duty ratio	D	0~50 %
Electrolytic solution	KNO_3 solution, 5 %dilution		

Typically, cBN abrasives require a speed of over 50 m/min for grinding Ti-6V-4Al [2], and the purpose of the experiment is to confirm the feasibility of the proposed UECG method and elucidate its fundamental machining characteristics in the grinding of Ti-6Al-4V. Therefore, the wheel speed was set at V_g=84.78 m/min, and the values of Δ and V_w were kept constant at 3 μm and 2 mm/min, respectively, based on the specification of the experimental setup in the current work. Thus, substituting the afore-determined values of a=18.88 μm, the employed wheel diameter of d_s=1.8 mm and the values of V_g=84.78 m/min, Δ=3 μm, V_w=2 mm/min into Eq. (1) yields the t_m=0.139 μm which is far smaller than the mean value of h=2.7 μm, sufficiently meeting the afore-mentioned precondition of t_m<h. The other process parameter including the grinding width, the ultrasonic vibration, and the pulse

electrolytic power supplying were as exhibited in Table 3.1. Due to the electrochemical reaction of Inconel 718 is too weak to reduce work hardness. The UECG process of Inconel 718 have no different with UAG process.

In experiments, CG operations neither with electrolysis nor with ultrasonic were also carried out for comparison. In each grinding test, the grinding forces were measured and the ground work surface was characterized by measuring its roughness and observing its topography using a 3D laser microscope (VK-9700 by Keyence Co., Ltd.). Besides, chemical elements analysis was also performed on the formed chips using the EDX function of the existing SEM to examine the oxidization of work materials by the electrochemical reaction.

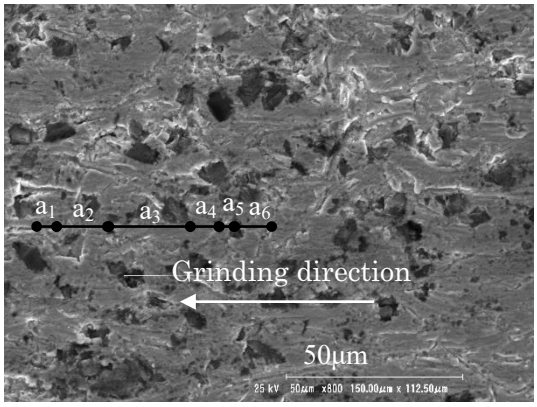

(a) 2D SEM image of a typical area on the wheel working surface

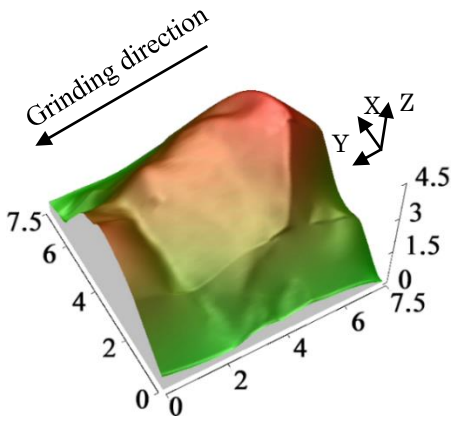

(b) 3D SEM image of a representative grain

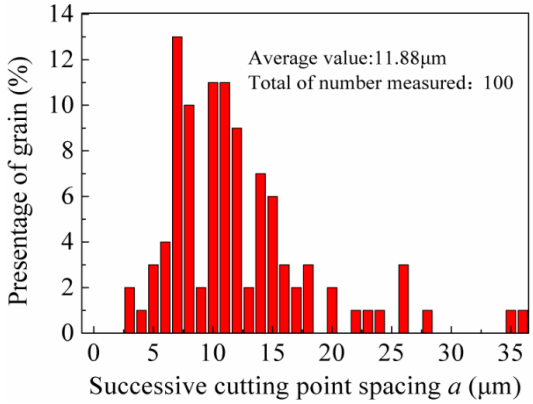

(c) Distribution percentage of *a*

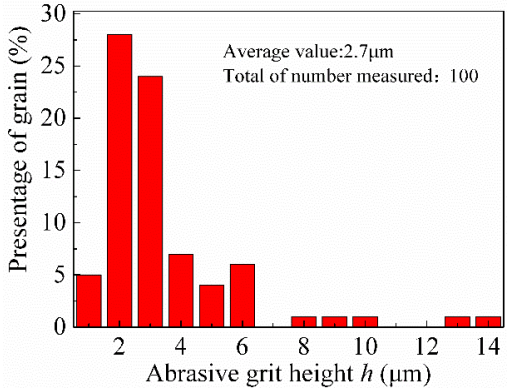

(d) Distribution percentage of *h*

Fig. 3.3 The successive cutting point spacing in grinding direction and grains extrusion height

3.3 Results and discussions

3.2.1 Electrochemical reaction

In ECG, the anodizing of Ti is carried out with the following electrochemical reaction:

$$Ti + 4OH^- \rightarrow TiO_2 + 2H_2O + 4e^- \quad (3)$$

In order to confirm whether the titanium dioxide (TiO_2) layer is actually generated on the work-surface by this reaction, a specimen was prepared by focused ion beam (FIB) machining technique and the SEM observation was carried out on the specimen as illustrated in Fig.3.4. Firstly, the workpiece was coated with a thin Au-layer of around 0.13 μm in thickness for protecting the work-surface from residual stress. Then, a micro-sized rectangle hollow of about L400×W100×D70 μm) was created by FIB machining. Finally, the specimen was placed with a tilted angle of 45°on the specimen stage inside a SEM for observing the side surface of the hollow and thus identifying the oxygen layer. Figs.3.5 (a) and (b) show the SEM images of specimens obtained in CG (U_I=0V without ultrasonic) and ECG (U_I=20V without ultrasonic), respectively. From Fig.3.5 (a) it is hard to find any layer between the Au-coated layer and the original material of Ti-6AL-4V, whereas a black oxygen layer with the mean thickness of about 78 nm can be distinctly observed between the Au-coated layer and the original material in Fig.3.5 (b). This demonstrates that the electrochemical reaction given by Eq.(3) exactly occurred in ECG.

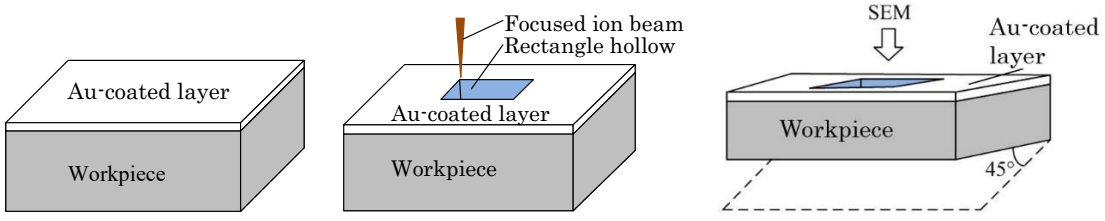

(a) Surface Au-coating (b) FIB machining (c) Tilted with 45° for SEM observation

Fig.3.4 Schematic diagram of FIB-SEM specimen preparation.

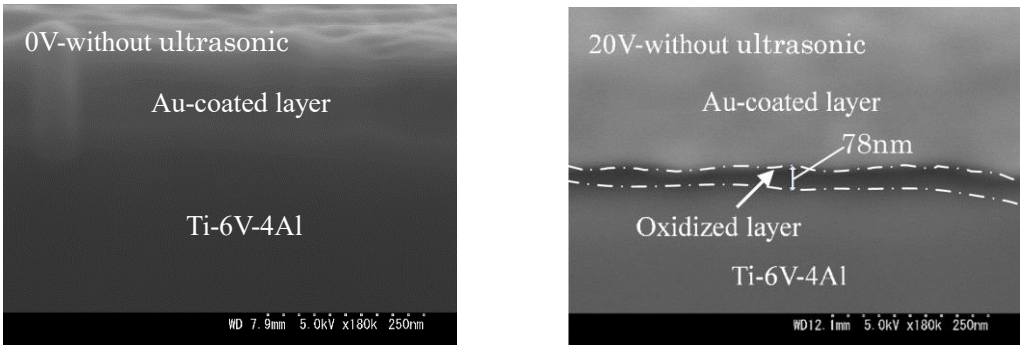

(a) (b)

Fig.3.5 The SEM image of workpiece cross-section

3.2.2 Voltage and current

Ti oxide thin films were deposited on unheated plasma by DC power. The higher voltage may be attributed to the optimum surface roughness, porosity, large surface area, grain size and high rate of oxidation. The resistance (current variations) of the TiO films that were exposed to environmental plasma at 200–400 ℃ [3], the measurement of the current and voltage was carried out by measuring the output current resulting from the exposure of the work surface.

The results of the change in the voltage vs. the change in the current are represented in Fig. 3.6. It can be seen from Fig. 3.6 that either in ECG or in UECG, with the increase of the U_I the current I were quickly increased. With ultrasonic vibration (UV) the measured current is lower than without UV. Considered the oxide film is insulation, the lower current means the oxide film is deeper.

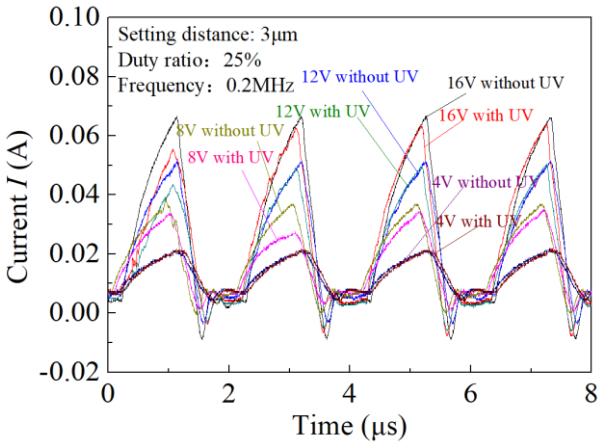

Fig. 3.6 Relationships between the current and the voltage

3.2.3 Grinding forces

As the grinding force is a crucial factor to measure the grinding characteristics, the effects of the voltage U_I, the frequency f_d and the duty ratio D of the pulse electrolytic power on the normal and tangential grinding forces, F_n and F_t, in UECG ($A_{p\text{-}p}$=8 μm) and ECG ($A_{p\text{-}p}$=0 μm) were obtained as shown in Figs. 3.7 (a), (b) and (c), respectively. It can be seen from Fig.3.7 (a) that either in ECG or in UECG, with the increase of the U_I both the F_n and the F_t were quickly decreased at beginning, and once the U_I reached the value of around 10 V their decrease rates became very small. Significantly, the F_n and the F_t were 3.24 N and 2 N, respectively, in CG (U_I=0, $A_{p\text{-}p}$=0), and reduced to 1.3 N and 0.7 N, respectively, in UECG (U_I=12 V, $A_{p\text{-}p}$=8 um), amazing decrease rates of 60 % and 65 %, respectively; whereas this kind of decrease rates owing to UAG (U_I=0V, $A_{p\text{-}p}$=8 um) only or ECG (U_I=12 V, $A_{p\text{-}p}$=0 um) only were 31 % for F_n and 37 % for F_t, indicating that a much greater grinding force decrease rate can be achieved by the synergy effect of the UAG and ECG compared with that by UAG only or ECG only.

Regarding the effect of the f_d on the F_n, F_t in UECG (Fig.3.7 (b)), it is evident that both the F_n and F_t decreased linearly as the f_d increased. However, the duty ratio D had the effect on the grinding forces with different tendency compared with the f_d (Fig.3.7 (c)); both the F_n and F_t decreased before the D reached 20 %, and then turned to increase, implying the D should be set at 20 % for minimizing the grinding forces under the current experimental conditions.

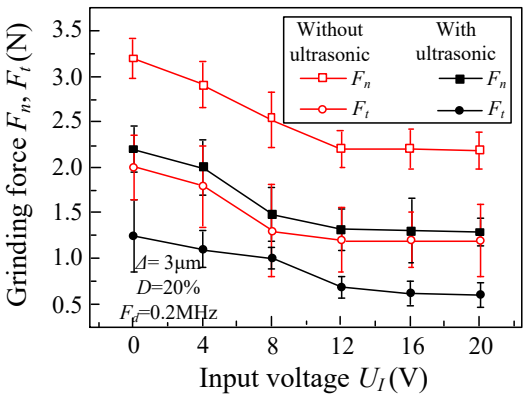

(a)

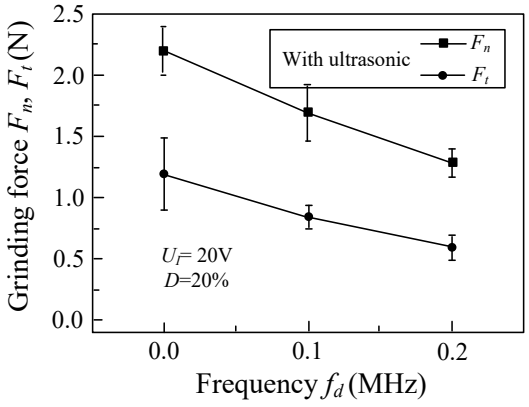

(b)

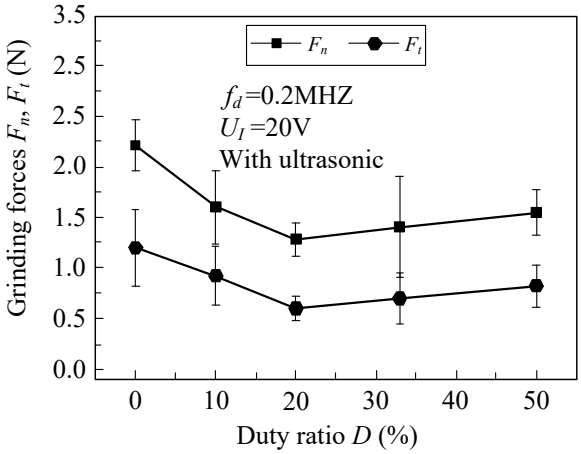

(c)

Fig.3.7 Relationships between the grinding forces and the process parameters

Either the ultrasonic vibration or the electrochemical reaction can decrease the grinding force. Especially, the combination of the two phenomenon decrease the grinding force significantly. For clarifying the respective reasons, first the effect of the ultrasonic only on the grinding force is considered. The present authors stated in their previous work that the tangential grinding force on a single grain, f_g, under the presence of the wheel axial ultrasonic vibration can be determined by Eq.(1)[4].

$$f_g = \frac{k_s \Delta V_w b l_c}{N_g V_g \int_0^{l_c} \sqrt{1+\left(\frac{2\pi A_{p-p} f}{V_g}\cos\frac{2\pi A_{p-p} f}{V_g} x\right)^2}\, dx} \tag{1}$$

Where k_s is the specific grinding force of the workpiece material; N_g is the number of acting abrasive grains; l_c is the contact arc length, x is the location of an abrasive grain in X-direction. It is easy to figure out from Eq.(1) that as long as the ultrasonic is applied, i.e., A_{p-p} >0, the value of f_g will become smaller than that in CG where A_{p-p}=0,

revealing that the grinding force decreases as a result of applying ultrasonic during grinding.

Next the effect of the electrochemical reaction on the grinding force is considered as below. In grinding process, the normal grinding force on a single grain, f_n, can be expressed as [5]:

$$f_n = \frac{1}{2} N_g \xi a_g^2 \tan^2 \frac{\alpha}{2} H_v \tag{2}$$

Where α is the rake angle of the grain cutting edge, a_g is the cutting depth of grain, H_v is the hardness of work-material, and ξ is the geometrical factor of grain. It is obvious that the f_n has a linear relationship with the workpiece hardness, indicating that the harder the work material is, the higher the grinding force gets.

Given that the workpiece hardness affects the grinding force significantly (see Eq.(2)), the dynamic Vickers micro-hardness (DHV) were obtained for work-surfaces by CG (U_I=0 without ultrasonic), UAG (U_I=0 with ultrasonic), ECG (U_I=20 V without ultrasonic) and UAG (U_I=20 V with ultrasonic), respectively, by using Dynamic Ultra Micro Hardness Tester (DUH-211). In measurement, a load of 1 mg was applied for duration of 5s and a Vickers indenter with an included angle of 115° was employed. As a result, the DHV values in CG, UAG, ECG and UAG were 512 HV, 512 HV, 453 HV and 436 HV, respectively, demonstrating that in the case without electrochemical reaction, i.e., in CG and UAG, the DHV was independent of the ultrasonic, and once the electrochemical reaction occurred, the DHV decreased from 512 HV to 453 HV without ultrasonic and further to 436 HV with ultrasonic. These imply that under the presence of electrochemical reaction the work-surface hardness becomes low and the ultrasonic encourages the decrease in the hardness, however under the absence of electrochemical reaction the ultrasonic does not affect the hardness.

On the other hand, according to H. Jamshidi and M.J. Nategh [2], 50–70 percent of the energy is spent to overcome the frictional forces at the tool-chip and workpiece-chip interfaces in grinding process; the TiO_2 layer formed on the work-surface is a well-known lubricating material, implying that the resultant TiO_2 leads to the significant decrease in the tangential grinding force f_t in addition to the reduction in the normal grinding force due to the lower hardness of TiO_2 layer.

In the UAG, the trajectory of a single grain is a spatial sinecure-like as shown in Fig. 3.8 where the grain trajectory in ECG is also displayed for comparison. The

wheel ultrasonic vibration brings a change of the Reynolds number of electrolyte fluid in the range of 100 - 400, resulting in the occurrence of vortex effects in the places where the crest of the sinecure-like trajectory of grain is located [6].

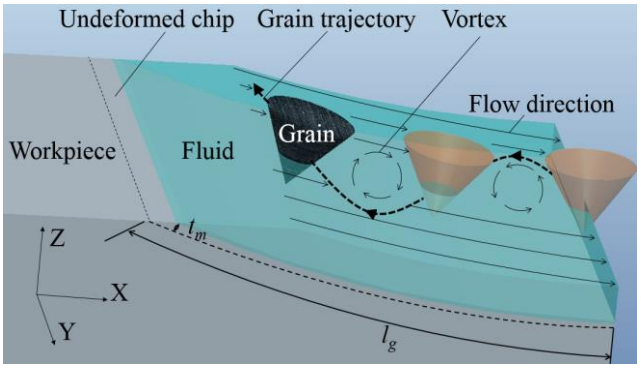

Fig. 3.8 Grain motion trajectory.

The contact arc length between the wheel and the workpiece, l_g, is given by Eq. (4) [7]:

$$l_g = \sqrt{\Delta d_s} \tag{4}$$

where d_s is the diameter of grinding wheel. Meanwhile the ultrasonic vibration wavelength λ is expressed as:

$$\lambda = \frac{1}{f}(V_g + V_f) \tag{5}$$

Consequently, the number of the crests, i.e., the vortexes, generated by a single grain within the grinding zone, N, would be:

$$N = 2\frac{l_g}{\lambda} = 2\frac{f\sqrt{\Delta d_s}}{V_g + V_f} \tag{6}$$

Substituting the process parameters (Table 1) into Eq. (6) yields that the vortex number was 136 in the current work.

O. A. Druzhinin [8] pointed out that the vortex has the ability to unify the ion concentration of electrolyte, and G. Bellanger et al. [9] concluded that the thickness of oxidized layer e depends on the concentration of ion OH^- c_{OH^-}, the diffusion coefficient D_d and the permeability p_m of the electrolyte employed as expressed by Eq. (7)

$$e = D_d c_{OH^-}/p_m \tag{7}$$

Therefore, thicker oxidized layer would be generated in UAG process compared with that in ECG.

In order to confirm the anodization of the work-material, the formed chips were observed with SEM and the weight percentage of the oxygen element on the chip and workpiece were measured. Figs. 3.9(a) and (b) show the SEM images of typical chips formed in ECG and UAG, respectively. It can be observed that the mean size of chips in UAG was larger than those in ECG. The mean areas of chips A_c were quantitatively obtained as exhibited in Fig. 3.9(c), showing the A_c decreased slightly with the increasing U_I. This phenomenon might be caused by the fact that the TiO_2 layer is more brittle and broken easily compared with the original material of Ti-6Al-4V. Besides, the ultrasonic decreased the chip size considerably, a phenomenon certainly occurring in UAG processes [10].

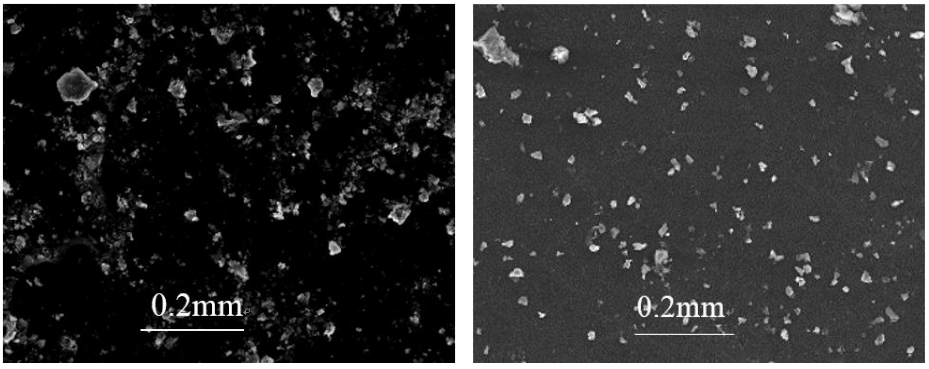

(a) U_I=20V without ultrasonic (b) U_I=20V with ultrasonic

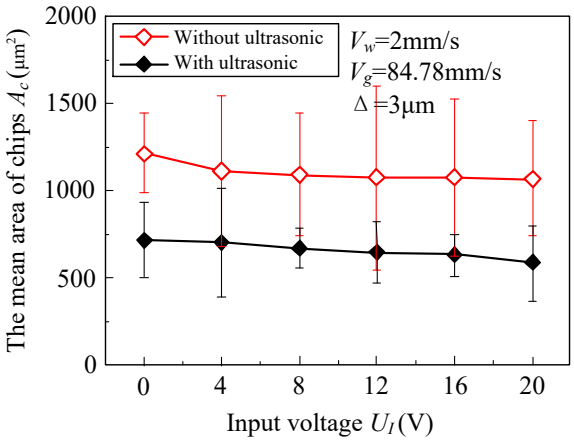

(c)

Fig. 3.9 Variations in mean area of chips A_c with different U_I

Fig.3.10 shows the weight percentages of oxygen on chips and work surfaces obtained at different values of U_I with and without ultrasonic. It can be seen that the percentages on both the chips and work surfaces increased with the increasing U_I either in the presence or in the absence of ultrasonic. In addition, the ultrasonic

distinctly increased the percentages of oxygen, implying that with ultrasonic, thicker TiO_2 lay is formed on the work surface and contributes to the decrease of grinding forces.

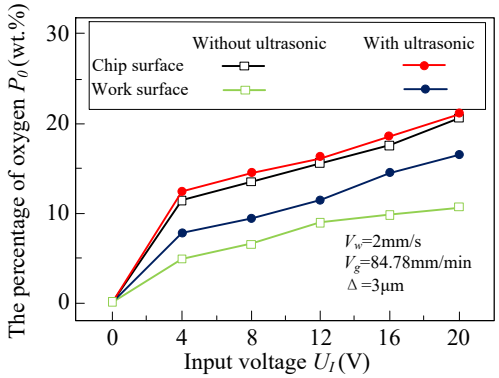

Fig. 3.10 Weight percentages of oxygen elements on chip and work surfaces at different U_I with/without ultrasonication

3.2.4 Work-surface integrity

Next, the effect of process parameters on the work-surface roughness in ECG and UECG are shown in Fig.3.11. It is found that the roughness either in ECG without ultrasonic or in UECG with ultrasonic decreased with the increasing of the U_I. Additionally, it is worth noting that the roughness Ra in UECG was smaller than that in ECG regardless of the value of U_I, meaning the presence of the ultrasonic improves the work-surface quality reasonably. The improvement of surface quality by UECG can be considered to be the contribution of the decreased grinding forces and friction coefficient caused by the formation of electrochemical product (TiO_2) which will be further discussed later.

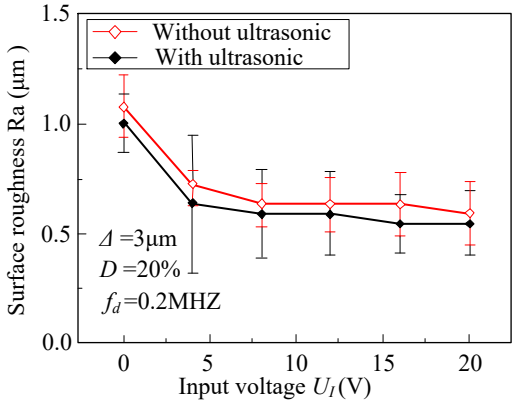

Fig.3.11 Surface roughness rate versus input voltage.

SEM images of the ground work surface are as shown in Figs. 3.12 (a) and (b). It can be observed that the main damages on the work-surface in CG were plastic deformation and crack (Fig. 3.12(a)), whereas in UECG (Fig. 3.12(b)) this kind of damage was not observed. The cross-section profile of the plastic deformation and crack in grinding direction can be illustrated as in Fig. 3.12 (c)); this kind of damage is caused by the residual stresses which are attributed to the fact that the abrasive grain is compressive at beginning, then gradually increasing to become tensile with the progress of grinding action. This trend was observed in the work-surface after CG where the residual stresses are very sensitive to machining parameters [6]. This implies that the grinding force and temperature in UECG are much smaller than those in CG; this issue will be further discussed later.

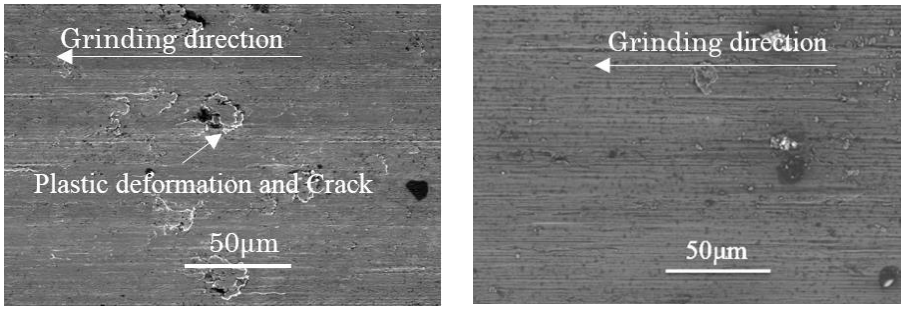

(a) in CG (b) in UECG with U_I=20V

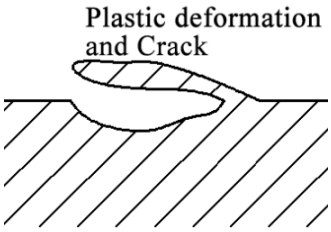

(c) Illustration of the cross section of plastic deformation and crack in grinding direction

Fig. 3.12 SEM images of ground work-surface.

As well known, under the presence of ultrasonic vibration, the wheel axial vibration causes an oscillatory rubbing motion of the grains over the work-surface, removing the material through the overlapping of adjacent grain trajectories. Moreover, due to the more micro-fracture behavior of grains, the number of active grain cutting edges is increased. Consequently, for the sake of the multiplier effect of the two phenomena, the work-surface roughness is decreased. In addition, the TiO_2

generated by the electrochemical reaction can act as a lubricant boundary layer, thus preventing the surface from forming any unwanted damage.

3.2.5 Grinding wheel wear

In order to confirm the merit of the UECG from the viewpoint of the grinding wheel working life, the radial wears of the wheel, Δ_{Rg}, in CG and UECG were experimentally compared. In experiments, the actual value of Δ_{Rg} was attained by measuring the wheel diameters before and after grinding. Fig. 3.13 exhibits the obtained results, showing that the wheel wear in UECG at U_I=20 V was 4 times smaller than CG (U_I=0 without ultrasonic). The higher the value of U_I was, the smaller the amount of wheel wear Δ_{Rg} became, and in the case of U_I<10 V the Δ_{Rg} in UECG with ultrasonic were considerably smaller than that in ECG without ultrasonic. In other words, the effect of the ultrasonic on the wheel wear was little once the U_I has been beyond 10 V.

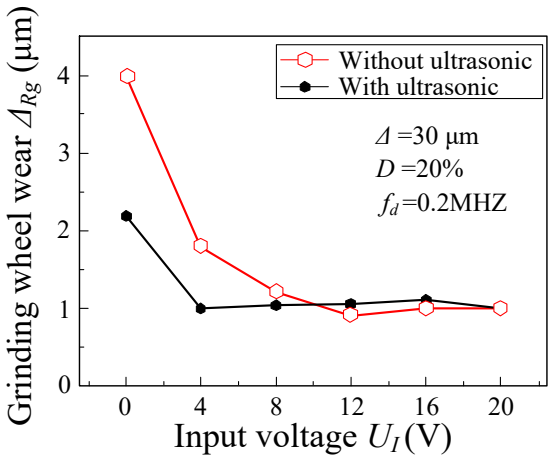

Fig. 3.13 the grinding wheel line wheel and input voltage.

Subsequently, in order to elucidate the wheel wear mechanism the conditions of wheel working surface in CG, ECG and UECG were investigated by SEM observation. For instance, Fig. 3.14 shows the obtained SEM images of typical grain damages on the wheel working surface before and after CG. Comparing the SEM images before and after grinding revealed that the grain damage was dominantly attributed to three different types, i.e., drop out, fracture and chip adhesion. Subsequently the effects of the U_I and the ultrasonic on the number percentage of the damage type, a ratio of the number of grains damaged with the given type in a given

area on the wheel working surface to the total number (50 in the current work) of grains in the same area, were obtained quantitatively to determine which type is the dominant reason for the wheel wear. Obviously as shown in Fig. 3.15, in the case without ultrasonic once the U_I has been applied even at a low value of 4 V the number percentage of the drop out dramatically decreased and gradually continued the decrease with the increase of U_I; amazingly once the ultrasonic has been imposed this type of grain damage disappeared, indicating that the grain drop out does not occur and thus reduce the wheel wear considerably. As for the chip adhesion, its number percentage tended to decrease as the U_I increased either with or without ultrasonic; in particular this percentages in UECG were significantly smaller than those in ECG by 8 %-21 % in the voltage range of U_I =0-20 V. However, the number percentage of grains fracture increased when the ultrasonic has been imposed regardless of the value of U_I.

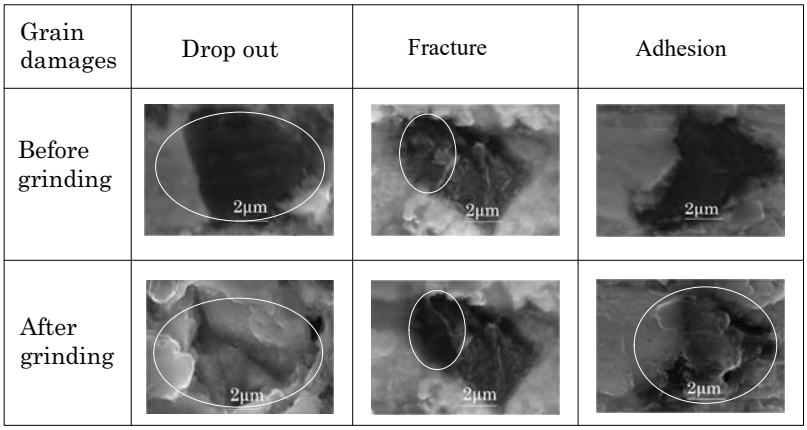

Fig. 3.14 Type of grain damage in CG (U_I=0 V without ultrasonic)

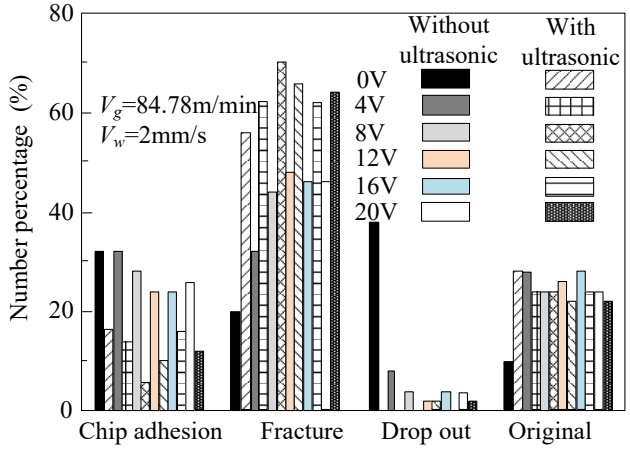

Fig. 3.15 Number percentages of grain damage in CG, ECG and UECG

According to P.D.h.c.m.D.-I.G. Spur, et al. [11], under the presence of ultrasonic the friction and thermal loading are reduced in grinding. In addition, the electrochemical product TiO_2 is also capable of decreasing the friction force. These enhance the grain fracture phenomenon and restrain the grain drop out, eventually result in the increase in the number of active grain cutting edges.

As for the chip adhesion, assuming a chip with a mass of m is adhered to the front face, i.e., the rake face, of the grain cutting edge and motions along with the grain, an inertia force in the wheel axial direction will be caused by the acceleration of the chip according to Newton‟s second law and acts on itself as expressed by Eq. (9)

$$F_V(t) = -m\pi^2 f^2 A_{p-p}\sin(2\pi f t) \tag{8}$$

At any of the sinusoidal peaks of the grain motion, the inertia force reaches maximum, for example, with a value of $3.14^2\times40^2\times4$ m=6,3101 m in the case of f=40 kHz and A_{p-p}=4 μm, meaning the inertia force would reach a huge value of 6439 times as great as chip weight of 9.8 m. This inertia force has non-significant effect on the material removal but help the chips escape from the grain surface because the inertia force acts in a direction opposite to the grain motion direction. In addition, the friction coefficient between grain and chip would be decreased for the sake of the generated TiO_2 layer, leading to not only the difficulty of chip adhesion but also the increase in shear angle which eventually decreases the undeformed chip thickness [12]. As a result, the chip adhesion is lightened and the chip cross section area is decreased once UAG process is performed.

3.4 Summary

In order to develop a novel technique for the high performance machining of difficult-to-machine materials such as Ti-6Al-4V, this paper proposed a hybrid material removal process, i.e., ultrasonic assisted electrochemical grinding (UAG). For confirming the feasibility of the proposed technique, an experimental setup capable of performing UAG process was constructed and fundamental machining characteristics of UAG in the grinding of Ti-6Al-4V were investigated followed by discussion. The obtained result can be summarized as following.

(1) Under the given ranges of the voltage U_I, the frequency f_d and the duty ratio D of the pulse electrolytic power in the current work, i.e., U_I=0~20 V, f_d=0~0.2 MHz, D=0~50 %, the lowest normal and grinding forces, F_n and F_t, in UAG were attained at U_I =20 V, D=20 % and f_d=0.2 MHz which were smaller than those in

CG (conventional grinding at U_I=0 V without ultrasonic) by around 60 % and 65 %, respectively.

(2) The work-surface roughness in UAG decreased with the increasing U_I; once the ultrasonic is stopped and the conventional electrochemical grinding (ECG) is performed, the roughness increased by a certain value regardless of the value of U_I. The plastic deformation and cracks which are often generated on the work-surface in CG were not observed in UAG.

(3) The wheel radius wear Δ_{Rg} in UAG decreased as the value of U_I increased when U_I<4 V, thereafter was almost kept constant; in the case of U_I<10 V the Δ_{Rg} in UAG were considerably smaller than that in ECG. The wheel wear in CG was attributed dominantly to the grain drop out, whereas in ECG and UAG the wheel working lives were affected dominantly by the chip adhesion and the grains fracture, respectively.

(4) A titanium dioxide (TiO_2) layer of 78 nm in thickness was actually generated on the work-surface by the electrochemical reaction at U_I=20 V, and thus the Vickers micro-hardness of work-surface decreased from 512 HV in CG and UAG to 436 HV in UAG, a reduction by 15 %. This would be one of the reasons why the grinding forces in UAG were significantly smaller than those in CG, UAG and ECG.

(5) The weight percentages of oxygen element on chips and work surfaces increased as the U_I increased either in ECG or in UAG and the ultrasonic enhanced the percentages of oxygen, implying that with ultrasonic, thicker TiO_2 lay is formed on the work surface and contributes to the decrease of grinding forces.

Reference

[1] V. Zwilling, M. Aucouturier, E. Darque-Ceretti, Anodic oxidation of titanium and TA6V alloy in chromic media. An electrochemical approach, Electrochimica Acta, 1999; 45 :921-930.

[2] J. H., N.M. J., Theoretical and experimental investigation of the frictional behavior of the tool–chip interface in ultrasonic-vibration assisted turning, International Journal of Machine Tools and Manufacture, 2013;65:1-7.

[3] S.Y. Hong, I. Markus, W.-c. Jeong, New cooling approach and tool life improvement in cryogenic machining of titanium alloy Ti–6Al–4V, International Journal of Machine Tools & Manufacture, 2001; 41 :2245-2260.

[4] Y.B. Wu, M. Nomura, Z.J. Feng, M. Kato, Modeling of Grinding Force in Constant-depth-of-cut Ultrasonically Assisted Grinding, Materials Science Forum, 2004;471-472:101-107.

[5] X. Xiao, K. Zheng, W. Liao, H. Meng, Study on cutting force model in ultrasonic vibration assisted side grinding of zirconia ceramics, International Journal of Machine Tools and Manufacture, 2016;104:58-67.

[6] E.M. Alawadhi, Numerical Simulation of Fluid Flow Past an Oscillating Triangular Cylinder in a Channel, Journal of Fluids Engineering, 2013;135 :1-10.

[7] M.C. Shaw, Principles of abrasive processing, Bookcaft (Bath)Ltd Midsomer Norton, Great Britain, 1996.

[8] O.A. Druzhinin, Concentration waves and flow modification in a particle-laden circular vortex, Physics of Fluids, 1994;6:3276.

[9] G. Bellanger, J.J. Rameau, Tritium recovery from tritiated water by electrolysis, Fusion Science and Technology, 2015;22:296-308.

[10] S. Agarwal, P.V. Rao, Experimental investigation of surface/subsurface damage formation and material removal mechanisms in SiC grinding, International Journal of Machine Tools and Manufacture, 2008;48 :698-710.

[11] P.D.h.c.m.D.-I.G. Spur, D.-I.S.-E. Holl, Ultrasonic assisted grinding of ceramics, Journal of Materials Processing Technology, 1996;62:287-293.

[12] K.K. Singh, V. Kartik, R. Singh, Modeling dynamic stability in high-speed micromilling of Ti–6Al–4V via velocity and chip load dependent cutting coefficients, International Journal of Machine Tools and Manufacture, 2015;96:56-66.

This page intentionally left blank.

Chapter 4 Machining characteristics of the UPOG of difficult-to-machine materials

4.1 Introduction

Ti-6Al-4V is considered to be among the most promising engineering materials across a range of application sectors. Because of its unique combination of high strength-to-weight ratio, melting temperature, and corrosion resistance, interest in the application of Ti-6Al-4V to mechanical and tribological components is growing rapidly in a wide range of industries [1]. However, it is classified as extremely difficult-to-machine material, owing to several inherent properties: low thermal conductivity, high specific strength, and exceptional resistance to corrosion [2]. Currently, most Ti-6Al-4V products are fabricated by precision casting first, followed by machining operations to remove excess material [3]. To improve surface quality and form/dimensional accuracy, machined parts need to be ground. During grinding, each of the abrasive grains removes a small amount of material from the workpiece. This removal mode contributes to improving the work-surface finish and form/dimensional accuracy. However, titanium alloys are generally known for their poor grindability, resulting in high costs and low efficiency with respect to the current grinding methods [4].

One way to increase grinding efficiency is to utilize ultrasonic-assisted grinding (UAG). This technique has attracted significant attention for decades because its smaller grinding force, higher material removal rate, longer grinding wheel working life, and lower grinding heat generation, which are achieved by a fundamental alteration in process kinematics [5]. Mohsen Ghahramani Nik et al. [6] found that a higher depth of cut and feed rate can be selected in the UAG of Ti-6Al-4V compared

to conventional grinding (CG), and superior surfaces can still be obtained by applying vibration on the workpiece in the feed direction. Pujana et al. [7] showed that lower feed forces and higher processing precision were achieved when ultrasonic vibration was superimposed on the drilling samples of Ti-6Al-4V. Further, rotary ultrasonic machining of brittle materials and titanium was studied experimentally and theoretically by Qin et al. [8].

Another way to increase grinding efficiency is to soften the work surface and then remove the softened layer using the cutting action of grains. Plasma electrolytic oxidation (PEO) is widely used to soften work surfaces by oxidizing the work materials. The oxidized layer would be much softer than the original material [9].

In particular, Dang Van Thanh et al. found in their work on the preparation of graphene sheets using electrochemical discharge [10] that the ultrasonic vibration of a cathode can strengthen the plasma electrolysis phenomenon. This is achieved by the breaking of van der Waals bonds, which increases the synthesis efficiency of graphene. This implies that the PEO phenomenon would be promoted by the ultrasonic vibration. However, no studies have been reported so far on grinding processed with the assistance of both ultrasonic vibration and PEO. Consequently, a hybrid process is proposed in this study to further improve the grindability of the titanium alloy Ti-6Al-4V. In the developed method, a PEO process is added to the UAG process, hereafter referred to as ultrasonic-assisted plasma oxidation grinding (UPOG). After the processing principle of UPOG and the experimental details have been introduced, the experimental results are described. Then, the discussion of the results is presented, and the feasibility of using UPOG for the improvement in grindability of Ti-6Al-4V is confirmed.

4.2 Machining principle and kinematic characteristics

4.2.1 Operation principle

Fig.1 shows the schematic of the processing principle of UPOG. A metal-bonded grinding wheel vibrating ultrasonically on its own axis at a frequency of f and a peak-peak amplitude of $A_{p\text{-}p}$ is rotated clockwise at a peripheral speed of V_g, and a workpiece is fed to right at a feed rate of V_w to perform an up-cut UAG operation. In

the grinding zone with a wheel-workpiece contact length of l_g, the grain depth of cut would gradually increase from zero to the maximum value, t_m, and then begin to decrease rapidly, eventually returning to zero. Let the grinding wheel be the cathode and the workpiece be the anode. Thus, the grinding wheel and the workpiece have a zero and positive charge, respectively. A thin oxidized layer is formed on the largest surface of the workpiece in the grinding zone by PEO. Then, the weakened thin layer is easily removed by the abrasive grains that move along with the peripheral surface of the rotating grinding wheel.

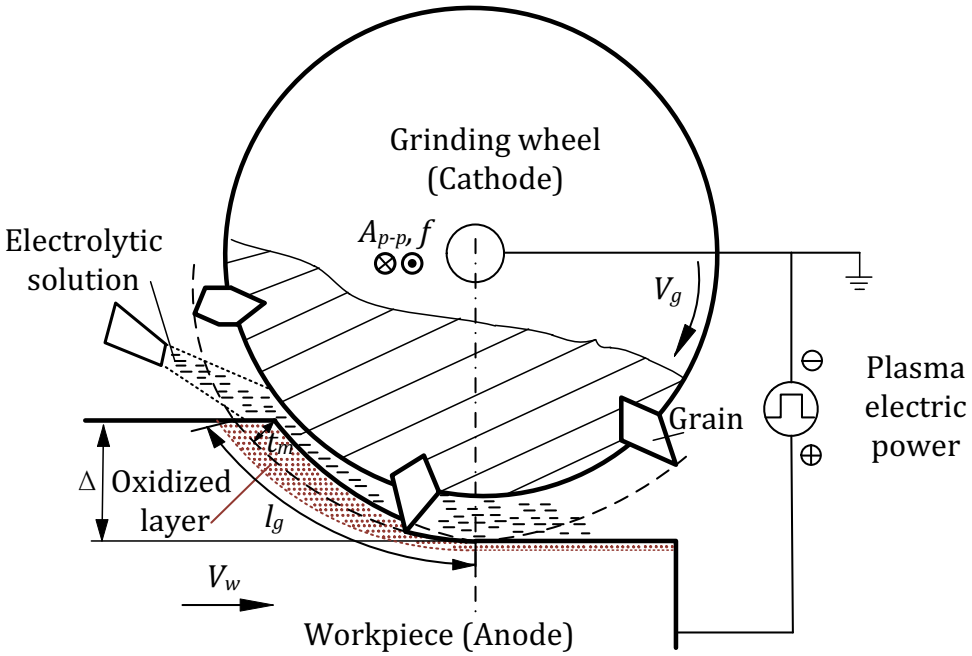

Fig 4.1. Schematic illustration of the processing principle of UPOG.

4.2.2 Kinematic characteristics

To facilitate the understanding, the grinding process of a single grain was chosen to study. During the single grain grinding process, the grain and the workpiece were treated as the two absolute rigid bodies. The arc length of contact between the grain and the workpiece was the geometric contact arc length l_g. According to the general grinding theory [11], l_g could be described by Eq. 9:

$$l_g = \sqrt{\Delta d_s} \tag{9}$$

where d_s was wheel. Meanwhile, the ultrasonic vibration wavelength λ could be

expressed as:

$$\lambda = \frac{1}{f}(V_g + V_f) \tag{10}$$

Therefore, the assume number of ultrasonic vibration wave was N, it could be described by Eq. 11:

$$N = \frac{l_g}{\lambda} = \frac{f\sqrt{\Delta d_s}}{V_g + V_f} \tag{11}$$

Subsequently, substituting the data shown in Table 1 and the values of Δ, ds, f, V_g and V_w shown in Table 1 into Eq.(4) yielded the N≈34. In order to study the effect of the ultrasonic vibration on concentration, vortex shedding formed two times after each cycle of oscillating [12]. Therefore, in our study the vortex number in single grinding grain was 78. And the number of pulsed discharge times N_d could be calculated by Eq.12:

$$N_d = \frac{f_d}{f} N = 170 \tag{12}$$

The discharge number was close to vortex number. This was the main difference between UACG and ECG. The details were discussed as follows.

First, the ultrasonic vibration charged the conservation of reacting electrolyte. The conservation equations for the fluid momentum and mass were described by Eq. 6 and 7. [13]

$$(1-c)\rho_f \frac{D\boldsymbol{U}}{D_t} = -\boldsymbol{\nabla} p + (1-c)\rho_f \boldsymbol{g} - c\boldsymbol{F} \tag{13}$$

$$\frac{\partial_c}{\partial_t} - div(1-c)\boldsymbol{U} = 0 \tag{14}$$

It was assumed the flow considered was regular and of a high Reynolds number, c was the concentration, $\boldsymbol{F}$ was the force acting on the ion from the ambient fluid specified below, g was the gravity acceleration, ρ_f was the density of fluid and assumed to be a uniform constant, $\boldsymbol{\nabla}$ was the nabla operator, here used to represent the pressure p, $\boldsymbol{U}$ was gradients of the velocity.

In this paper, the grain velocity in CG Vg =84.78 m/min had been already known as exhibited in Table 1 and the grain velocity in UACG $84.78 \leqslant V_U \leqslant 103.2$ m/min was calculated by differentiating Eq. (1) with respect to time t. Meanwhile the material properties of electrolyte did not charge by UECG. Therefore, the $\boldsymbol{U}$ in UECG was larger than ECG and the charge of c could be faster.

4.3 Experimental setup and procedure

Figs. 4.2(a) and (b) show the schematic of the experimental setup and a photograph of the main portion of the setup constructed, respectively. A commercially available ultrasonic spindle (R2 by Industrial Co., Ltd., Japan) capable of vibrating axially at f = 40 kHz and $A_{p\text{-}p} \leq 4$ μm was installed on a 3-axis CNC machine tool (Multi Pro 3 by Takashima Sangyo Co., Ltd., Japan). On the lower end of the spindle, a metal-bonded #1000 cBN grinding wheel of diameter d_s = 1.8 mm was fixed. A nozzle was employed to supply the electrolyte solution to the grinding zone. A Ti-6Al-4V specimen (L14 × W10 × T6 mm) was used as the workpiece and was held on the work-table of the machine tool using a 3D-dynamometer (9254 by Kistler Co., Ltd.) and a work-holder. A plasma power supply, composed of a high frequency switch and a DC power source, was employed to induce plasma oxidation between the electrodes. The anode output of the power supply was connected to the work-holder directly, whereas the cathode output was connected to the spindle though a spring/carbon brush mechanism.

Surface grinding experiments were conducted under the conditions listed in Table 4.1. Typically, cBN abrasives require a cutting speed of over 50 m/min when grinding Ti-6V-4Al [11]. The purpose of the experiment is to confirm the feasibility of the proposed UPOG method and elucidate its fundamental machining characteristics in the grinding of Ti-6Al-4V. The values of V_g, Δ, and V_w were all kept constant at 84.78 m/min, 3 μm, and 2 mm/s, respectively, based on the specifications of the experimental setup used in this study. The wave pattern of the pulse electric power was set as triangular, and its frequency, f_d, and duty ratio, D, were kept constant at 0.2 MHz and 20 %, respectively. Its voltage, U_I, was set to a range of 0–160 V to generate plasma with different strengths. The UPOG of Inconel 718 was also selected as work material.

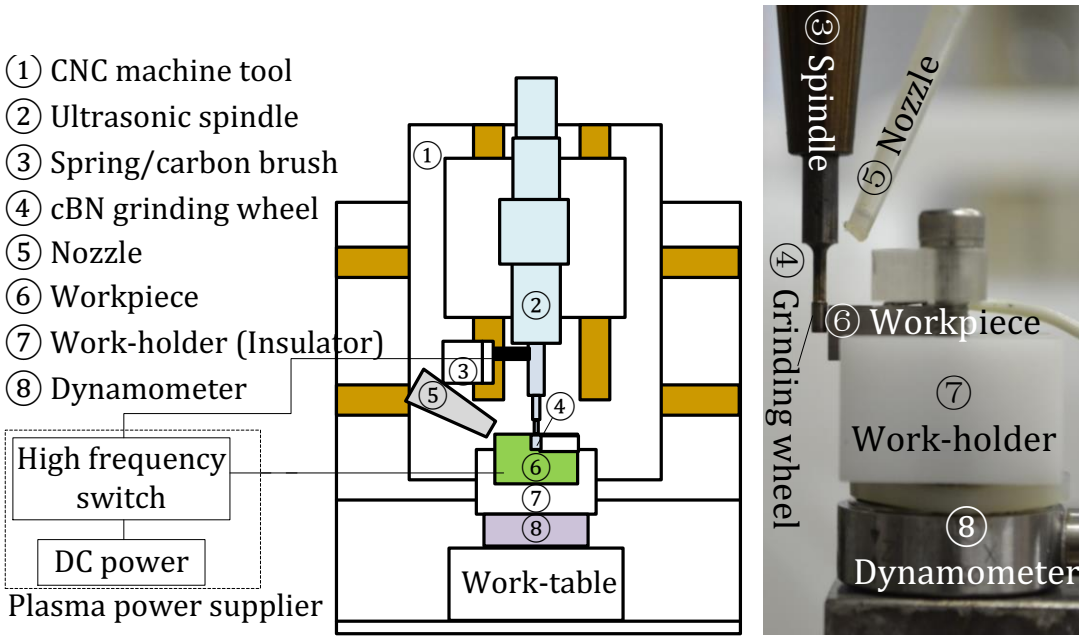

(a) (b)

Fig 4.2. Schematic of experimental setup (a) and a photograph of the main portion of experimental setup (b).

Table 4.1 Experimental conditions

Ultrasonic vibration	Frequency f	40 kHz
	Amplitude $A_{p\text{-}p}$	4.0 μm
Grinding wheel and process parameters	cBN1000N100M	
	Diameter d_s	1.8 mm
	Peripheral speed V_g	84.8 m/min
	Depth of cut Δ	3 μm
	Grinding width b	2.5 mm
	Feed rate V_w	2.0 mm/s
Workpiece	Inconel718, Ti-6Al-4V(L14×W10×T6 mm)	
Plasma electric power supplying	Pattern	Triangle
	Plasma voltage U_I	0~160 V
	Pulse frequency f_d	0.2 MHz
	Duty ratio D	20 %
Electrolytic solution	KNO_3 solution, 5 %dilution	

In these experiments, conventional grinding (CG) operations (U_I = 0 V, $A_{p\text{-}p}$ = 0 μm) were also carried out for comparison. In each grinding test, the grinding forces

were measured with the 3D-dynamometer, and the ground work-surface was characterized by measuring its roughness using a laser scanning microscope (VK-9700 by KEYENCE Co., Ltd with a measurable area of 520 × 700 μm^2) and by observing its topography using a scanning electron microscope (ERA-8900 by ELIONIX Co., Ltd.).

4.4 Experimental results and discussions

4.4.1 Plasma oxidation test of Ti-6Al-4V

Consequently, the formation of the oxidized layer on the largest surface of the workpiece by PEO was experimentally confirmed, and the Vickers microhardness of the oxidized layer was investigated. For this purpose, Ti-6Al-4V work samples were first oxidized by PEO at different values of U_I with or without ultrasonic vibration. In PEO, the grinding wheel was replaced with a rod-shaped Cu cathode, 1.8 mm in diameter, and a gap of 7 μm was given between the cathode and the anode (work sample). The cathode was rotated at 15,000 rpm and fed leftward at a feed rate of 2.0 mm/s for a stroke of 10 mm. Then, the work-surfaces oxidized under different values of U_I with or without ultrasonic vibration were optically observed, and the Vickers hardness of the oxidized work samples was measured by using a dynamic ultra micro hardness tester (DUH-211).

Figs. 4.3(a) and (b) show the optical images of the work-surfaces oxidized at different values of U_I without and with ultrasonic vibration, respectively. Evidently, the value of U_I significantly affected the color of the work-surface, implying that the thickness or hardness of the oxidized layer would be different at different values of U_I; however, a small difference between the colors of the work-surface with and without ultrasonic vibration can be observed. Subsequently, the dynamic Vickers microhardness (DVH) of the oxidized work-surfaces was obtained and is shown in Fig.4.4. It can be seen from the figure that regardless of the value of U_I, the DHV of the surfaces subjected to ultrasonic vibration was lower than those without ultrasonic vibration, implying that ultrasonic vibration promoted the PEO. This finding correlates with the findings of the study conducted by Dang Van Thanh, et al. wherein they revealed that the ultrasonic vibration of the electrode can break the van der Waals bonds and strengthen the plasma electrolysis phenomenon [10]. As for the

effect of U_I on the DHV, once the plasma voltage was applied, the hardness decreased. Under the presence of ultrasonic vibration, the DHV decreased from 512 HV at U_I =0 V to 312 HV at U_I =80 V, a decrease of 39 %. Comparing this phenomenon to that in Fig.3 (b) demonstrated that the PEO benefitted from the reduction in grinding forces. However, when U_I was beyond 100 V, the plasma discharge intensity became higher locally [14], which resulted in the formation of melt-quenched, high-temperature oxides on the work-surface. The formed oxides are analogous to TiO_2 ceramic sintering [9], eventually increasing the DHV in UPOG from 320 HV (U_I = 80 V) to 400 HV (U_I = 160 V).

The effects of the ultrasonic vibration and PEO on the integrity of the work-surface are also considered. It is well known that wheel axis vibration causes an oscillatory rubbing motion of the grains over the work-surface, removing the material through the overlapping of adjacent grain trajectories. Moreover, because of the more microfracture behavior of grains, the number of active grain cutting edges is increased. Consequently, for the sake of the multiplier effect of the two phenomena, the work-surface roughness is decreased. On the other hand, as R.M. Arunachalam, et al. explained in their work on the machining of age-hardened Inconel 718 [15], the grain-induced stress in CG is compressive in the beginning; then, it gradually increases to become tensile as grinding action progresses, resulting in the formation of residual stresses that are very sensitive to machining parameters. This eventually leads to plastic deformation and fractures in the work-surface in CG and UAG (Fig.4). In contrast, the oxidized layer is softer and more ductile in POG and UPOG than the original Ti-6Al-4V material [9], and thus, the grindability is significantly improved. This eventually decreases the occurrence of work-surface damage and improves work-surface integrity. However, when U_I exceeded 100 V, the higher local plasma discharge intensity resulted in the formation of oxides that can easily break down [16] and eventually deteriorate work-surface integrity.

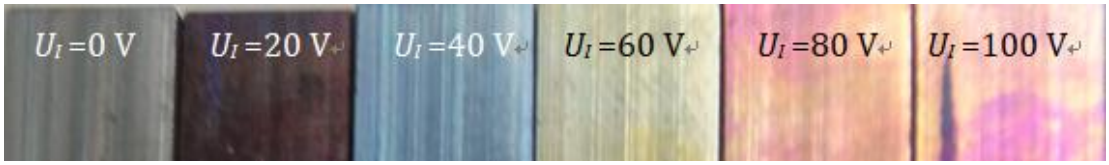

(b) Without ultrasonic

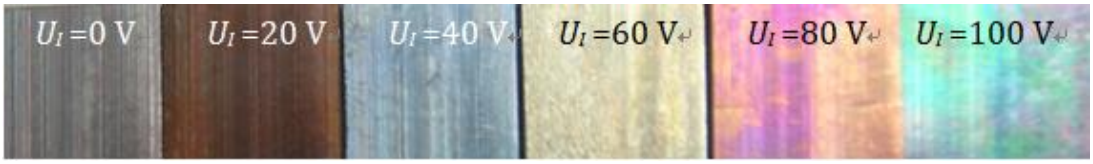

(b) With ultrasonic

Fig 4.3. Optical images of oxidized workpiece surface.

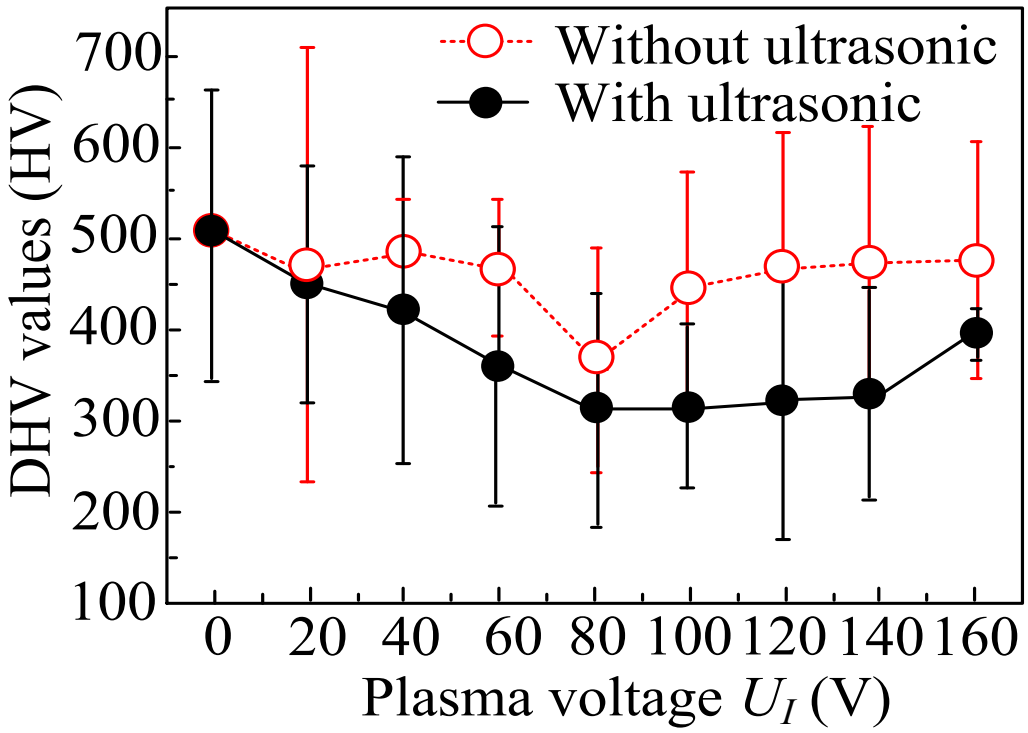

Fig 4.4. Relationship between microhardness and plasma voltage.

4.4.2 Grinding forces of Ti-6Al-4V

The grinding forces were measured at different values of U_I with and without ultrasonic vibration. Fig.4.5 (a) shows the variations of the normal and tangential grinding forces, F_n and F_t, during grinding typically obtained in CG (U_I = 0 V, $A_{p\text{-}p}$ = 0 μm) and UPOG (U_I = 100 V, $A_{p\text{-}p}$ = 4 μm). It can be seen from the figure that in both the processes, the grinding forces fluctuated during grinding. This is mostly likely due to the forced vibration of the setup, but their mean values, i.e., $\overline{F}_{n\text{-}CG}$, $\overline{F}_{t\text{-}CG}$, $\overline{F}_{n\text{-}UAPOG}$, and $\overline{F}_{t\text{-}UAPOG}$, were stable. In particular, it was observed that the mean values in UPOG, i.e., $\overline{F}_{n\text{-}UAPOG}$ and $\overline{F}_{t\text{-}UAPOG}$, were considerably smaller than those in CG ($\overline{F}_{n\text{-}CG}$ and $\overline{F}_{t\text{-}CG}$) by 60 % and 70 %, respectively.

Subsequently, the effects of the plasma voltage, U_I, and the ultrasonic vibration on

the mean grinding forces, $\overline{F}_n$ and $\overline{F}_t$, were obtained as shown in Fig.4.5 (b). Obviously, all the force components exhibited a similar variation tendency as U_I increased. First, in CG (U_I = 0 V without ultrasonic vibration), $\overline{F}_n$ = 3 N and $\overline{F}_t$ = 2 N. Once ultrasonic vibration was applied to perform UAG (U_I = 0 V with ultrasonic vibration), the values of $\overline{F}_n$ and $\overline{F}_t$ were reduced by 33 % and 40 % to 2 N and 1.2 N, respectively. Then, as the plasma electric power was applied to perform plasma oxidation grinding (POG) (20 V ≤ U_I ≤ 160 V without ultrasonic vibration) and UPOG (20 V ≤ U_I ≤ 160 V with ultrasonic vibration), $\overline{F}_n$ and $\overline{F}_t$ decreased as U_I increased until 40 V was observed in all the force components. However, once U_I was beyond 100 V, the mean forces increased rapidly, implying that U_I should be set in the range of 40–100 V to minimize the grinding forces under the current experimental conditions.

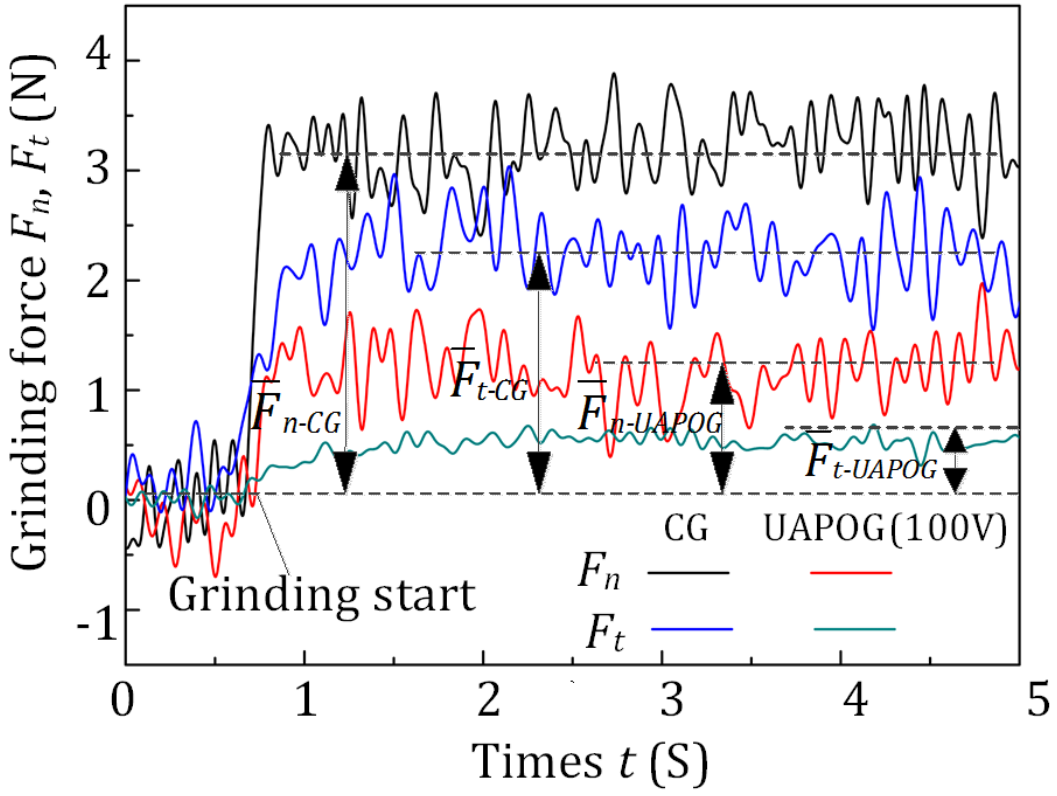

(a)

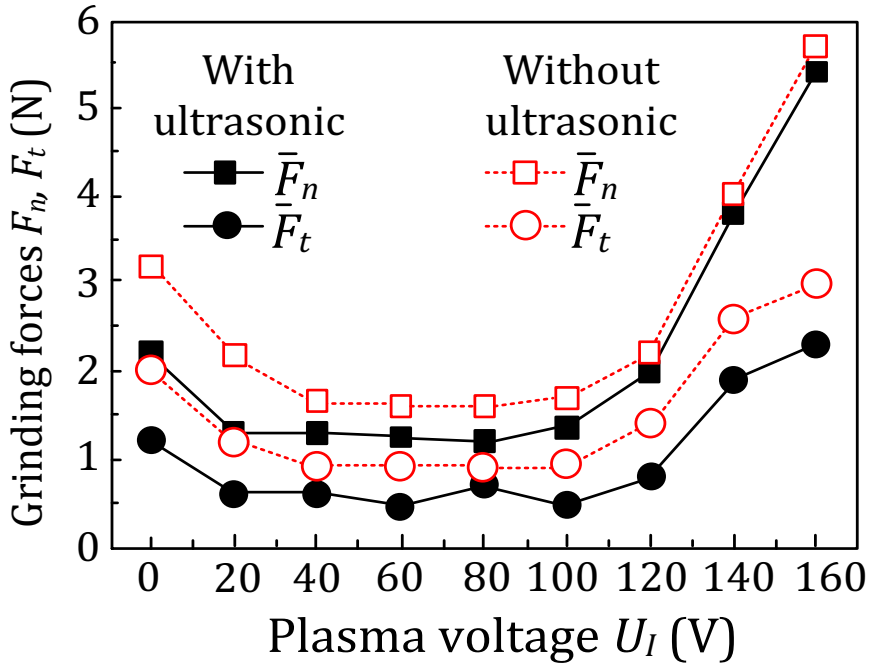

(b)

Fig 4.5. Relationship between the grinding forces and plasma voltage.

The effects of the plasma voltage and ultrasonic vibration on the work-surface integrity were investigated as well. Figs. 4.6(a) through (f) show the SEM images of typical work-surfaces ground by CG, UAG, POG (U_I= 100 V and 160 V), and UPOG (U_I= 100 V and 160 V), respectively. In CG (Fig. 4.6(a)), both plastic deformation and fractures can be observed on the work-surface, and in UAG, fractures only occurred on the ground work-surface (Fig.4.6(b)). On the other hand, once the plasma voltage of U_I= 100 V is supplied, either in POG (Fig.4.6(c)) or in UPOG (Fig.4.6(e)), only a minor damage is observed on the work-surfaces. However, when the plasma voltage was elevated to U_I= 160 V, the work-surfaces became jagged after grinding, with (Fig.4.6(f)) or without (Fig.4.6(d)) ultrasonic vibration. The reason for this phenomenon will be discussed later.

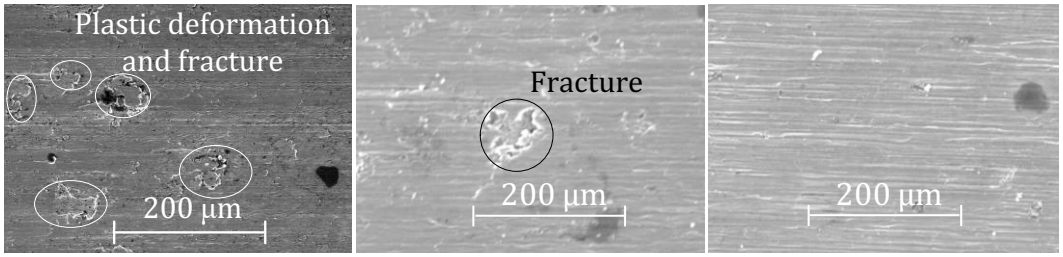

(a) CG (b) UAG (c) POG (U_I=100V)

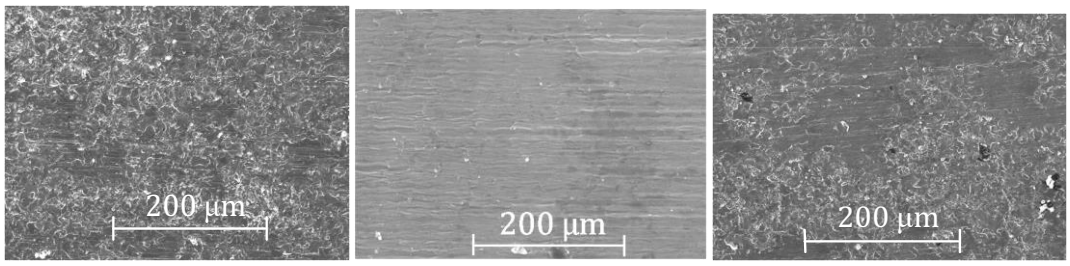

(d) POG (U_I=160 V) (e) UPOG (U_I=100 V) (f) UPOG (U_I=160 V)

Fig 4.6. SEM images of work surfaces obtained in various processes.

4.4.3 Chips deformation of Ti-6Al-4V

The mean area of chip at different plasma voltage with/without ultrasonic were obtained as shown in Figs.4.7, where the error bars indicate the size variations of 50 chips in the corresponding test with the same grinding conditions. It is evident in Fig.4.4 that both the mean area of 50 chips was decreased monotonously with ultraconic. Shifting the attention to the effect of the plasma voltage revealed that the mean area of chip either in UAG or in CG decreased slightly with the increasing plasma voltage; however, the plasma voltage is larger than 140 V the mean area of chip increased with plasma voltage increase. In a word, the chip size is distinctly affected by the ultrasonication and plasma voltage was observed. It is further worthy to note that the cross-section area of chips became increased when U_I is larger than 140 V.

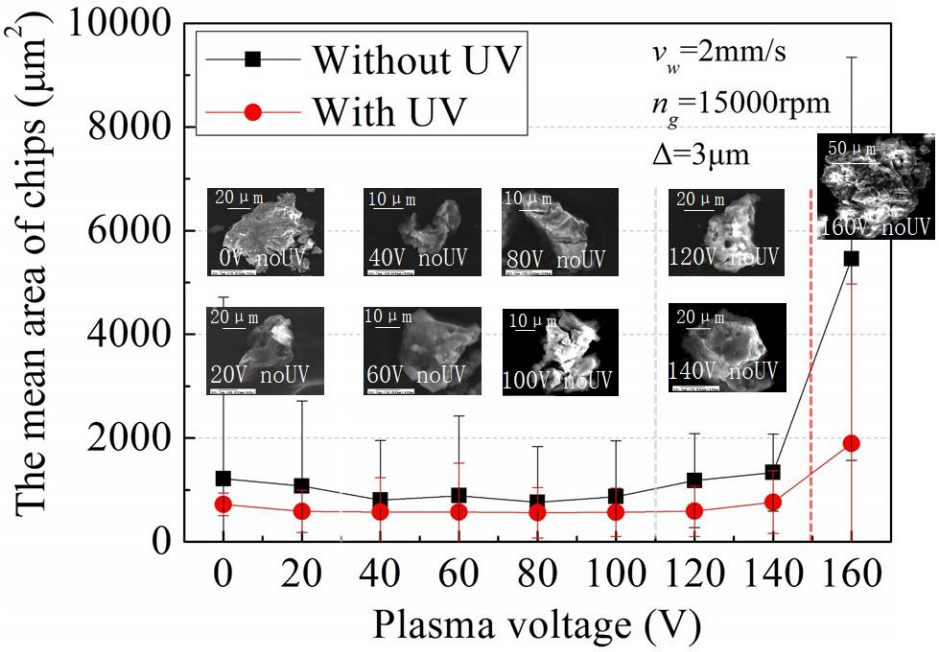

Fig. 4.7 Effects of plasma voltage and ultrasonic on chip size

4.4.4 Grinding efficiency of Ti-6Al-4V

To investigate the grinding efficiency of the UPOG process, actual removal ratio $\eta=\Delta_r/\Delta$, where Δ_r is the material removal depth, Δ is setting depth of grinding, are studied. As shown in Fig. 4.8, η shows a slow increasing trend both in POG and UPOG with voltage increase. Further, grinding ratio is the ratio of the volume of ground material removed from the workpiece to the volume removed from the grinding wheel. As shown in Fig 4.9, the grinding ratio G is increased with the increasing of input voltage. It is further worthy to note that with ultrasonic vibration the grinding ratio is higher than without ultrasonic vibration.

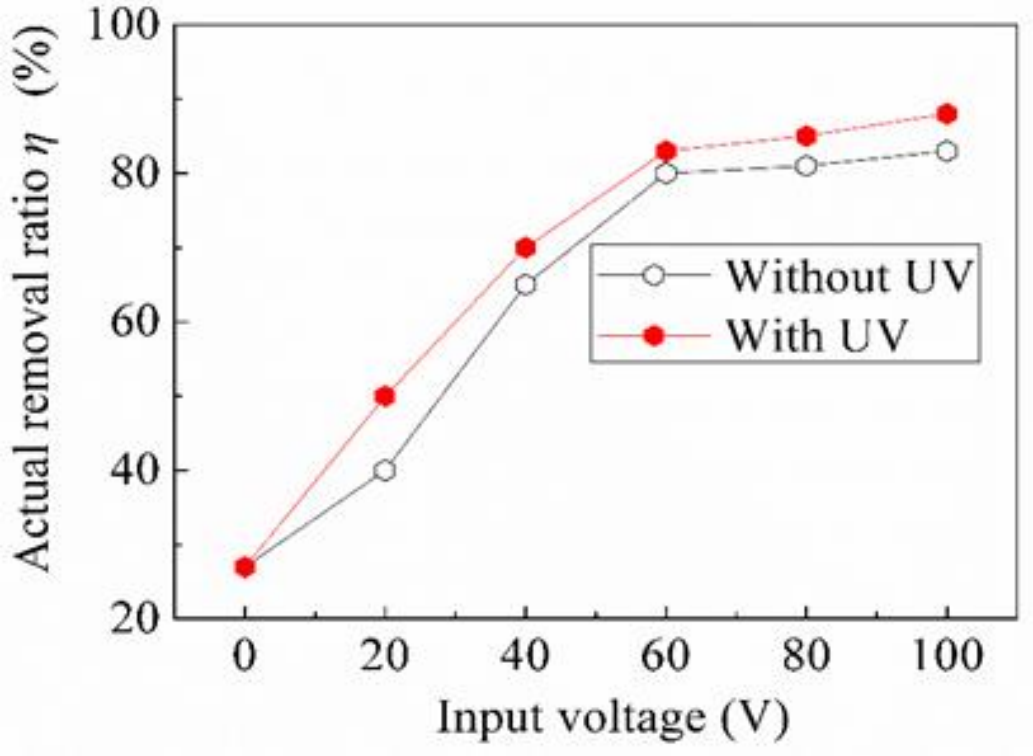

Fig.4.8 Effect of input voltage on actual removal ratio with/without ultrasonication.

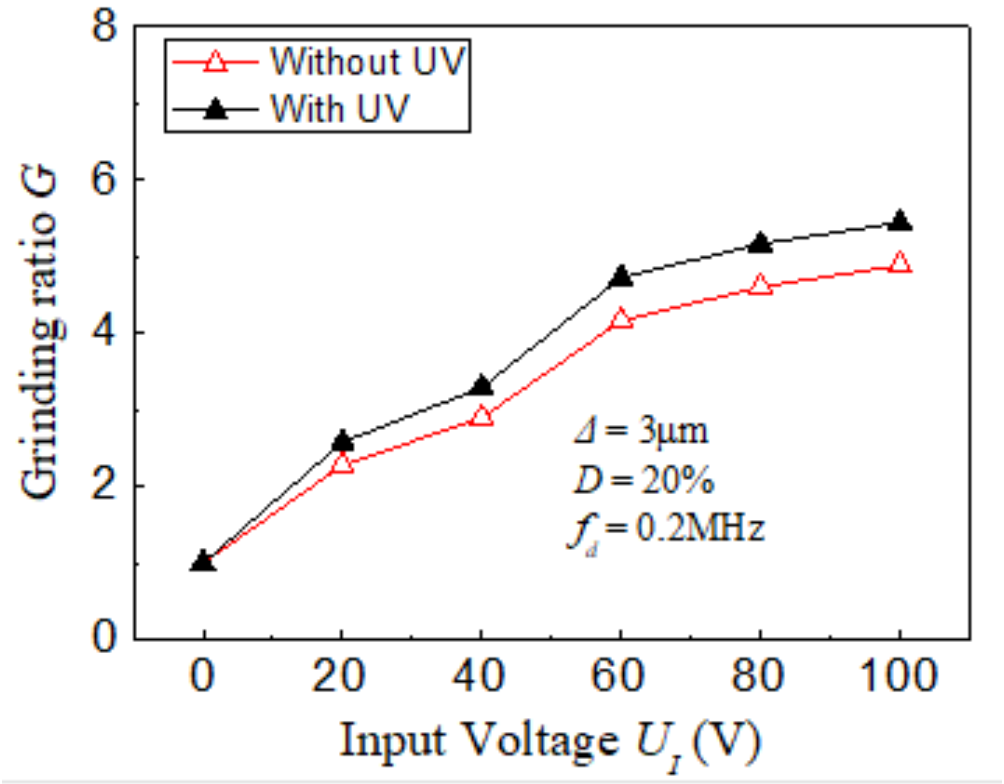

Fig.4.9 Effect of input voltage on grinding ratio with/without ultrasonication.

4.4.5 UPOG of Inconel 718

In Charpter 4.4.1 to 4.4.4, it has been confirmed that the Ti-6Al-4V can be machined well by the UPOG. However, in aeronautical materials not only Ti-6Al-4V but also Inconel 718 need to be effectively machined. For this purpose, the UPOG of Inconel 718 were carried out.

First, the optical images of the Inconel 718 work-surfaces oxidized at different values of U_I without and with ultrasonic vibration, respectively. First, no difference between the colors of the work-surface with voltage change can be observed with U_I $\leqslant$100V. When U_I is higher than 100 V the surface layer is turn to yellow. Evidently, this change implying that the thickness or hardness of the oxidized layer would be different at high value of U_I. Subsequently, the hardness of the oxidized work-surfaces was obtained and is shown in Fig.4.10. It can be seen from the figure that regardless of the value of U_I, the hardness of the surfaces subjected to ultrasonic vibration was no different with those without ultrasonic vibration, implying that ultrasonic vibration hardly change the oxidation process of Inconel 718.

Subsequently, the effects of the plasma voltage, U_I, and the ultrasonic vibration on the grinding forces, F_n and F_t of Inconel 718 were obtained as shown in Fig.4.11. Obviously, F_n decreased with U_I increased, when U_I is higher than 100 V. Then, as the F_n turn to stable with U_I increase ever with or without ultrasonic vibration. And there is a small change can be found in F_t.

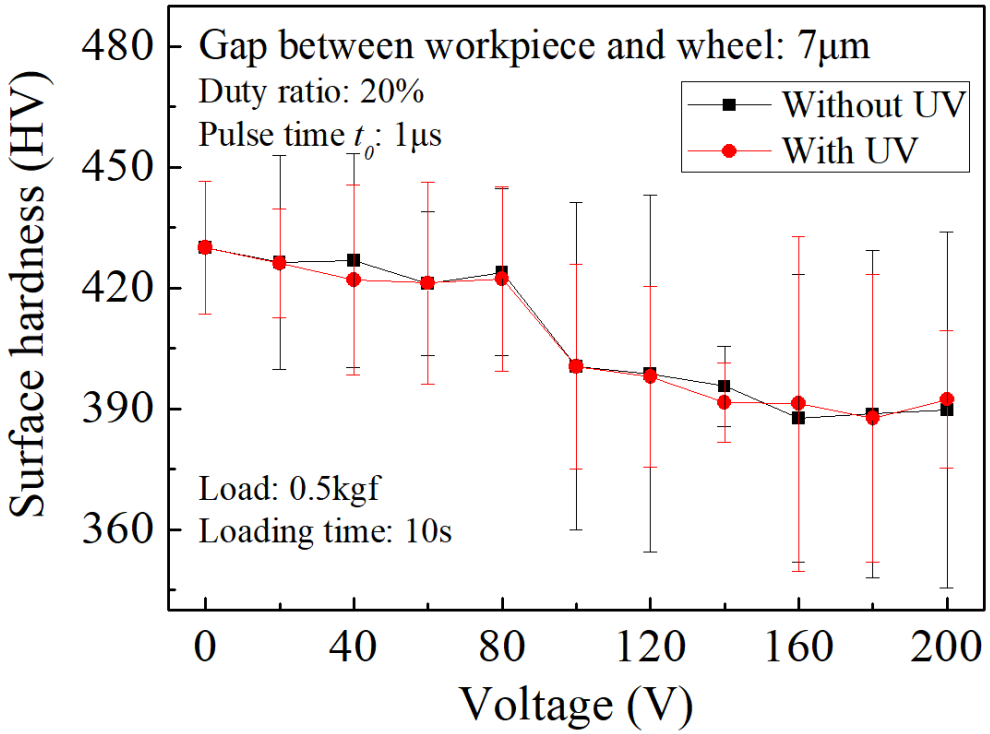

Fig.4.10 Effect of input voltage on surface hardness with/without ultrasonication.

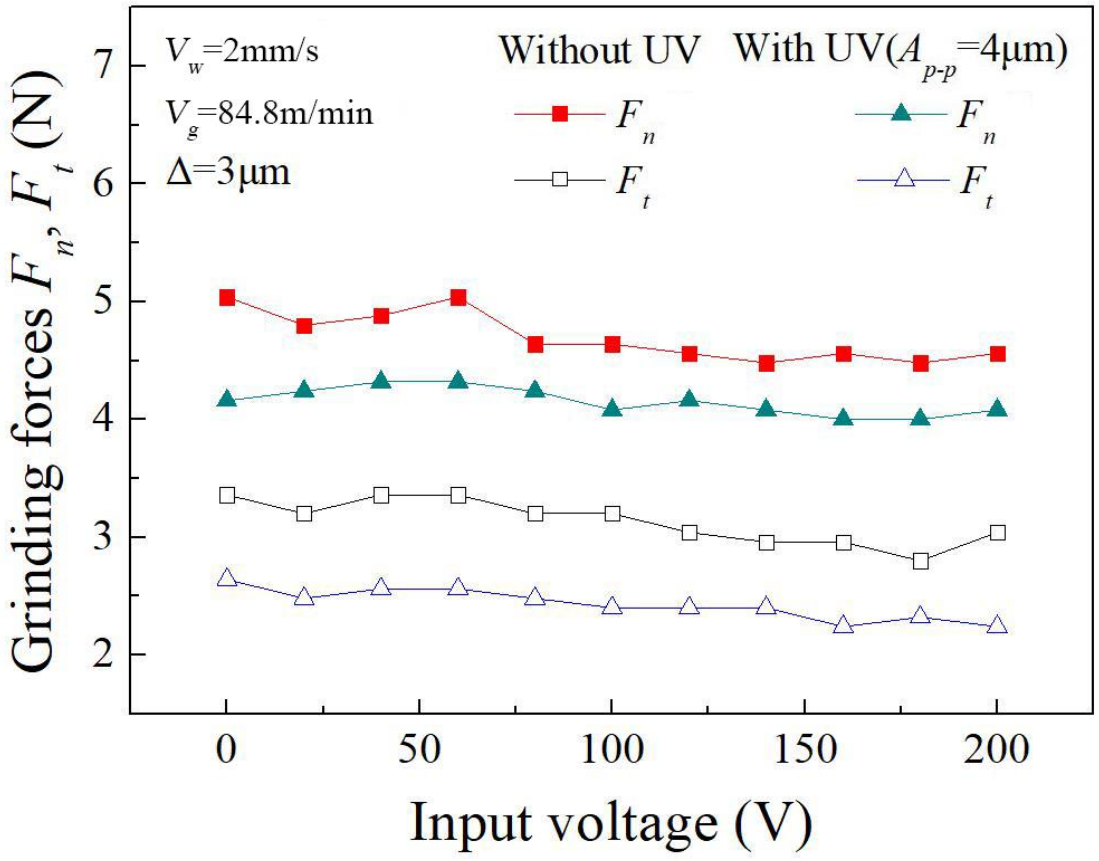

Fig.4.11 Effect of input voltage on grinding forces with/without ultrasonication.

4.5 Summary

(1) Under the current experimental conditions, the lowest normal and tangential grinding forces and work-surface roughness in UPOG were obtained at the plasma voltage U_I = 100 V and are lower than those obtained in conventional grinding by 60 %, 70 %, and 46 %, respectively.

(2) The plasma oxidation tests confirmed the generation of an oxidized layer through observation of the work-surface color. The minimum Vickers microhardness of the oxidized work-surface was obtained at U_I = 80 V, and was lower than that of the original material by 39 %.

(3) Ultrasonic vibration promoted plasma electrolysis oxidation of the work-surface, resulting in reduced work-surface hardness and decreased grinding forces.

Reference

[1] S.Y. Hong, I. Markus, W.-c. Jeong, New cooling approach and tool life improvement in cryogenic machining of titanium alloy Ti-6Al-4V, International Journal of Machine Tools & Manufacture, 2001;41:16.

[2] E.O. Ezugwu, Z.M. Wang, Titanium alloys and their machinability - a review, Journal of Materials Processing Technology, 1997;68:12.

[3] A. Thakur, S. Gangopadhyay, State-of-the-art in surface integrity in machining of nickel-based super alloys, International Journal of Machine Tools and Manufacture, 2016;100:25-54.

[4] E.O. Ezugwu, Key improvements in the machining of difficult-to-cut aerospace superalloys, International Journal of Machine Tools and Manufacture, 2005;45:1353-1367.

[5] D. Setti, M.K. Sinha, S. Ghosh, P. Venkateswara Rao, Performance evaluation of Ti–6Al–4V grinding using chip formation and coefficient of friction under the influence of nanofluids, International Journal of Machine Tools and Manufacture, 2015;88:237-248.

[6] S. Sun, M. Brandt, M.S. Dargusch, Machining Ti–6Al–4V alloy with cryogenic compressed air cooling, International Journal of Machine Tools and Manufacture, 2010;50:933-942.

[7] M.J. Bermingham, S. Palanisamy, D. Kent, M.S. Dargusch, A comparison of cryogenic and high pressure emulsion cooling technologies on tool life and chip morphology in Ti–6Al–4V cutting, Journal of Materials Processing Technology, 2012;212:752-765.

[8] S. Palanisamy, S.D. McDonald, M.S. Dargusch, Effects of coolant pressure on chip formation while turning Ti6Al4V alloy, International Journal of Machine Tools and Manufacture, 2009;49:739-743.

[9] C.R. Dandekar, Y.C. Shin, J. Barnes, Machinability improvement of titanium alloy (Ti–6Al–4V) via LAM and hybrid machining, International Journal of Machine Tools and Manufacture, 2010;50:174-182.

[10] Dang Van Thanh, Phung Phi Oanh, Do Tra Huong, Phuoc Huu Le, 2017, Ultrasonic-assisted cathodic electrochemical discharge for graphene

synthesis, Ultrasonics Sonochemistry, 34:978-–983.

[11] M.C. Shaw, Principles of abrasive processing, Bookcaft (Bath)Ltd Midsomer Norton, Great Britain, 1996.

[12] E.M. Alawadhi, Numerical Simulation of Fluid Flow Past an Oscillating Triangular Cylinder in a Channel, Journal of Fluids Engineering, 2013;135: 041202.

[13] O.A. Druzhinin, Concentration waves and flow modification in a particle-laden circular vortex, Physics of Fluids, 1994;6:3276.

[14] D.Z. K.P. Rajurkar, J.A. McGeough, J. Kozak, A. De Silva, New Developments in Electro-Chemical Machining, CIRP Annals - Manufacturing Technology, 1999;48:12.

[15] A.B. Suvadeep Roy, Simul Banerjee, Analysis of effect of voltage on surface texture in electrochemical grinding by autocorrelation function, Tribology International, 2007;40:6.

[16] Z.J. Pei, P.M. Ferreira, Modeling of ductile-mode material removal in rotary ultrasonic machining, International Journal of Machine Tools and Manufacture, 1997;38:20.

Chapter 5 Machining apparition of drilling Ti alloy by UPOG

5.1 Drilling principal and experimental procedure

The schematic of UPOG technique in drilling of Ti-6Al-4V is shown in Fig. 5.1 (a), where a metal bonded cBN grinding wheel ultrasonically vibrating in its own axis at a frequency of f and a peak-peak amplitude of $A_{p\text{-}p}$ is rotated at a peripheral speed of V_g and fed at a feed rate of V_w. Let the grinding wheel be the cathode and the workpiece be the anode. Thus, the grinding wheel and the workpiece are positively and zero charged, respectively, when an electric voltage V is applied between them. In the meantime if an ionic liquid is supplied into the grinding zone between the wheel and the workpiece, the work-material is oxidized and a thin oxidized layer is formed on the most surface of workpiece in the grinding zone for the sake of PEO. Then the weakened thin layer is easily removed by the abrasive grans which is moving along with the peripheral surface of the rotating grinding wheel. The ionic liquid is a key part of the PEO process. In this work, electrochemical reaction is used to form the oxygen layer on workpiece surface to make it is easy to be removed by the cBN grains. Therefore, KNO_3 solution is selected as ionic liquid.

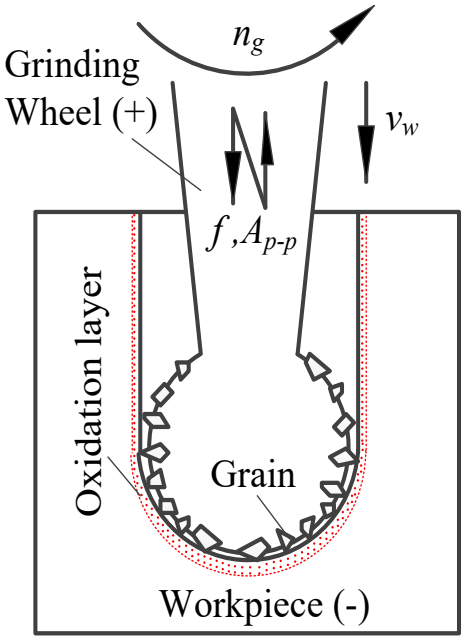

(a) Pinciple schematic

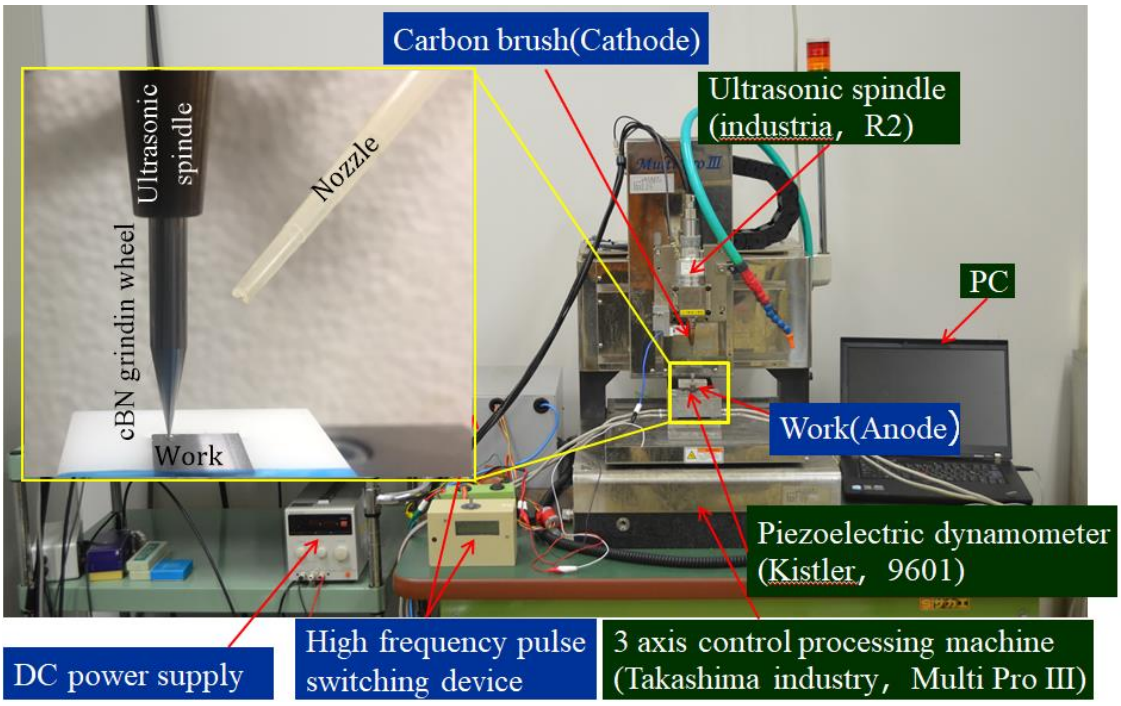

(b) Experimental setup

Fig. 5.1. Schematic and setup of Ultrasonic Assisted Plasma Oxidation Grinding Technique in Drilling of Ti-6Al-4V.

To practice the processing principle described above, an experimental setup was constructed as shown in Fig.1 (b). A commercially available ultrasonic spindle (R2 by industrial Co., Ltd., Japan) capable of vibrating at a frequency of 40 kHz and an

peak-peak amplitude of up to $A_{p\text{-}p}$=4 μm was installed on the vertical axis of an existing desktop sized 3D CNC machine tool (Multi Pro III by Takashima Sangyo Co., Ltd., Japan). On the lower end of the spindle, a metal bonded cBN grinding wheel with a diameter of 1mm was screwed. A grinding fluid nozzle was employed to supply the electrolyte fluid into the grinding zone with a given flow. A Ti-6Al-4V specimen with dimensions of L14× W10 × T6 mm was held on the work-table of the 3D CNC machine tool as the workpiece through a 3-components dynamometer (9254 by Kistler Co., Ltd.) and a work-holder. Actual UPOG operations of Ti-6Al-4V were conducted under the processing parameters as shown in Table 5.1.

Table 5.1. Experimental conditions

Ultrasonic vibration	Frequency f	40 kHz
	Amplitude $A_{p\text{-}p}$	4.0 μm
Grinding wheel and process parameters	cBN1000N100M	
	Diameter d_s	1 mm
	Roational speed n_g	20000 rpm
	Depth of cut Δ	1.5 mm
	Grinding width b	2.5 mm
	Feed rate V_w	0.001 mm/s
	Grinding time	25 min
Workpiece	Ti-6Al-4V(L10×W10×T1 mm)	
Plasma electric power supplying	Pattern	Triangle
	Plasma voltage U_I	0~160 V
	Pulse frequency f_d	0.2 MHz
	Duty ratio D	20 %
Electrolytic solution	KNO_3 solution, 5 %dilution	

5.2 Experimental results and discussions

5.2.1 Grinding efficiency

At first, UPOG tests were performed under different plasma variables to elucidate the influences of the processing parameters on the grinding forces. For comparison, plasma grinding (hereafter called POG for simplicity) tests were also carried out under the same plasma variables. As a result, Figs. 5.2 (a) and (b) show the influences of the parameters U_I on the normal grinding forces F_n and maximum grinding force $F_{n\text{-}max}$ in UPOG and POG ($A_{p\text{-}p}$=0 μm), respectively. Obviously, the F_n

in UPOG were charged stable with time increased (Fig. 5.2 (a)), whereas, in CG, POG or UAG (10V) were more likely to be dramatic changed. Father, it can be found that the F_n in UPOG at U_I =20 V were decreased by 60 %, compared with those in either CG or POG. Meanwhile, either in the POG, the $F_{n\text{-}max}$ decreased with increasing U_I, until U_I = 10 V in POG or U_I = 30 V in UPOG; thereafter, $F_{n\text{-}max}$ began to increase as U_I continued to increase. At U_I = 10 V, $F_{n\text{-}max}$ reached 2.1 N where $F_{n\text{-}max}$ with ultrasonic vibration was smaller by 30 % than that in CG. This indicates that the plasma voltage considerably affects grinding force. The higher grinding force leads to serious wheel wear and affect removal volume.

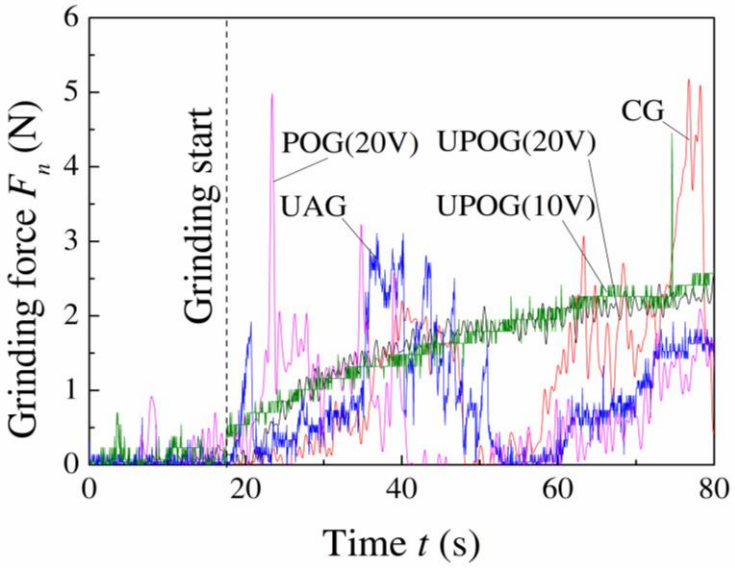

(a) Grinding force vs time

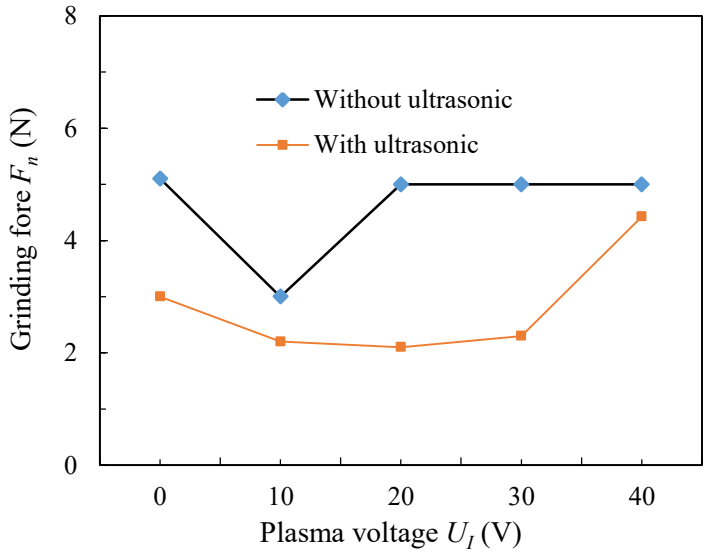

(b) Maximum grinding force

Fig.5.2 Effect of the ultrasonic vibration and plasma oxidation on grinding force

To explain the reasons why ultrasonic vibration and PEO can decrease the grinding force, the effect of the ultrasonic vibration on the grinding force is considered first. The normal grinding force on a single grain, F_{gn}, can be expressed as follows [1]:

$$F_{gn} = \frac{1}{2} N_g \xi t_m^2 \tan^2 \frac{\alpha}{2} H_v \tag{15}$$

where ξ is the geometrical factor of the grain, α is the rake angle of the grain cutting edge, and H_v is the hardness of the work material. The assumption that factors related to the grinding wheel, such as N_g, ξ, α, and the process parameter related factor, t_m, are only minimally affected by plasma electrolysis indicates that F_{gn} predominantly depends on workpiece hardness during grinding. This indicates that the softer the work material is, the smaller the grinding force becomes. In order to confirm whether the titanium dioxide (TiO_2) layer is actually formed on the work-surface by this reaction, Ti-6Al-4V work samples were oxidized by electrochemical reaction with U_I = 0 V and U_I = 20 V. In electrochemical reaction, the grinding wheel was replaced with a Nickel-made rod-shaped cathode of 1 mm in diameter and a gap of 7 μm was given between the cathode and the anode (work sample). The cathode was rotated at a rotational speed of 20,000 rpm and fed leftward at a feed rate of 2.0 mm/s for a stroke of 10 mm. The dynamic Vickers micro-hardness (DHV) was obtained for work-surfaces by original (U_I = 0 V, without ultrasonic), plasma electronic oxidation (U_I = 20 V without ultrasonic) and ultrasonic assisted plasma electronic oxidation (U_I = 20 V with ultrasonic), respectively, by using Dynamic Ultra Micro Hardness Tester (DUH-211). In measurement, a load of 1 mg was applied for a duration of 5 s and a Vickers indenter with an included angle of 115° was employed. As a result, the DHV values in original, electrochemical, and ultrasonic assisted electrochemical were 512 HV, 453 HV and 436 HV, respectively. These values demonstrate that in the case without electrochemical reaction, i.e., in original, the DHV was independent of the ultrasonic vibration, and once the electrochemical reaction occurred, the DHV decreased from 512 HV to 453 HV without ultrasonic vibration, and decreased further to 436 HV with ultrasonic vibration. These results imply that under the presence of electrochemical reaction the work-surface hardness becomes low and ultrasonic vibration encourages the decrease in the hardness. However, in the absence of electrochemical reaction, the ultrasonic does not affect the hardness.

To explain the reasons why ultrasonic vibration and PEO can decrease the grinding force, the effect of the ultrasonic vibration on the grinding force is considered first. The normal grinding force on a single grain, F_{gn}, can be expressed as follows:

$$F_{gn} = \frac{1}{2} N_g \xi t_m^2 \tan^2 \frac{\alpha}{2} H_v \tag{16}$$

where ξ is the geometrical factor of the grain, α is the rake angle of the grain cutting edge, and H_v is the hardness of the work material. The assumption that factors related to the grinding wheel, such as N_g, ξ, α, and the process parameter related factor, t_m, are only minimally affected by plasma electrolysis indicates that F_{gn} predominantly depends on workpiece hardness during grinding. This indicates that the softer the work material is, the smaller the grinding force becomes. In order to confirm whether the titanium dioxide (TiO_2) layer is actually formed on the work-surface by this reaction, Ti-6Al-4V work samples were oxidized by electrochemical reaction with U_I = 0 V and U_I = 20 V. In PEO the grinding wheel was replaced with a Cu-made rod-shaped cathode of 1 mm in diameter and a gap of 7 μm was given between the cathode and the anode (work sample). The cathode was rotated at a rotational speed of 20,000 rpm and fed leftward at a feed rate of 2.0 mm/s for a stroke of 10 mm. The dynamic Vickers micro-hardness (DHV) was obtained for work-surfaces by original (U_I = 0V, without ultrasonic), plasma electronic oxidation (U_I = 20 V without ultrasonic) and ultrasonic assisted plasma electronic oxidation (U_I = 20 V with ultrasonic), respectively, by using Dynamic Ultra Micro Hardness Tester (DUH-211). In measurement, a load of 1 mg was applied for a duration of 5 s and a Vickers indenter with an included angle of 115° was employed. As a result, the DHV values in original, electrochemical, and ultrasonic assisted electrochemical were 512 HV, 453 HV and 436 HV, respectively. These values demonstrate that in the case without electrochemical reaction, i.e., in original, the DHV was independent of the ultrasonic vibration, and once the electrochemical reaction occurred, the DHV decreased from 512 HV to 453 HV without ultrasonic vibration, and decreased further to 436 HV with ultrasonic vibration. These results imply that under the presence of electrochemical reaction the work-surface hardness becomes low and ultrasonic vibration encourages the decrease in the hardness. However, in the absence of electrochemical reaction, the ultrasonic does not affect the hardness. Meanwhile,

increase U_I caused the grain damage increase in POG process cause the grinding force increased.

5.2.2 Tool wear and form accuracy

Form accuracy of drilling Ti-6Al-4V were explained with Fig. 5.3. The form error of the hole was observed in CG, UAG and POG process, however, no appeared on in UPOG process. Further compare the cross-section image of them, the hole did not cross though the workpice in CG and UAG. Meanwhile, the diameter of hole was decreased with the depth increase in CG process. In UAG process, the end part was plastic deformation which means grinding wheel was lose material removal able.

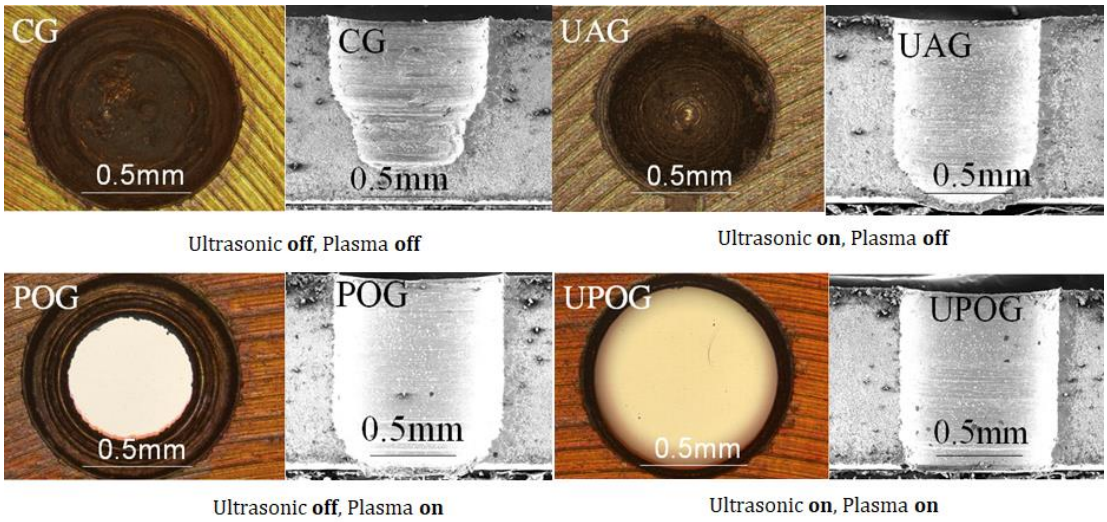

Fig. 5.3 Form accuracy of the drilling Ti alloy by UPOG

5.2.3 Surface roughness

The effect of process parameters on the surface roughness in POG and UPOG are shown in Fig 5.4. It is evident that regardless of the value of U_I, Ra with ultrasonic vibration was smaller than that without ultrasonic vibration. This is a phenomenon similar to that seen in conventional UAG, demonstrating that under the presence of plasma oxidation, ultrasonic vibration also reasonably improves the work-surface quality. Interestingly, either in the presence or absence of ultrasonic vibration, the Ra value decreased with increasing U_I, until U_I = 10 V; thereafter, Ra began to increase as U_I continued to increase. At U_I = 10 V, Ra reached 5.4 μm where Ra with ultrasonic

vibration was smaller by 19 % than that in CG. This indicates that the plasma voltage considerably affects work-surface roughness.

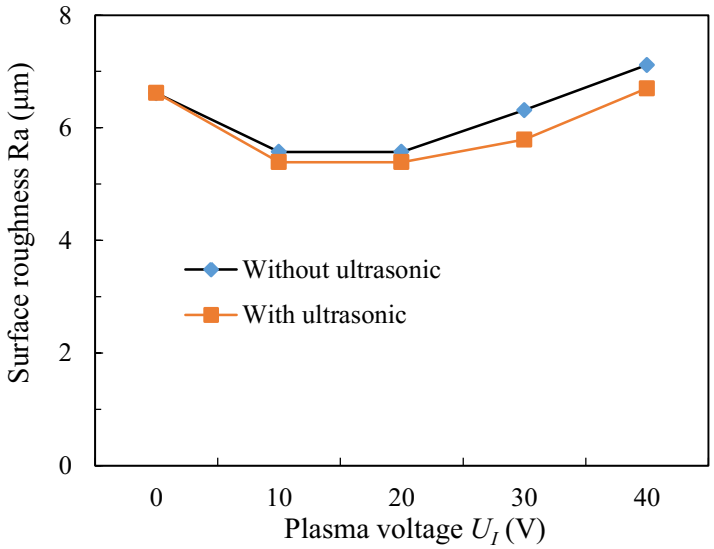

Fig.5.4 Surface roughness rate versus process parameters

5.2.4 Burr volume

Removal volume V_r and Volume of burrs V_b at different values of U_I were investigated as shown in Fig. 5.5. Indeed, the increase of the U_I resulting in the increase of the residual removal ratio, either in the presence or absence of ultrasonic vibration (Figs. 5.5(a)). For example, at U_I =10 V the values of V_r in UPOG (10V) and CG were 0.7 mm^3 and 0.6 mm^3, the difference reached 14 %. Subsequently, the effects of the plasma voltage, U_I, and the ultrasonic vibration on the volume of burrs were obtained as shown in Fig. 5.5 (b). Obviously, the volume burrs exhibited a similar variation tendency as U_I increased. First, in CG (U_I = 0 V without ultrasonic vibration), V_b= 9.2×10^5 μm^3. Once ultrasonic vibration and plasma was applied to perform UPOG (U_I = 10 V with ultrasonic vibration), the values of burrs was reduced by 73 % to V_b= 2.5×10^5 μm^3. Then, as the plasma electric power was applied to perform plasma oxidation grinding (POG) (U_I = 10 V without ultrasonic vibration) and UPOG (10 V ≤ U_I ≤ 30 V with ultrasonic vibration), and decreased as U_I = 10 V was observed. However, once U_I was beyond 10 V, the volume of burrs increased rapidly in POG, implying that U_I should be set in 10 V to minimize the volume of burrs under the current experimental conditions.

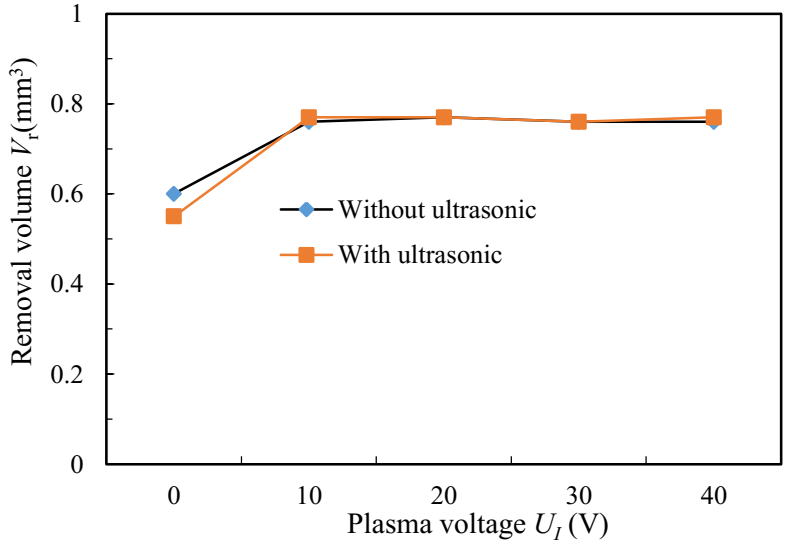

(a) Removal volume

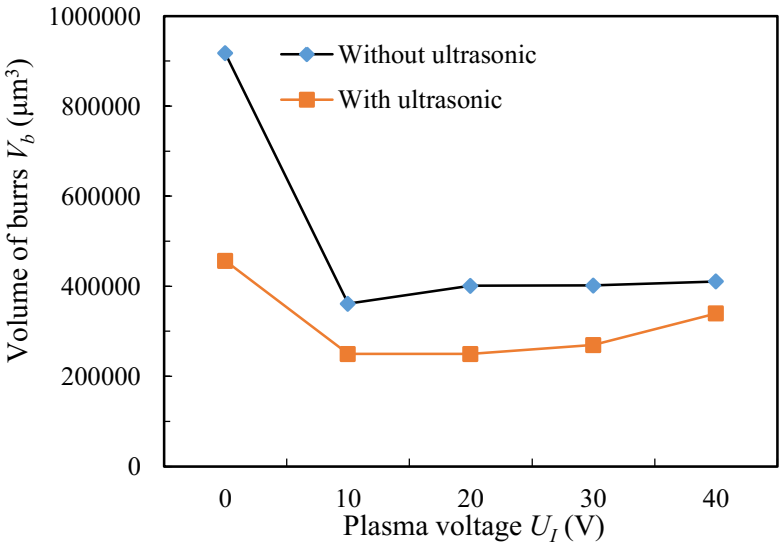

(b) Volume of burrs

Fig.5.5 Effect of the ultrasonic vibration and plasma oxidation on removal volume and volume of burrs

5.3 Summary

The drilling process of Ti-6Al-4V was processed by UPOG with different process parameters. The results obtained in this work are summarized as follows:

(1) Under the current experimental conditions, the lowest normal grinding force, volume of burrs and work-surface roughness in UPOG were obtained at the

plasma voltage U_I = 10 V and are lower than those obtained in conventional grinding by 60 %, 73 %, and 19 %, respectively.

(2) The plasma oxidation tests confirmed the Vickers micro-hardness of the work-surface decreased from 512 HV in original to 436 HV in ultrasonic assisted plasma electronic oxidation by 15 %.

Reference

[1] I.D. Marinescu, M.P. Hitchiner, E. Uhlmann, W.B. Rowe, I. Inasak, Handbook of Machining with Grinding Wheels, in, CRC Press, USA, 2006.

Chapter 6 Conclusions and future recommendation

6.1 Conclusions

In this study, toward the development of an alternative machining method for the grinding of hard-to-machine materials, the ultrasonic, electrochemical and plasma oxidation technique is applied to the grinding of hard-to-machine materials. For this purpose, an experimental rig was constructed by installing an ultrasonic spindle and pulse power onto grinder and experimental investigations on the machining characteristics of Ti and Inconel 718 workpiece were performed on the constructed rig. The obtained results of this study can be summarized as following:

In chapter 1, prevailing technologies, i.e., UAG, ECG and PEO was outlined. The classical and recent works were reviewed. The motivations for this study were outlined.

In chapter 2, experimental investigations on the machining characteristics of the UAG of Inconel 718 materials were performed on the constructed rig. The conclusions are obtained as follows:

(1) In UAG at the ultrasonic vibration amplitude of $A_{p\text{-}p}$=9.4 μm the normal and tangential grinding forces were smaller by 42.5 % and 40 %, respectively, compared to those in CG, when the wheel peripheral speed was 138.2 m/min.

(2) The specific grinding energy u in UAG is smaller than that in CG and intended to decrease as the $A_{p\text{-}p}$ increases, demonstrating that the ultrasonication benefits the reduction in the specific grinding energy.

(3) The wear of electroplated cBN grinding wheel in grinding of Inconel 718 are dominantly attributed to chips adhesion, grains releasing and grains fracture. Both the percentage of chips adhesion area and the size of chips adhered tend to decrease as the vibration amplitude increases; in contrast, the effect of ultrasonic vibration on the number of chips adhesion are not noticeable;

(4) The percentage of the number of grains released/fractured decreases as the vibration amplitude rises; e.g., the percentage in UAG at $A_{p\text{-}p}$=9.4 μm was decreased by 40 % compared to that in CG;

(5) The chip size, i.e., cross-section area and length, are distinctly affected by the ultrasonication but little effect of wheel peripheral speed is observed. The UAG is potentially avoiding the formation of shear chips and prefers the flow chips especially at larger amplitude;

(6) In conventional grinding (CG) without ultrasonication the wheel peripheral speed would affect the chip formation significantly, whereas in UAG the chip formation is hardly affected by the speed.

In chapter 3, in order to develop a novel technique for the high performance machining of difficult-to-machine materials such as Ti-6Al-4V, this paper proposed a hybrid material removal process, i.e., ultrasonic assisted electrochemical grinding (UAG). For confirming the feasibility of the proposed technique, an experimental setup capable of performing UAG process was constructed and fundamental machining characteristics of UAG in the grinding of Ti-6Al-4V were investigated followed by discussion. The obtained result can be summarized as following.

(1) Under the given ranges of the voltage U_I, the frequency f_d and the duty ratio D of the pulse electrolytic power in the current work, i.e., U_I =0~20 V, f_d=0~0.2 MHz, D=0~50 %, the lowest normal and grinding forces, F_n and F_t, in UAG were attained at U_I =20 V, D=20 % and f_d =0.2 MHz which were smaller than those in CG (conventional grinding at U_I =0V without ultrasonic) by around 60 % and 65 %, respectively.

(2) The work-surface roughness in UAG decreased with the increasing U_I; once the ultrasonic is stopped and the conventional electrochemical grinding (ECG) is performed, the roughness increased by a certain value regardless of the value of U_I. The plastic deformation and cracks which are often generated on the work-surface in CG were not observed in UAG.

(3) The wheel radius wear R_g in UAG decreased as the value of U_I increased when U_I <4 V, thereafter was almost kept constant; in the case of U_I <10 V the Rg in UAG were considerably smaller than that in ECG. The wheel wear in CG was attributed dominantly to the grain drop out, whereas in ECG and UAG the wheel working lives were affected dominantly by the chip adhesion and the grains fracture, respectively.

(4) A titanium dioxide (TiO_2) layer of 78 nm in thickness was actually generated on the work-surface by the electrochemical reaction at U_I =20 V, and thus the Vickers micro-hardness of work-surface decreased from 512 HV in CG and UAG to 436 HV in UAG, a reduction by 15 %. This would be one of the reasons why the grinding forces in UAG were significantly smaller than those in CG, UAG and ECG.

(5) The weight percentages of oxygen element on chips and work surfaces increased as the U_I increased either in ECG or in UAG and the ultrasonic enhanced the percentages of oxygen, implying that with ultrasonic, thicker TiO_2 lay is formed on the work surface and contributes to the decrease of grinding forces.

In chapter 4, experimental investigations on the machining characteristics of the UPOG of Ti-6Al-4V materials were performed on the constructed rig. The conclusions are obtained as follows:

(1) Under the current experimental conditions, the lowest normal and tangential grinding forces and work-surface roughness in UPOG were obtained at the plasma voltage U_I = 100 V and are lower than those obtained in conventional grinding by 60 %, 70 %, and 46 %, respectively.

(2) The plasma oxidation tests confirmed the generation of an oxidized layer through observation of the work-surface color. The minimum Vickers microhardness of the oxidized work-surface was obtained at U_I = 80 V, and was lower than that of the original material by 39 %.

(3) Ultrasonic vibration promoted plasma electrolysis oxidation of the work-surface, resulting in reduced work-surface hardness and decreased grinding forces.

(4) The UPOG is also effectively to machining Inconel 718 with high voltage.

In chapter 5, the drilling process of Ti-6Al-4V was processed by UPOG with different process parameters. The results obtained in this work are summarized as follows:

(1) Under the current experimental conditions, the lowest normal grinding force,

volume of burrs and work-surface roughness in UPOG were obtained at the plasma voltage U_I = 10 V and are lower than those obtained in conventional grinding by 60 %, 73 %, and 19 %, respectively.

(2) The plasma oxidation tests confirmed the Vickers micro-hardness of the work-surface decreased from 512 HV in original to 436 HV in ultrasonic assisted plasma electronic oxidation by 15 %.

6.2 Future recommendation

The research in the ultrasonic assisted plasma oxidation grinding is still in preliminary stage. There are many topics and unclear points that need to be investigated to ensure the reliability to apply this technology on the actual machining. In what follows, some recommendations and notes were list for future work:

(1) Although the material removal behavior in UPOG has been sufficiently studied in this study, the material removal mechanism has not been explored fully. This work should be done in the future work.

(2) In this study, it is found that actual removal rate in UPOG is deeper than that in the conventional grinding. However, the reason why actual removal rate becomes deeper in ultrasonic assisted grinding has not been explored fully.

(3) Much more works should be devoted to the feasibility of the technique in practice.

Acknowledgements

This thesis work is a result of three years of hard work. It would be impossible to complete this work without the assistance and encouragement of many people. I would like to take this opportunity to express my appreciation to many people who have been helping me during my PhD study.

First and foremost, I must thank my first advisor, Prof. Yongbo Wu. I still remember the moment I came to Akita Prefectural University about three years ago. At that time, I knew nothing about the knowledge of manufacturering, how to do research, how to write a good paper, how to be a good researcher… In a word, I was a blank sheet of paper at that time. However, with Prof. Wu‟s constant support, guidance, sage advice, and infinite patience, the blank sheet of paper three years ago became a rich and colorful picture today. What I have learned from Prof. Wu will spur me to go on with scientific research and to be a good man throughout the rest of my life.

Next, I must thank my second advisor, Prof. Teruo Bitoh. When my first advisor changed his position and leaved Akita Prefectural University, I am boarding in Prof. Teruo Bitoh‟s laboratory. Without his undeserved kindness, there is no hope to finish my last year of PhD study. He has walked me through all the stages of last school year. Without his consistent and illuminating instruction, this thesis could not have reached its present form.

Also, I am thankful to Associate Professor Mitsuyoshi Nomura and Dr. Tatsuya Fujii for their invaluable instructions during my PhD study. I also have to thank the Lab technical staff Mr. Seiichi Kimura for his extraordinarily technique support. I would like to thank Dr. Jia Gu for his kind help and assistance in my journal paper revision. Without his countless help, papers could not be successfully published.

I was very fortunate to have participated in Prof. Wu‟s laboratory, and grateful thanks go to my peer research lab members, including but not limited to, Prof. Yuebo Ji, Dr. Masakazu Fujimoto, Dr. Youliang Wang, Dr. Jianguo Cao, Dr. Huiru Guo, Mr. Zongliang Yao, Mr. Qiang Wang, Mr. Ming Feng,…..

Thanks are due to, including but not limited to, the following people for sharing happy and indelible experience in Akita Prefectural University.

Sisi Li

March, 2018

Accomplishments

I. 博士学位論文に関するもの

著書(分担執筆)

1. Yongbo Wu, Qiang Wang, Sisi Li, Dong Lu, Ultrasonic Assisted Machining of Nickle-based Superalloy Inconel 718, Superalloys, **InTech - open science**, Full Chapter Review

学術論文

1. Sisi Li, Yongbo Wu, Masakazu Fujimoto, Mitsuyoshi Nomura. Improving the Working Surface Condition of Electroplated Cubic Boron Nitride Grinding Wheel in Surface Grinding of Inconel 718 by the Assistance of Ultrasonic Vibration. **Journal of Manufacturing Science and Engineering** (IF: 3.48), 2016, 138(7): 8 pages. [DOI: 10.1115/1.4032080] (第二章)
2. Sisi Li, Yongbo Wu , Mitsuyoshi Nomura. Effect of grinding wheel ultrasonic vibration on chip formation in surface grinding of Inconel 718. **The International Journal of Advanced Manufacturing Technology** (IF: 1.458), 2016, (Online). [DOI 10.1007/s00170-015-8149-0] (第二章)
3. S. Li, Y. Wu, K. Yamamura, M. Nomura, T. Fujii, Improving the grindability of titanium alloy Ti-6Al-4V with the assistance of ultrasonic vibration and plasma electrolytic oxidation, **CIRP Annals Manufacturing Technology** (IF: 2.49), 2017, 66(1):345-348. (第四章)
4. Sisi Li, Yongbo Wub, Mitsuyoshi Nomura, Tatsuya Fujii. Proposal of an ultrasonic assisted electrochemical grinding method and its fundamental machining characteristics in the grinding of Ti–6Al–4V, **Journal of**

Manufacturing Science and Engineering (IF: 3.48), (修正中) (第三章).

5. Sisi Li, Yongbo Wu and Mitsuyoshi Nomura, Fundamental Investigation of Ultrasonic Assisted Surface Grinding of Inconel 718, **Advanced Materials Research**, 2016, 1136: 365-370.(EI) (第二章)
6. Sisi Li, Yongbo Wu, Mitsuyoshi Nomura. Fundamental Investigation of Ultrasonic Assisted Pulsed Electrochemical Grinding of Ti-6Al-4V, Proc. of ISAAT2016, **Materials Science Forum**, Volume 874:279-284. (EI) (第三章)

国際学術会議

1. Sisi Li , Yongbo Wu, Mitsuyoshi Nomura, Fundamental Investigation of Ultrasonic Assisted Surface Grinding of Inconel 718, **The 18th International Symposium on Advances in Abrasive Technology (ISAAT 2015)**, 2015.10.6-7. (第二章)
2. Sisi Li, Yongbo Wu, Mitsuyoshi Nomura, Ji Yuebo, On the chip formation in ultrasonic assisted grinding of Inconel 718, **The 11th China-Japan International Conference on Ultra-Precision Machining Process (CJUMP2015)**, 2015.11.25-26. (第二章)
3. Sisi Li , Yongbo Wu, Mitsuyoshi Nomura, Fundamental Investigation of Ultrasonic Assisted Pulsed Electrochemical Grinding of Ti-6Al-4V, **The 19th International Symposium on Advances in Abrasive Technology (ISAAT 2016)**, 2016.10.2-4. (第三章)
4. S. Li, Y. Wu, K. Yamamura, M. Nomura, T. Fujii, Improving the grindability of titanium alloy Ti-6Al-4V with the assistance of ultrasonic vibration and plasma electrolytic oxidation, **CIRP Annals Manufacturing Technology**, 2017. 10.5-8. (第四章)
5. Sisi Li, Teruo Bitou, Yongbo Wu, Mitsuyoshi Nomura and Tatsuya Fujii, Study on Ultrasonic Assisted Plasma Oxidation Grinding technology in micro drill-grinding of Ti-6Al-4V, **The 20th International Symposium on Advances**

in Abrasive Technology (ISAAT 2017), 2017. 11. 23-30. (第五章)

国内学術会議

1. 李　偲偲，呉　勇波，野村光由，インコネル 718 の超音波援用円筒プランジ研削の試み，**2015 年度精密工学会秋季大会学術講演会講演**，2015.9
2. 李　偲偲，呉　勇波，野村光由，立花　亨，小林　敏，チタン合金 Ti–6Al–4V の超音波援用電解研削の試み，**2016 年度精密工学会春季大会学術講演会講演**，2016.3
3. 李　偲偲，呉　勇波，野村光由，藤井達也，立花　亨，小林　敏，超硬合金の超音波援用プラズマ研削の試み，**2016 年度精密工学会秋季大会学術講演会講演**，2016.9
4. 李　偲偲，呉　勇波，野村光由，藤井達也，立花　亨，小林　敏，超音波援用プラズマ研削によるチタン合金 Ti-6Al-4V の穴あけ，**2017 年度精密工学会春季大会学術講演会講演**，2017.3

受賞

1. 平成 27 年 11 月　CJUMP2015 国際会議の発表論文が”Excellent Paper Award”を受賞した
2. 平成 28 年三豊科学技術振興協会国際交流助成
3. 平成 28 年本荘由利産学振興財団国際交流助成

Ⅱ. その他関連業績

学術論文

1. Yongbo Wu, Sisi Li, Mitsuyoshi Nomura, Satoshi Kobayahi, Toru Tachibana. Ultrasonic Assisted Electrolytic Grinding of Titanium Alloy Ti-6Al-4V, **International Journal of Nanomanufacturing**, 2017, 13 (2) :152-154. (EI) (第三章)

国内学術会議

1. 顧 嘉, 呉 勇波, 野村 光由, 汪 強，李 偲偲，王 有良超音波潤滑を利用した Ti-6Al-4V の旋削における基礎加工特性，**2016 年度精密工学会春季大会学術講演会講演**，2016.